Humboldt-Universität zu Berlin
Mathematisch-Naturwissenschaftliche Fakultät
Institut für Physik

Vertex correction to the electron-phonon interaction in the homogeneous electron gas

Masterarbeit

zur Erlangung des akademischen Grades
Master of Science (M. Sc.)

eingereicht von: Axel Hübner
geboren am: 13.11.1995
geboren in: Berlin

Gutachter/innen: Prof. Dr. Dr. hc. Claudia Draxl
Prof. Dr. Jan Plefka

eingereicht am: ..... verteidigt am: .....

Contents

1. Introduction

The interaction between bosons and fermions is a fundamental component of many-body physics. One of the manifestations in materials is the interaction of electrons with collective vibrational modes, the (bosonic) phonons. Electron-phonon interaction influences the properties of matter and contribute to multiple phenomena. These include the temperature dependence of the electrical resistivity and carrier mobility in semiconductors [27, 35], optical absorption in indirect gap semiconductors [28], the temperature dependence of band structures [22, 23, 42], the formation of kinks, polaronic satellites and Kohn anomalies in photoemission spectra [17, 19, 39, 50, 64, 66, 68, 69], as well as conventional superconductivity [4]. Additionally, the scattering of electrons and phonons results in dissipation phenomena, such as hot-carrier relaxation [11, 12, 16], phonon damping [28], and the decay of collective charge-density fluctuations (plasmons) [10, 14, 18, 55].

A quantitative understanding of electron-phonon interaction from *ab initio* calculations can help to find materials for applications, in which the time-scales of dissipation phenomena are important for the device function [18]. Such applications are plasmonic devices [25, 34] which employ charge-density fluctuations, the plasmons and surface-plasmon-polaritons (SPP's) [13, 65], that exist in nanostructured materials. SPP's allow for the amplification, concentration, and manipulation of light-waves at the nanoscale, exhibit large excitation cross-sections, and can cause field strengths around the nanoparticles, significantly larger than this of the incident light beam [25, 41]. Plasmonic devices allow to overcome the diffraction limit of conventional optics and may help to increase the resolution and sensitivity of optical probes [25]. The applications of plasmon excitations range from ancient stained glass [35], up to modern biomedicine [24, 29], and especially radiation therapy [31, 57], energy generation [6, 37, 46, 62], environmental protection [7, 38, 51], information technology [8, 45, 58] and sensing [32]. The number of applications for plasmonics increases rapidly with the capability to manifacture nanomaterials [25]. As large enough plasmon lifetimes are indispensable for the device functionality [34], the development of predictive theories, that account for the damping mechanisms of plasmons may contribute to the development of plasmonic applications.

Plasmon excitations correspond to the roots of the macroscopic dielectric function ε of the system, and have a dispersion relation between their momenta $\mathbf{k}$ and frequencies ω_{pl} [18, 44]. Plasmons can be observed in electron-energy-loss spectroscopy (EELS). In EELS an electron beam is directed on a specimen [21] and the change of the electron energy and momentum after interacting with the sample is measured to deduce information about the structural and chemical properties of the system [20]. The electron loss can be described by the loss function $\mathscr{L}$

$$\mathscr{L}(\mathbf{k}, \omega) = \Im(\varepsilon(\mathbf{k}, \omega)^{-1}), \tag{1}$$

which exhibits poles for values $(\mathbf{k}, \omega)$, at which plasmons or electron-hole pairs can be excited [56]. The loss function for the free electron gas (in the random-phase approximation [4]) in three dimensions as depicted in Fig.1, exhibits plasmon excitations

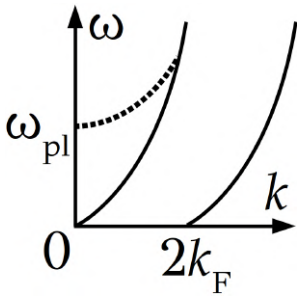

Figure 1: Poles of the loss function for the free electron gas [53, p.239], with frequency ω over momentum $k = |\mathbf{k}|$. k_F is the Fermi wavevector [35] and ω_{pl} the plasma frequency, that marks the onset of the plasmon mode in the system (dashed line). The parabolic lines mark the boundaries, in which electron-hole pairs can be excited.

(the dashed line).

The lifetime of the plasmon modes can be calculated by including electron-phonon and electron-electron interactions in the dielectric function. In recent years, substantial advancements have been made [5, 48, 52, 59, 73, 74], though most of these approaches concentrated on absorption spectroscopy. Recently, the effects of plasmon damping in the homogeneous electron gas have been calculated, relying on corrections of the electron Green's function [18]. However, the impact of electron-hole interactions in this model, the electron-phonon vertex correction, has not yet been considered.

In this work, I will use the Hedin-Baym equations, which constitute an exact formalism to investigate interacting electrons and phonons in the harmonic approximation [18, 27], to calculate the electron-phonon vertex correction to the homogeneous electron gas. In the model, electron-electron interaction is neglected to focus on electron-phonon interaction, which is appropriate for small energy excitations [2, p.187]. To allow by hand calculations, a single optical phonon is considered, that interacts with electrons with a non-dispersive coupling strength. The calculations will be done in a zero temperature framework and exemplified for carrier densities representative of metals. Within this model, I will investigate the properties of the vertex function. I aim to check the validity of Migdal's theorem [47], that the vertex correction can only have a small impact on the dielectric function. Additionally, I investigate whether compensation effects between the correction from Green's functions [18] with the vertex correction take place, similar to the findings for the electron-electron interacting systems [9]. Eventually, I will assess the influence of the vertex correction on the plasmon lifetimes.

2. Theoretical background and methodology

In this section, I first present the model Hamiltonian of the homogeneous electron gas, then introduce the method of Green's functions, the Feynman rules of the theory, the equation of motion for the Green's functions and the concept of the self-energy. Afterwards, I discuss the scope of this methodology, the dielectric function, the random-phase approximation, the Hedin-Baym equations and I outline the calculation procedure that I used and how I validated my results. The model that I investigate is the homogeneous electron gas with electron-phonon interactions and phonons in the harmonic approximation[1] at zero temperature. The treatment is simplified by neglecting the Coulomb interactions between the electrons, so that the effect of electron-phonon interactions can be more easily assessed. Additionally, I approximate the coupling of electrons and phonons and the phonon frequency ω_{ph} as non-dispersive. The scope of this approximation is discussed in Secs. 2.5 and 3.3.

The Hamiltonian of the system, which can be found for example in [27], is, in second quantization[2]

$$\widehat{\mathscr{H}} = \sum_{\mathbf{k}} \epsilon(\mathbf{k}) c^\dagger_{\mathbf{k}} c_{\mathbf{k}} + \sum_{\mathbf{q}} \omega_{\text{ph}} \left(a^\dagger_{\mathbf{q}} a_{\mathbf{q}} + \frac{1}{2} \right) + \sum_{\mathbf{k},\mathbf{q}} g \; c^\dagger_{\mathbf{k}+\mathbf{q}} c_{\mathbf{k}} (a_{\mathbf{q}} + a^\dagger_{-\mathbf{q}}) \tag{3}$$

where $c_{\mathbf{k}}$ denotes an electron annihilation operator for momentum $\mathbf{k}$, $a_{\mathbf{q}}$ an annihilation operator for a phonon of momentum $\mathbf{q}$, and the † denotes the Hermitean conjugate creation operators. $\epsilon(\mathbf{k})$ denotes the energy of an electron with momentum $\mathbf{k}$ (in the non-interacting system). The non-dispersive electron-phonon coupling strength g depends in real materials on the momenta $\mathbf{k}$ and $\mathbf{q}$ and additionally on the band indices of the involved phonon and electron. To make by hand calculations of the vertex tractable, I work in the homogeneous electron gas with one parabolic electron band and one phonon mode only, so the band-indices are omitted for brevity. I aim to predict the behaviour of the system, especially regarding charge-density fluctuations (plasmons) [53]. For this purpose, I employ field theoretical methods - more precisely the Hedin-Baym equations [27], that constitute a rigorous formalism to investigate interacting electrons and phonons in the harmonic approximation, and the diagrammatic expansion [33]. The field theory approach is for my purpose preferable to other methods [67]. Other approaches, such as the Schödinger formulation of perturbation theory, suffer drawbacks: Their perturbation formulas get tediously complex at low orders and one needs to know the eigenstates of the system [53]. Both the Hedin-Baym equation and the diagrammatic approach build on the methods of Green's functions in the treatment of

[1] There is no unmediated phonon-phonon interaction.

[2] I work in atomic units

$$\hbar = \text{Ha} = m_e = \frac{1}{4\pi\varepsilon_0} = 1, \tag{2}$$

where $\hbar$ denotes the reduced Planck constant, Ha the unit of energy, Hartree, m_e the free electron mass and ε_0 the vacuum permittivity.

interacting many-particle systems, which is discussed in the next sections.

2.1. Green's function approach to many-body systems

Green's functions allow a mathematical treatment of interacting many-particle systems without knowledge of the precise partition function [53]. I discuss here their definition and connection to experimental data, for example from spectroscopic measurements [30, 63]. The discussion in this and the next section follows Ref. [53, p.109 ff.] closely.

2.1.1. Definition of Green's functions

I investigate a system under an external perturbation. For that reason I aim to compute response functions of the system, that allow to evaluate the evolution of an expectation value $\langle\widehat{\mathscr{O}}\rangle$ of an operator $\widehat{\mathscr{O}}$ in the presence of an external perturbation $P(t)$, where t is the time. The field P, that is assumed scalar, may couple to an operator $\widehat{\mathscr{M}}$, yielding a perturbation to the Hamiltonian of the unperturbed system $\widehat{\mathscr{H}_0}$. The Hamiltonian of the perturbed system is then

$$\widehat{\mathscr{H}}(t) = \widehat{\mathscr{H}_0} + \widehat{\mathscr{M}}P(t) = \widehat{\mathscr{H}_0} + \widehat{\mathscr{H}_p}. \tag{4}$$

In the presence of this perturbing field, I want to calculate the change of $\langle\widehat{\mathscr{O}}(t)\rangle$ with the help of the linear-response theory. In this framework, the time evolution of the system, represented by the density matrix ρ, is truncated at first order in the perturbation. This approach is justified if the perturbation P is sufficiently small. I discuss in Sec. 2.5 what "sufficiently" means. For a rigorous derivation of the linear-response, the interested reader is referred to [4, p.360ff.] or [53, p.115ff.]. Assuming that the perturbation was turned off at $t = -\infty$, the change in the observable $\langle\Delta\widehat{\mathscr{O}}\rangle$ is [53, p.118]:

$$\langle\Delta\widehat{\mathscr{O}}\rangle(t) = \langle\widehat{\mathscr{O}}\rangle(t) - \langle\widehat{\mathscr{O}}\rangle(-\infty) = \int_{-\infty}^{t} dt' P(t')\langle[\widehat{\mathscr{O}}(t), \widehat{\mathscr{M}}(t')]\rangle_0 \tag{5}$$

where $[,]$ means the commutator $[a, b] = ab - ba$, and $\langle ...\rangle_0$ indicates that the average is taken for the unperturbed system.

The retarded Green's function of the operators $\widehat{\mathscr{M}}$ and $\widehat{\mathscr{O}}$ is

$$G_{\widehat{\mathscr{O}},\widehat{\mathscr{M}}}(t, t') = -i\theta(t - t')\langle[\widehat{\mathscr{O}}(t), \widehat{\mathscr{M}}(t')]\rangle_0. \tag{6}$$

Here, the operators are in the Heisenberg picture, and θ is the Heaviside function. In terms of Green's functions, Eq.(5) can be recast as

$$\langle\Delta\widehat{\mathscr{O}}\rangle(t) = \int_{-\infty}^{\infty} dt' P(t') G_{\widehat{\mathscr{O}},\widehat{\mathscr{M}}}(t, t'). \tag{7}$$

This representation justifies the term Green's function in the mathematical sense [49, p.795] and makes evident that the system response to small external perturbations is given by retarded Green's functions.

Important is the Fourier transformed version of Eq.(5), the Kubo equation

$$\langle \Delta \widehat{\mathscr{O}} \rangle(t) = \int_{-\infty}^{\infty} d\omega P(\omega) G_{\widehat{\mathscr{O}},\widehat{\mathscr{M}}}(\omega) \exp(-i(\omega + i0)t). \tag{8}$$

2.1.2. The dielectric function

In this work the dielectric function is the most important response function. The dielectric function describes the linear-response of a system to a perturbing external charge density ρ_p. In a medium with free charge carriers, this perturbing charge density is screened: Charge carriers in the system are attracted or repelled in such a way to compensate the perturbation locally. A measure of this screening is the dielectric function ε.

I use the Fourier decomposition of the perturbing charge density

$$\rho_p(\mathbf{r}, t) = \int_{\mathbb{R}} \frac{d\omega}{2\pi} \sum_{\mathbf{q}} \rho_p(\mathbf{k}, \omega) \exp(i\mathbf{k}\mathbf{r} - i(\omega + i0)t). \tag{9}$$

This charge density couples via the Coulomb interaction to the other charge carriers in the system. The interaction energy is

$$\mathscr{H}_p(t) = -\int d\mathbf{r} \int d\mathbf{r}' \frac{\rho(\mathbf{r})\rho_p(\mathbf{r}', t)}{|\mathbf{r} - \mathbf{r}'|}. \tag{10}$$

With the space-like Fourier transform of the density of the valence electrons $\rho(\mathbf{k})$,

$$\int d\mathbf{r} d\mathbf{r}' \frac{\exp(i(\mathbf{k}\mathbf{r} + \mathbf{k}'\mathbf{r}'))}{|\mathbf{r} - \mathbf{r}'|} = \delta_{\mathbf{k},-\mathbf{k}'} \frac{4\pi}{\mathbf{k}^2}, \tag{11}$$

$\delta_{x,y}$ being the Kronecker delta, and the Fourier transform of the Coulomb interaction $v(\mathbf{k}) = \frac{4\pi}{\mathbf{k}^2}$ one obtains

$$\mathscr{H}_p(t) = \int_{\mathbb{R}} \frac{d\omega}{2\pi} \exp(i(\omega + i0)t) \sum_{\mathbf{q}} v(\mathbf{q}) \rho_p(\mathbf{q}, \omega) \rho(-\mathbf{q}). \tag{12}$$

I assume now, that the background of ions just compensates the electronic charges. The total charge density is

$$\rho_t = \rho_p + \rho_i \tag{13}$$

where ρ_i represents the induced charge density. With Maxwell's equations [54]

$$i\mathbf{k} \cdot \mathbf{D}(\mathbf{k}, \omega) = \rho_p(\mathbf{k}, \omega), \tag{14}$$

$$i\mathbf{k} \cdot \mathbf{E}(\mathbf{k}, \omega) = 4\pi(\rho_p(\mathbf{k}, \omega) + \rho_i(\mathbf{k}, \omega)), \tag{15}$$

and the material equation

$$\mathbf{D}(\mathbf{k},\omega) = \frac{1}{4\pi}\varepsilon(\mathbf{k},\omega)\mathbf{E}(\mathbf{k},\omega), \tag{16}$$

one obtains

$$\rho_i(\mathbf{k},\omega) = \left(\frac{1}{\varepsilon(\mathbf{k},\omega)} - 1\right)\rho_p(\mathbf{k},\omega). \tag{17}$$

The screened or effective Coulomb potential is then

$$W(\mathbf{k},\omega) = \frac{v(\mathbf{k})}{\varepsilon(\mathbf{k},\omega)}. \tag{18}$$

Up to now, the considered theory is not quantized. The quantization is achieved by introducing the density operator $\widehat{\rho}$, for the internal electrons:

$$\widehat{\rho}(\mathbf{k}) = \sum_{\mathbf{q}'} c^{\dagger}_{\mathbf{q}'} c_{\mathbf{q}'+\mathbf{k}}. \tag{19}$$

Then, the perturbation becomes

$$\widehat{\mathscr{H}_p}(t) = \sum_{\mathbf{q}} \widehat{\rho}^{\dagger}(\mathbf{q}) F_t(\mathbf{q}) \tag{20}$$

where F_t is a perturbing field (but no operator here):

$$F_t(\mathbf{k}) = v(\mathbf{k}) \int_{\mathbb{R}} \frac{d\omega}{2\pi} \exp(-i(\omega + i0)t)\rho_p(\mathbf{k},\omega). \tag{21}$$

In the linear-response theory, the expectation of the induced charge density is

$$\begin{aligned} \langle \Delta\widehat{\rho}_i(\mathbf{k},t)\rangle &= \sum_{\mathbf{q}'} \int_{\mathbb{R}} dt' F_{t'}(\mathbf{q}') G_{\widehat{\rho}(\mathbf{k}),\widehat{\rho}(\mathbf{q}')}(t,t') \\ &= \int_{\mathbb{R}} dt' F_{t'}(\mathbf{k}) \chi(\mathbf{k},t,t') \end{aligned} \tag{22}$$

where $G_{\widehat{\rho}(\mathbf{k}),\widehat{\rho}(\mathbf{q}')}(t,t') = \chi(\mathbf{k},t,t')$ is the density-density response function, that is by translation symmetry diagonal in $\mathbf{k}$. One obtains finally

$$\frac{1}{\varepsilon(\mathbf{k},\omega)} = 1 + v(\mathbf{k})\chi(\mathbf{k},\omega). \tag{23}$$

It is evident from Eq.(23) that charge-density fluctuations are directly related to the dielectric function. The dielectric function will later be calculated with the aid of approximations to the density-density response χ.

2.1.3. Spectral density

It should be clarified how direct the connection between Green's functions and experiment is. The most direct fashion is the introduction of a spectral density: In spectroscopy experiments, such as photoemission, inverse photoemission or electron loss spectroscopy, beams of incident light or electrons hit a material and thereby cause elementary excitations in the material, which in turn cause the emission of either light or electrons. The emitted particle's properties disclose information about the electronic structure of the material.

I consider the transition operator $\widehat{\mathscr{T}}$, that is for electron emission $\hat{c}_{\mathbf{k},n}$, where $\mathbf{k}, n$ denote a quasi-electron state in the material. The spectral density is defined as [53]

$$S(t,t') = \frac{1}{2\pi}\langle[\widehat{\mathscr{T}}(t), \widehat{\mathscr{T}}^\dagger(t')]\rangle_0 \tag{24}$$

and can be related to the current of photoelectrons that leave the sample [30]: While moving out of the sample, the photoelectron interacts with the solid, leading to an energy loss of the photoelectron, so that the measured current is not only dependent on the excitation process. However, if the energy loss of the photoelectron can be approximately neglected, the photoelectron spectra can be directly related to the Fourier transform of the spectral density (Eq.(24)), that actually only encapsulates the excitation process itself. Interested readers can find a profound discussion in [30].

As the spectral density is a Green's function, it is evident that Green's functions can be related to experiments. It can be shown [2, p.50,51], that the Fourier transform of a Green's function has poles corresponding to the excitations of the system. The entire macroscopic thermodynamics of a system is determined by the Green's functions [53, p.141 ff.]. To obtain information about a system, it remains to calculate the Green's functions. For this purpose I introduce calculation methods for Green's functions.

2.2. Diagrammatic methods for Green's functions

To simplify later discussions, I introduce two equivalent calculation methods of Green's functions: the method of Feynman diagrams, in this section, and the equations of motion for Green's functions Sec.2.4. As the latter is less discernible, and diagrams lead to the same results, I begin with a brief derivation of the diagrammatic method. This can be done for a Green's function that is related to the retarded Green's function defined in Eq. (6). The derivation will only address objects that are relevant for this thesis and thus be a short glimpse on the theory. Interested readers can find profound discussions in Refs. [4, 36, 53, 61].

Recall the Hamiltonian of the system, Eq.(3). There, the last term can be interpreted as a perturbation to the free electron-phonon system

$$\widehat{\mathscr{H}_p} = g\sum_{\mathbf{k},\mathbf{q}} c^\dagger_{\mathbf{k}+\mathbf{q}} c_{\mathbf{k}} (a_{\mathbf{q}} + a^\dagger_{-\mathbf{q}}). \tag{25}$$

If g is sufficiently small (see Sec. 2.5), the interpretation as a perturbation is justified. Two additional definitions are necessary: Wick's time-ordering operator is

$$\hat{T}_c(\hat{\mathcal{O}}_1(t), \hat{\mathcal{O}}_2(t')) = \theta(t-t')\hat{\mathcal{O}}_1(t)\hat{\mathcal{O}}_2(t') + r\theta(t'-t)\hat{\mathcal{O}}_2(t')\hat{\mathcal{O}}_1(t), \tag{26}$$

where r is the commutation factor of the operators, which is $+1$ for bosonic and -1 for fermionic operators. The time-ordered Green's function is

$$G^c_{\hat{\mathcal{O}}_1,\hat{\mathcal{O}}_2}(t,t') = -i\langle \hat{T}_c(\hat{\mathcal{O}}_1(t), \hat{\mathcal{O}}_2(t'))\rangle. \tag{27}$$

To obtain a "new" perturbation expansion, assume that the system was unperturbed at time $t = -\infty$ and the interaction is turned on "adiabatically" until t reaches the measuring time $t \approx 0$, before it is turned off again to lead to a non-interacting system at $t = +\infty$.

One can then write the time-dependent Hamiltonian in terms of the unperturbed Hamiltonian $\widehat{\mathscr{H}_0}$ as

$$\widehat{\mathscr{H}} = \widehat{\mathscr{H}_0} + \widehat{\mathscr{H}_p}\exp(-\eta|t|) \tag{28}$$

where η is a positive infinitesimal. Switching to Dirac's interaction picture, the perturbing Hamiltonian then becomes

$$\widehat{\mathscr{H}_p^D} = \exp\left(i\widehat{\mathscr{H}_0}t\right)\widehat{\mathscr{H}_p}\exp(-i\widehat{\mathscr{H}_0}t), \tag{29}$$

and the corresponding time evolution operator of the system is

$$U_\eta(t,t') = \sum_{n=0}^{\infty}\frac{1}{n!}\int_t^{t'} dt_1...dt_n \exp\left(-\eta\sum_{i=1}^{n}|t_i|\right)\hat{T}(\widehat{\mathscr{H}_p^D}(t_1)...\widehat{\mathscr{H}_p^D}(t_n)). \tag{30}$$

With these preparations I can use the Gell-Mann-Low theorem:

Theorem 1. *Be $|0\rangle$ the non-interacting ground state. If the state*

$$\lim_{\eta\to 0}\frac{U_\eta(0,-\infty)|0\rangle}{\langle 0|U_\eta(0,-\infty)|0\rangle} =: \lim_{\eta\to 0}\frac{|\psi_\eta(0)\rangle}{\langle 0|\psi_\eta(0)\rangle} \tag{31}$$

exists to any order in perturbation theory, then it is an exact eigenstate to $\widehat{\mathscr{H}}$.

I aim to compute the expectation value of an operator $\hat{\mathcal{O}}$ in the Heisenberg picture. Therefore, one has to evolve the system from the non-interacting ground state to time 0 and then back to the non-interacting ground state. Assuming that the exact ground state is normalized, one finds

$$\langle\psi(0)|\hat{\mathcal{O}}(t=0)|\psi(0)\rangle = \lim_{\eta\to 0}\frac{\langle 0|U_\eta(\infty,0)\hat{\mathcal{O}}(0)U_\eta(0,-\infty)|0\rangle}{\langle 0|U_\eta(\infty,-\infty)|0\rangle}. \tag{32}$$

The rest of this section aims to compute this expectation value $\langle\psi(0)|\widehat{\mathscr{O}}(t=0)|\psi(0)\rangle$. In the denominator one finds the scattering matrix $S_\eta = U_\eta(\infty,-\infty)$. The same fashion that was used to find the expectation of $\widehat{\mathscr{O}}$ can be used for the time-ordered Green's functions. The machinery cannot be applied to the other Green's functions [53], so that the now developed diagrammatic machinery only applies to the time-ordered Green's functions, which, however, can be transformed into the others.

Two more definitions are necessary: The normal product is the product where all creation operators stand at the left (by commutation in arbitrary order) and all destruction operators stand to the right. This defines the operator $N(\widehat{\mathscr{O}}_1...\widehat{\mathscr{O}}_n)$. Note that any average over a normal product vanishes at zero temperature. The contraction C is defined as

$$C(\widehat{\mathscr{O}}_1,\widehat{\mathscr{O}}_2) = \widehat{T}(\widehat{\mathscr{O}}_1,\widehat{\mathscr{O}}_2) - N(\widehat{\mathscr{O}}_1,\widehat{\mathscr{O}}_2). \tag{33}$$

With these definitions I can now introduce key theorems that enable the computation of expectation values in a diagrammatic perturbation theory. The first theorem is Wick's theorem

Theorem 2. *The time ordered product of any operators can be written in terms of all normal products of all partially contracted operators*

$$\begin{aligned}\widehat{T}(\widehat{\mathscr{O}}_1...\widehat{\mathscr{O}}_n) = {} & N(\widehat{\mathscr{O}}_1...\widehat{\mathscr{O}}_n) \\ & + \sum_{\textit{one contraction in normal product}} N(...) \\ & + \sum_{\textit{two contractions in normal product}} N(...) \\ & + ... + \sum_{\textit{all operators pairwise contracted}} (...).\end{aligned} \tag{34}$$

Note that all operators can only be contracted, if the number of operators is even. In this case, a corollary of Wick's theorem is

$$\langle 0|\widehat{T}(\widehat{\mathscr{O}}_1...\widehat{\mathscr{O}}_n)|0\rangle = \sum_{\text{all operators pairwise contracted}} (...), \tag{35}$$

which only enables the computation of any expectation value.

The contractions can now be interpreted in a diagrammatic way. In that manner, any perturbation to any correlation function can be computed - formally. The identification procedure of operators and diagrams can be found in [53, p.341] - only the computation rules for the diagrams are important, which will be introduced shortly, after additional simplifications. A Green's function corresponds in diagrammatic language to the sum of all diagrams with a fix number of external phonons and electrons. To compute the Green's function to order n of the perturbation, one has to compute all diagrams composed of n vertices and all possible connections between them, with this fixed number of external particles, see Fig. 2.

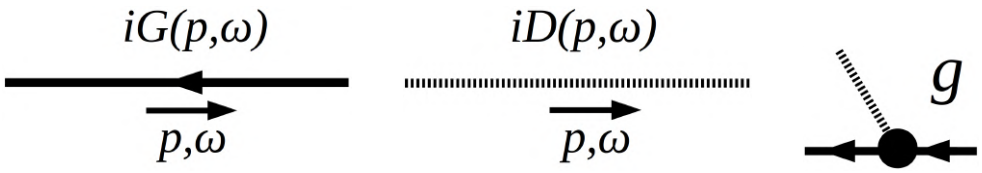

Figure 2: Diagram rules for the model system Eq.(3). The arrows on the electron line denote the charge flow.

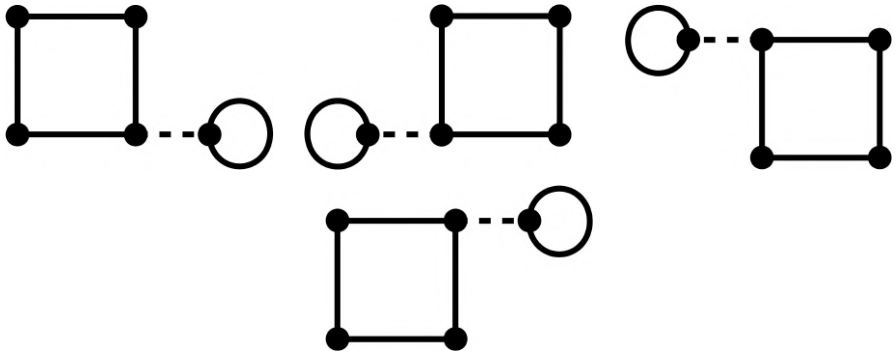

Figure 3: Topologically identical diagrams. All four diagrams can be transformed into each other by flipping or rotating.

I am about to draw combinatorially many diagrams, to calculate the denominator and the numerator in Eq.(32). Fortunately, there are two more theorems that reduce the number of diagrams to draw dramatically.

Theorem 3 (Linked cluster theorem)**.** *Diagrams that have the same topology (i.e. that can be transformed into each other by rotating, flipping, or distorting), have to be considered only once.*

The theorem is illustrated by Fig. 3 - and only one such diagram has to be computed, as the others are topologically identical. I define connected diagrams, to be the diagrams that have paths from each one-particle Green's function to the other, and closed diagrams, to be any diagrams that have no external legs. With these definitions, the corollary of the linked cluster theorem can be derived [53, p.349]: Every expectation value can be computed from connected diagrams values $\mathscr{D}$ only

$$\langle 0|U_\eta|0\rangle = \exp\left(\sum_{v\in\text{connected diagrams}} \mathscr{D}_v\right). \tag{36}$$

The other theorem is the theorem of closed diagrams: The scattering matrix expectation value is the sum of all closed diagrams.

So, the denominator in the calculation cancels the unconnected diagrams that contribute to the numerator. Thus, by the linked cluster theorem, any expectation

value can be computed by connected diagrams only

$$\langle\psi|\widehat{\mathscr{O}}(t=0)|\psi\rangle = \sum_{\text{connected diagrams for } \widehat{\mathscr{O}}} \mathscr{D}_{\widehat{\mathscr{O}}}. \tag{37}$$

2.3. Feynman rules

Now I can write down the Feynman rules for the model theory Eq. (3), that are explicitly derived in Refs. [2, p.52,53], [27] and [53]. Note that a line of the diagram is a one-particle Green's function. The electron Green's function is

$$iG(\mathbf{k},\omega) = \frac{i}{\omega - \epsilon(\mathbf{k}) + i\eta_{\mathbf{k}}}, \tag{38}$$

with $\eta_{\mathbf{k}} = \eta\ \mathrm{sgn}(|\mathbf{k}| - k_F)$. η is considered a positive infinitesimal and k_F is the Fermi wavevector. The Fermi wavevector denotes the highest occupied momentum state of the free electron gas at zero temperature. By Pauli exclusion, electrons in the homogeneous electron gas cannot occupy the same state. This means, that the states are filled from the lowest energy up to the Fermi energy ϵ_F, that corresponds to the Fermi wavevector. The electron Green's function accounts for this change in occupation by a change of the sign of the infinitesimal $\eta\ \mathrm{sgn}(|\mathbf{k}| - k_F)$, distinguishing between excited electrons (with energies higher than the Fermi energy) and empty electron states below the Fermi surface, holes.

The phonon Green's function of the theory is

$$iD(\omega) = \frac{i}{\omega - \omega_{\mathrm{ph}} + i\eta} - \frac{i}{\omega + \omega_{\mathrm{ph}} - i\eta}. \tag{39}$$

The interaction vertex is non-dispersive and is simply a factor g (see above). The remaining rules stem from [53].

- As the system is translation invariant in space and time, Noether's theorem guarantees at each vertex energy and momentum conservation [4, 36].
- The momenta and energies of particles that are created and destroyed in the process (internal particles), are integrated over.
- Every closed fermion loop is summed over spins and contributes the factor -1.
- Every vertex, including external ones, contributes a factor $(-i)$.
- Self-energy diagrams, like the polarizability χ_0 carry an additional factor i.

The term "self-energy diagram" will be clarified shortly.

2.4. Equation of motion for Green's functions

In this section, I define the equation of motion for the Green's function and the self-energy, following [15, p.23,24] closely[3]. I define the one-particle Green's function to be

$$G(\mathbf{r},t;\mathbf{r}',t') = -i\langle\Omega|\widehat{T}_c[c(\mathbf{r},t)c^\dagger(\mathbf{r}',t')]|\Omega\rangle \tag{40}$$

where c and $c^\dagger$ denote annihilation or creation operators at a spacetime point and Ω denotes the ground state. The generalization of the Green's function to N particles is then

$$G^N(\mathbf{r}_1,t_1;...;\mathbf{r}_N,t_N|\mathbf{r}'_1,t'_1;...;\mathbf{r}'_N,t'_N) = \\ (-i)^N\langle\Omega|\widehat{T}_c[c(\mathbf{r}_1,t_1)...c(\mathbf{r}_N,t_N)c^\dagger(\mathbf{r}'_1,t'_1)...c^\dagger(\mathbf{r}'_N,t'_N)]|\Omega\rangle \tag{41}$$

. The Bogoliubov-Born-Green-Kirkwood-Yvon (BBGKY) hierarchy now determines the function G^N, if G^{N+1} is known. This "equation of motion" for the single-particle Green's function is

$$\left[i\frac{\partial}{\partial t_1} - h_0(\mathbf{r}_1,t_1)\right]G(\mathbf{r}_1,t_1;\mathbf{r}_2,t_2) + i\int d\mathbf{r}_3dt_3v(\mathbf{r}_1;\mathbf{r}_3)\delta(t_1-t_3)\times \\ \times G^2(\mathbf{r}_1,t_1;\mathbf{r}_3,t_3^+|\mathbf{r}_2,t_2;\mathbf{r}_3,t_3^{++}) = \delta(\mathbf{r}_1-\mathbf{r}_2)\delta(t_1-t_2). \tag{42}$$

Here, $t^+ = t + i\eta$, and h_0 is the Hamiltonian for the single electron, which is here simply the kinetic term. Equation (42) can be obtained from the anticommutation relations of the involved operators. However, Eq.(42) is not very helpful for actual calculations, but it can be rewritten in a profitable way, introducing the self-energy.

The self-energy Σ is formally defined by

$$\int d\mathbf{r}_3dt_3\left[v_H(\mathbf{r}_3)\delta(t_3)\delta(\mathbf{r}_1-\mathbf{r}_3)\delta(t_1-t_3) + \Sigma(\mathbf{r}_1,t_1;\mathbf{r}_3,t_3)\right]G(\mathbf{r}_3,t_3;\mathbf{r}_2,t_2) = \\ -i\int d\mathbf{r}_3dt_3v(\mathbf{r}_1;\mathbf{r}_3)\delta(t_1-t_3)G^2(\mathbf{r}_1,t_1;\mathbf{r}_3,t_3^+|\mathbf{r}_2,t_2;\mathbf{r}_3,t_3^{++}) \tag{43}$$

where v_H is the Hartree potential, which vanishes in the model system due to the absence of Coulomb interactions. Then, Eq.(42) can be written as

$$\left[i\frac{\partial}{\partial t_1} - h_0(\mathbf{r}_1,t_1)\right]G(\mathbf{r}_1,t_1;\mathbf{r}_2,t_2) - \int d\mathbf{r}_3dt_3\Sigma(\mathbf{r}_1,t_1;\mathbf{r}_3,t_3)G(\mathbf{r}_3,t_3;\mathbf{r}_2,t_2) \\ = \delta(\mathbf{r}_1-\mathbf{r}_2)\delta(t_1-t_2). \tag{44}$$

The self-energy accounts for possible events that a particle encounters while propagating

[3]Even though this derivation includes only Coulomb interactions, the result is transferable to the model system with Eq.(3).

through the system - such as electron-hole-pair formation. These virtual processes affect the propagation of the particle and so the Green's function.

For the model system, that is invariant under spacetime translations, Eq.(44) can be simplified, by Fourier transformation [49, p.465]. Most importantly, the Fourier transform of the interacting one-particle Green's function is

$$G(\mathbf{k},\omega) = [\omega - \epsilon(\mathbf{k}) + \Sigma_{\mathbf{k}}(\omega)]^{-1}, \tag{45}$$

where $\Sigma_{\mathbf{k}}(\omega)$ is the Fourier transformed self-energy.

2.5. Scope of the methodology

In this section, I want to discuss the scope of the methodology, work out the interpretation of Eq.(45) for elementary excitations, explain why the one-particle description of the system is useful and what one can say about the excitations of the interacting system, if the excitations of the non-interacting counterpart are known. The discussion follows Ref. [63, p.6 ff.].

The methodology I describe is applicable to the "normal" Fermi liquid, that is the system that evolves smoothly from the non-interacting Fermi gas when the interaction is turned on adiabatically, similar to Eq.(31). So, I have to assume that the system evolves smoothly into the interacting state for an infinitely slow switching procedure. If this assumption is true, there is a one-to-one correspondence between the states of the non-interacting and the interacting system and perturbation theory is applicable.

Now, the excitations of the interacting system can be put in relation to their non-interacting counterparts in a similar way. Imagine a particle is plugged into the non-interacting system and the interaction is switched on adiabatically. If the particle evolves smoothly into an elementary excitation of the interacting system, there is a one-to-one correspondence between the excitations of the two system. However, for this procedure to be successful, the excitation in the interacting system has to be long-lived enough to not decay during the switching. This means, only long-lived excitations remain in one-to-one correspondence. The presence of the (long-lived) excitation in the interacting system deforms the surrounding of the former particle. This deformation is said to be the self-energy cloud, that dresses the particle. The dressed particle is considered to be an independent entity, the quasiparticle.

As the interaction is encoded in this particle-like entity, it is plausible why a one-particle description of the system is useful. However, many-body effects are still present, and the one-particle theory is in this sense incomplete. One can rewrite and interpret Eq.(45) with the bare one-particle Green's function Eq.(38), to obtain Dyson's equation

$$G(\mathbf{k},\omega) = G_0(\mathbf{k},\omega) + G_0(\mathbf{k},\omega)\Sigma_{\mathbf{k}}(\omega)G(\mathbf{k},\omega), \tag{46}$$

that helps to interpret the quasiparticle interacts with it's environment, yielding a self-energy Σ, see Fig. 4. The Dyson equation, however, describes the whole system and not only elementary excitations.

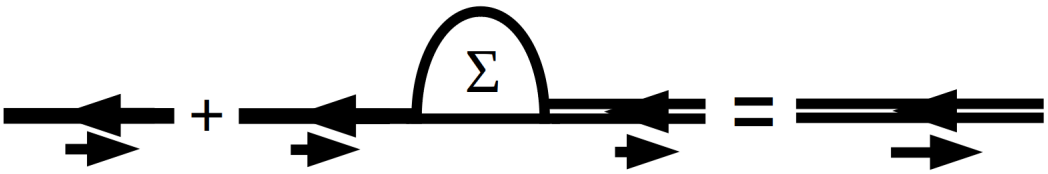

Figure 4: The Dyson equation for electron Green's functions in diagrammatic language. The self-energy operator dresses the Green's functions with interactions.

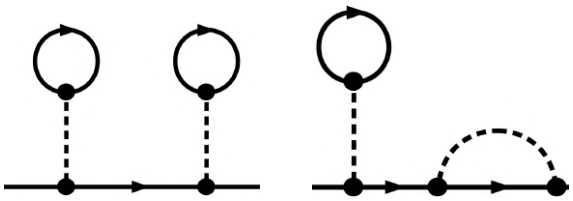

Figure 5: Diagrams that do not contribute to the self-energy, because they can be disconnected by removing a single line.

In general, elementary excitations of the system are well defined if they have a long lifetime. This holds also for collective modes, that are elementary excitations where the system undergoes a coherent motion. The collective mode to be discussed in this text is the plasmon.

2.6. Calculation of the self-energy

As I defined the scope of the theory, it remains to clarify, which diagrams contribute to the self-energy. The contributing diagrams are called "irreducible" [61, p.216]: A connected diagram is called one particle irreducible, if it cannot be disconnected by removing a single line from the diagram.

Thus the diagrams in Fig. 5 do not contribute to Σ, while the diagrams in Fig. 6 do. In the following I proceed to discuss some of the implications of these considerations for the dielectric function.

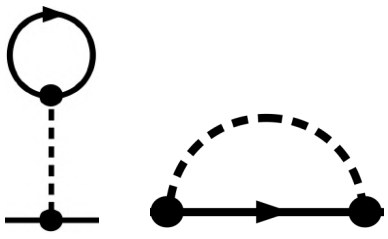

Figure 6: One-particle irreducible diagrams that do contribute to the self-energy.

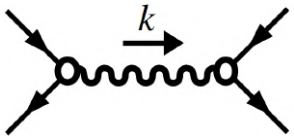

Figure 7: Coulomb vertex of the Coulomb interacting homogeneous electron gas. The value of the vertex is $v(\mathbf{k}) = \frac{4\pi}{\mathbf{k}^2}$.

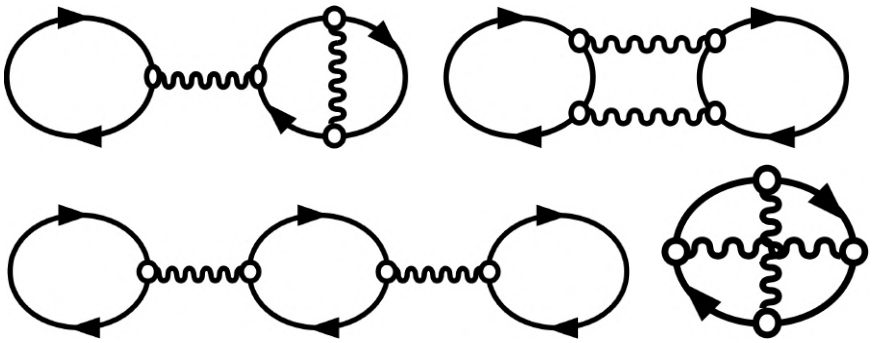

Figure 8: Diagrams that contribute to the free energy of the system at the second order in the interaction, so they all have two interaction lines. The diagrams to the left contain interaction lines that cannot transport momentum, and vanish therefore. The right two diagrams are discussed in the text.

2.7. The dielectric function and the random-phase approximation

In this section, I want to put attention to the computation of the dielectric function with the methods developed in the last sections. Therefore I introduce the random-phase approximation (RPA) to the density-density response function, following the line of Ref. [4, p.211 ff.][4]. Reference [4] introduces the free energy of the system F, which is the sum of all connected closed diagrams. The dominant contributions to this free energy come from a certain class of diagrams which, considered alone, constitute the RPA of the free energy. This free energy in the RPA can be linked to an effective Coulomb interaction and the dielectric function. The diagram rules for the Coulomb-interacting electron gas are given by the vertex with the bare Coulomb potential $v(\mathbf{k})$ Fig. 7 and by the bare electron Green's function, see also Secs. 2.1.2 and 2.3.

The idea behind the RPA is best explained by writing the second-order contributions to the free energy. At this order of the interaction, one can draw four diagrams, see Fig. 8, of which two (the left ones) are zero by charge neutrality (which causes $v(0) = 0$).

[4]Even though this derivation is made for the Coulomb-interacting electron gas it provides the basis for the calculation in the model system, provided by Eq.(3).

The right two can be written in terms of the Feynman rules[5]

$$F_1 = -4 \sum_{\mathbf{p}_1,\mathbf{p}_2,\mathbf{q}} \int_{\mathbb{R}\times\mathbb{R}\times\mathbb{R}} \frac{d\omega_1 d\omega_2 d\nu}{(2\pi)^3} G(\mathbf{p}_1,\omega_1) G(\mathbf{p}_1+\mathbf{q},\omega_1+\nu) \times \\ \times G(\mathbf{p}_2,\omega_2) G(\mathbf{p}_2+\mathbf{q},\omega_2+\nu) v(\mathbf{q})^2 \tag{47}$$

$$F_2 = 2 \sum_{\mathbf{p},\mathbf{q}_1,\mathbf{q}_2} \int_{\mathbb{R}\times\mathbb{R}\times\mathbb{R}} \frac{d\omega d\nu_1 d\nu_2}{(2\pi)^3} G(\mathbf{p},\omega) G(\mathbf{p}+\mathbf{q}_1,\omega+\nu_1) G(\mathbf{p}+\mathbf{q}_2,\omega+\nu_2) v(\mathbf{q}_1) v(\mathbf{q}_2). \tag{48}$$

In the homogeneous electron gas, at low temperatures, excitations near the Fermi surface are responsible for transport. Thus, the Green's functions acquire large values only if their momenta are near the Fermi momentum $|\mathbf{p}| \approx k_F$. In the first case, if the momentum $|\mathbf{q}|$ is small, all Green's function can have momenta near to the Fermi surface - so that two unbound summations over momentum shells near the Fermi-surface can take place with all Green's functions having large values. In the second case on the other hand, one needs to fine tune both photon momenta $\mathbf{q}_i$ and then just one unbound sum over a momentum shell near the Fermi-surface remains, so that the term F_1 dominates F_2. This can be generalized to multiple ring diagrams of the form in Fig. 9, that are the dominant contributions to the free energy F and constitute the RPA. As the free energy is directly related to the partition sum of the system [36, p.71], the dominant contributions to the free energy are important also for the effective Coulomb interaction in the system. In the RPA the effective Coulomb interaction is

$$W(\mathbf{k},\omega) = \frac{v(\mathbf{k})}{1-\chi_0(\mathbf{k},\omega)v(\mathbf{k})} = \frac{v(\mathbf{k})}{\varepsilon(\mathbf{k},\omega)}, \tag{49}$$

which is diagrammatically represented by Fig. 10. The dielectric function in the RPA[6] is then defined as

$$\varepsilon(\mathbf{k},\omega) = 1 - v(\mathbf{k})\chi_0(\mathbf{k},\omega), \tag{50}$$

where χ_0 is the single polarizability "bubble"

$$\chi_0(\mathbf{k},\omega) = -2i \int \frac{d\mathbf{q} d\omega'}{(2\pi)^4} G_0(\mathbf{q}+\frac{\mathbf{k}}{2},\omega'+\frac{\omega}{2}) G_0(\mathbf{q}-\frac{\mathbf{k}}{2},\omega'-\frac{\omega}{2}). \tag{51}$$

Eq.(51) has been evaluated by Lindhard for zero-temperature and an electron dispersion $\epsilon(\mathbf{q}) = \frac{\mathbf{q}^2}{2m}$ [26, p.161],

[5] I have choosen to write here sums for the momenta as in Ref. [4]. For the homogeneous electron gas, the sums can be transformed into integrals.

[6] Note that the contribution of $g^2 D(\omega)$ to the effective interaction is neglected throughout this work, which is feasible for large frequencies and small momenta.

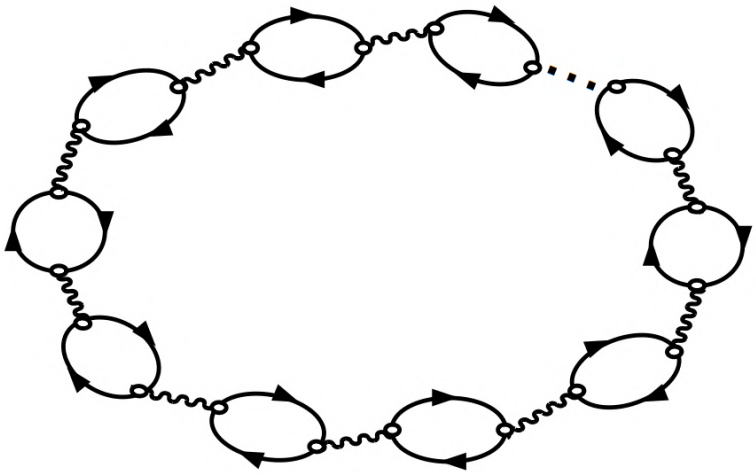

Figure 9: Ring diagram that contributes to the free energy. The inclusion of only those ring diagrams to calculate the free energy is known as the random-phase approximation. As virtual electron-hole pairs are generated in the diagram, the single bubble is called polarizability χ_0. The RPA diagrams therefore reflect the contribution to the free energy through independent virtual electron-hole pairs.

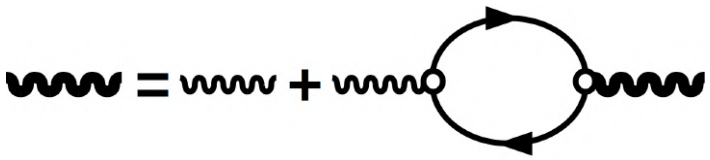

Figure 10: The Dyson equation for the effective interaction in the RPA. The thick wiggly line corresponds to the effective interaction W, the thinner wiggly line to the bare interaction v, and the bubble corresponds for the homogeneous electron gas at zero temperature to the Lindhard polarizability χ_0^L Eq. (52).

Theorem 4. *In three space dimensions the polarizability of the free electron gas at zero temperature is*

$$\chi_0^L(k,\omega) = N\frac{k_F}{k}\left[\Phi(\frac{\omega+i\eta}{kv_F}-\frac{k}{2k_F})-\Phi(\frac{\omega+i\eta}{kv_F}+\frac{k}{2k_F})\right] \tag{52}$$

where $\Phi(z) = \frac{z}{2}+\frac{1-z^2}{4}\log(\frac{z+1}{z-1})$, $N = \frac{mk_F}{\pi^2}$ *and* $v_F = \frac{k_F}{m}$. m *is the effective mass of the quasi-electrons in the system.*

The effective Coulomb interaction in the material can become very large, if $\Re(\varepsilon) \to 0$. When this condition is obeyed, the material exhibits collective oscillations of the charge density, the plasmons [63, p.211]. One can Taylor expand the result for χ_0 for $\frac{v_F\mathbf{k}}{\omega} \ll 1$,

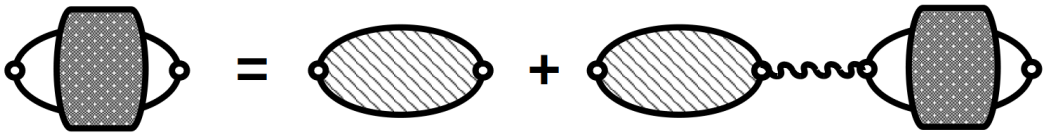

Figure 11: Diagrammatic representation of the Dyson equation for the density-density response function, which is the object to the left. The lighter shaded bubble is the irreducible polarizability and the wiggly line represents the bare Coulomb interaction v.

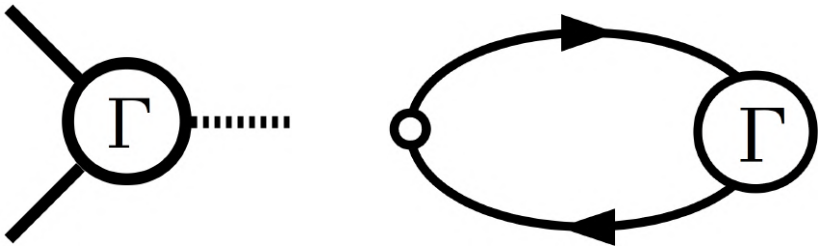

Figure 12: The diagrammatic representation of the vertex function (to the left) and the vertex correction to the polarizability (to the right).

where v_F is the Fermi velocity to obtain for small $\mathbf{k}$ [4, p.221]

$$W(\mathbf{k},\omega) = \frac{4\pi e^2}{\mathbf{k}^2}\frac{1}{1-\frac{\omega_{\rm pl}^2}{\omega^2}} \tag{53}$$

where $\omega_{\rm pl} = (4\pi n e^2/m)^{1/2}$ is the plasma frequency of the material. If the perturbing potential has just this frequency, it causes a resonance in the system, denoted as "plasmon". Plasmons have a dispersion relation and can be observed by electron energy loss spectroscopy.

I now introduce corrections to the dielectric function in the RPA approximation by the use of the Dyson equation of the density-density response function [53, p.388]:

$$\chi(\mathbf{k},\omega) = \chi_0(\mathbf{k},\omega) + \chi_0(\mathbf{k},\omega)v(\mathbf{k})\chi(\mathbf{k},\omega), \tag{54}$$

where χ_0 is the irreducible polarizability. Eq.(54) can be put diagrammatically as in Fig. 11.

In the following I go beyond the RPA and explore the influence of the electron-phonon interaction on the dielectric properties of simple metals. In particular, I include the electron-phonon interaction by dressing the Green's function of the electrons and by including vertex corrections. The Green's function corrections can be calculated using the dressed Green's functions from the Dyson equation (46). The irreducible vertex-contribution Γ is a higher Green's function that is defined as the diagram Fig. 12 to the left, and contributes to the polarizability (to the right).

Now, the formal calculation techniques for the diagrams are complete. Before I start

real calculations for the homogeneous electron gas, I will briefly address the full set of equations of motion for the system, the Hedin-Baym equations.

2.8. Hedin-Baym equations

The Hedin-Baym equations are a set of exact integro-differential equations for the coupled electron-phonon system in the harmonic approximation. Reference [27] gathered the equations of motion of the system in real space and time. To obtain their Fourier transforms I use [49, p.465].

$$\varepsilon(1,2) = \delta(1,2) - \int d3v(1,3)\chi(3,2) \tag{55}$$

$$\chi(1,2) = -i \int d(3,4)G(1,3)G(4,1)\Gamma(3,4,2) \tag{56}$$

$$G(1,2) = G_0(1,2) + \int d(3,4)G_0(1,3)\Sigma(3,4)G(4,2) \tag{57}$$

$$\Sigma(1,2) = i \int d(3,4)G(1,3)\Gamma(3,4,2)D(4,1) \tag{58}$$

$$\Gamma(1,2,3) = \delta(1,2)\delta(1,3) + \int d(4,5,6,7)\frac{\delta\Sigma(1,2)}{\delta G(4,5)}G(4,6)G(7,5)\Gamma(6,7,3). \tag{59}$$

Here, Γ is the vertex function, $1, 2, ...$ stand for spacetime points and $\frac{\delta}{\delta G}$ denotes the functional differential with respect to the Green's function G [71, p.113]. The Hedin-Baym's equations allow for a different viewpoint on the interacting electron-phonon system and are especially valuable for calculations for real materials [18, 27]. These equations will later be used to independently derive the vertex correction and self-energy contribution to the theory.

2.9. Calculational procedure

Finally, I aim to start real calculations for the homogeneous electron gas. Thereby I am mostly concerned with integrals of the following type

$$\chi_0(\mathbf{k},\omega) = -2i \int \frac{d\mathbf{q}d\omega'}{(2\pi)^4} G(\mathbf{q}+\frac{\mathbf{k}}{2},\omega'+\frac{\omega}{2})G(\mathbf{q}-\frac{\mathbf{k}}{2},\omega'-\frac{\omega}{2}). \tag{60}$$

To work out this integral, usually the integration over ω' is carried out first followed by a, possibly numerical, integration over $\mathbf{q}$ [18, 26]. Now, the integration over ω' is analytically impossible, due to the self-energy term Σ, but the integration over $\mathbf{q}$ remains tractable, as the self-energy that I consider is not depending on the wavevector $\mathbf{q}$. Therefore I first integrate $\mathbf{q}$ and then ω'. This method, however, suffers a serious problem, that already piles up for the Lindhard function:

$$\chi_0(\mathbf{k},\omega) = -2i \int_{\mathbb{R}} \frac{d\omega'}{2\pi} \int_{\mathbb{R}^3} \frac{d\mathbf{q}}{(2\pi)^3} G(\mathbf{q}+\frac{\mathbf{k}}{2},\omega'+\frac{\omega}{2})G(\mathbf{q}-\frac{\mathbf{k}}{2},\omega'-\frac{\omega}{2}). \tag{61}$$

I define

$$K_\chi(\mathbf{k},\omega,\omega') = \int_{\mathbb{R}^3} \frac{d\mathbf{q}}{(2\pi)^3} G(\mathbf{q}+\frac{\mathbf{k}}{2},\omega'+\frac{\omega}{2})G(\mathbf{q}-\frac{\mathbf{k}}{2},\omega'-\frac{\omega}{2}), \tag{62}$$

so that

$$\chi_0(\mathbf{k},\omega) = -2i\int_{\mathbb{R}} \frac{d\omega'}{2\pi} K_\chi(\mathbf{k},\omega,\omega'). \tag{63}$$

It is now proven in Sec. B.2.2 that for large ω'

$$K_\chi(\mathbf{k},\omega,\omega') \propto \frac{1}{\sqrt{\omega'}}. \tag{64}$$

So, by definition from algebra, one sees that

$$\begin{aligned} |\chi_0(\mathbf{k},\omega)| &\propto |\int_{\mathbb{R}} \frac{d\omega'}{2\pi} K_\chi(\mathbf{k},\omega,\omega')| \\ &\propto \lim_{\Lambda\to\infty} |\int_{-\Lambda}^{\Lambda} \frac{d\omega'}{\sqrt{\omega'}}| \\ &\propto \lim_{\Lambda\to\infty} \Lambda^{1/2} > c, \end{aligned} \tag{65}$$

where c can be any real number. Then, the left side is said to diverge, by definition. There is no cancellation between any terms in the proportionality. This is a serious problem, as the integrals that I encounter are not well defined and can, thus, not be calculated in this way[7]. However, there exists a method from quantum field theory [61, p.265 ff.], which can be proven to be applicable here - renormalization[8]. I did not find any literature reporting about this problem in the homogeneous electron gas. To make sure, that the procedure, which is explained below, is correct, I have tested especially whether the Lindhard function Eq.(52) can be reproduced by this method. The result is affirmative, see Sec. B.2.4 and Fig. 29. Therefore I consider the method of renormalization to be applicable.

The renormalization procedure that I use can be found in [61, p.377]. Suppose a quantity Q is ill-defined, as in Eq.(65). In the first step, a well defined quantity is introduced

$$Q(\Lambda) = \int_{-\Lambda}^{\Lambda} dx f(x), \tag{66}$$

which should be related to the object Q for large Λ. To take the limit $\Lambda\to\infty$, I search

[7] It remains unclear whether this in my method appearing divergence is reasoned in the Fourier transform of the theory [49, p.458 ff.] with respect to the Hedin-Baym equations. Maybe the issue can be resolved by summing a convergent partial series [53, p.382]. As I am unable to proof and use any of these options, I choose to renormalize the integrals.

[8] The proof of renormalizability can be found in Sec. A.

a function h such that

$$Q - C = \lim_{\Lambda \to \infty} \int_{-\Lambda}^{\Lambda} dx f(x) - h(x) \tag{67}$$

is well defined. In this text, h never depends on any momenta or energies, that Q may depend on. Then, C is considered a constant. As C is unknown, I use physical reasoning to find C. Therefore I fix "renormalization conditions" [61, p.325] which meet the expectations of solid state theory: The polarizability of the theory vanishes for large frequencies

$$\lim_{\omega \to \infty} \chi_0(\mathbf{k}, \omega) = 0 \tag{68}$$

and the self-energy term vanishes at the Fermi-surface [43]

$$\Sigma(\epsilon_F) = 0. \tag{69}$$

The procedure of renormalization leads to unique results if the renormalization conditions are fixed, and the theory allows physical predictions from perturbation theory if it is renormalizable [61, p.265 ff.], see Sec. A.

Unfortunately, the above described procedure is numerically not stable, as the integrands are subtracted from each other, that are similar of magnitude. To reduce the calculation error, I truncate the integrals as in Eq.(63), similar to renormalizing them. To correct the error, the integrand is expanded in orders $\frac{1}{\omega'}$, and then only the part of the series is integrated that leads to convergent contributions. This procedure is appropriate, if renormalization is applicable. I can then calculate the polarizability from Eq.(63) shifted by a constant of the order 10^{-8}, see Sec. B.2.2. Technical details can be found in Sec. C, and the mathematical expansions are in Secs. B.1.2,B.2.2 and B.3.3.

2.10. Checks and tests

I finally want to give an overview of the validation procedure. For the calculated integrals, I carried out tests against their numerical implementation. Be the function F represented by

$$F(\mathbf{x}) = \int_{\Omega} f(\mathbf{x}, \mathbf{y}) d\mathbf{y} \tag{70}$$

calculated over some region Ω, then the by hand result of F was tested against the numerical integral Eq. (70) for at least a thousand random inputs $\mathbf{x}$. If two by hand calculated integrals should converge against each other for some vanishing parameter, I did convergence tests. This has especially been done for the polarizability with $g \to 0$ and the Lindhard function and for the vertex corrections to the polarizability with and without dressed Green's functions. When integrals needed to be expanded in ω', I checked their asymptotic expansions to converge against the function for large values

ω' with the correct scaling. This has been done up to order $\frac{1}{(\omega')^5}$ for every integral. I additionally tested the calculated functions for expected symmetries. Moreover, the implementation is checked by benchmarking, and parallelization tests. All these tests are automated and have been performed on a weekly basis to minimize the chances that mistakes in the implementation remain undiscovered. The tests are explained in detail and denoted per calculated integral in Secs.B.1.4,B.2.4,B.3.6, B.4 and C.

3. Results and discussion

In this chapter I present the results of my work, which are

- an analytic expression for the electron-phonon self-energy in the homogeneous electron gas to order g^2,
- the application of this self-energy in the calculation of the polarizability of the homogeneous electron gas,
- the calculation of the vertex function of the homogeneous electron gas to order g^2,
- and the calculation of the vertex correction to the polarizability of the homogeneous electron gas.

This programme is visualized in Fig. 13. Additionally I have tried to obtain the impact of these corrections on the plasmon lifetimes.

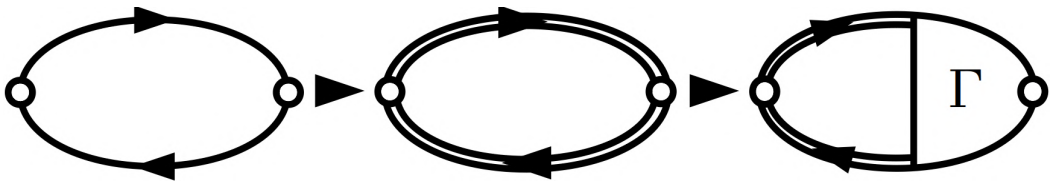

Figure 13: The plan of my master project in terms of approximations to the polarizability. I start with the well-known Lindhard function Eq.(52) (left) and then dress the electron Green's function with an electron-phonon self-energy term (middle). Afterwards, a vertex correction is added to the calculated diagrams (right). The results are accurate to second order in the electron-phonon interaction.

3.1. Self-energy and dressed Green's function

To obtain the self-energy to second order in the interaction, it is necessary to draw all diagrams with two interaction vertices, see Fig. 14. The left diagram simply contributes a constant to the self-energy, as the phonon Green's function carries no momentum. The right diagram contributes a dynamical function, and is known as Fan-Migdal term [27, p.26],

$$\Sigma_{\mathrm{FM}}(\mathbf{k},\omega) = ig^2 \int \frac{d\mathbf{q}\; d\omega_1}{(2\pi)^4} G(\mathbf{k}+\mathbf{q},\omega+\omega_1) D(\mathbf{q},\omega_1). \tag{71}$$

This term can be found with the diagram rules or the Hedin-Baym equations. If one considers a non-dispersive model for the phonon (Einstein model), the phonon Green's

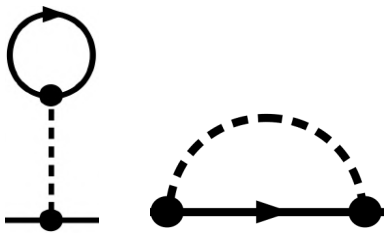

Figure 14: Diagrams that contribute to the electron-phonon self-energy at second order. The small circles denote interaction vertices with value g.

function does not depend on momentum, so that one finds

$$\Sigma_{\mathrm{FM}}(\omega) = ig^2 \int \frac{d\mathbf{q}\ d\omega_1}{(2\pi)^4} G(\mathbf{q}, \omega + \omega_1) D(\omega_1). \tag{72}$$

The result for the Fan-Migdal self-energy, as well as the calculation and validation of the result can be found in Sec. B.1. The main task is to consider the multiple infinitesimals of the integrand in a correct manner. Straightforward Feynman parametrization [61, p.195] is no option, because the infinitesimals may have different signs, and the use of the residue theorem[9] is not possible, because the resulting functions may have denominators with subtractions between infinitesimals, which is ambiguous. To circumvent this issue, I use Dirac's identity [70]

$$\frac{1}{x - a^{\pm}} = \frac{1}{x - a^{\mp}} \pm 2\pi i \delta(x - a), \tag{73}$$

where $a^{\pm} = a \pm i0$. With this identity, I shift the poles of the integrand for the ω_1 integration subsequently out of the contour, as illustrated in Fig. 15. When the contour encloses no poles anymore, the resulting integral is zero, by holomorphy. If the arc of the contour vanishes, the integral over ω_1 vanishes.

The resulting function can be seen in Fig. 16. The calculated self-energy fits the theoretic expectations, that are:

- The self-energy close to the Fermi surface has a vanishing imaginary part - which assures that excitations near the Fermi surface have a long lifetime.
- The imaginary part switches sign at the Fermi energy. This is important to make sure that the non-interacting Green's function and the integrals over it, evolve smoothly into their interacting counterparts when the interaction is switched on [4, p.380].
- The self-energy does not grow faster than ω for large frequencies [2, p.164 ff.].

This self-energy model exhibits multiple effects that are expected: The excitation energies in the interacting system are shifted and finite lifetime effects come into

[9]For function theory purposes, I use the language of Ref. [49].

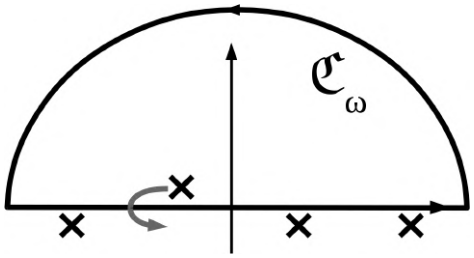

Figure 15: Complex ω plane, with a directed half-circle as integration contour. The y axis denotes the imaginary part, the x axis the real part of ω. The figure illustrates the use of Eq.(73) on an integrand with four poles, indicated by the crosses. The arrow denotes which pole is shifted. After this shift the contour integral is zero, because of holomorphy. If then the arc in the integration contour is zero, the integral over the real axis vanishes as well.

play [18]. In a numerical simulation, Ref. [27, p.31] found also dynamical features in the spectral function of this interacting system, such as satellites and phonon kinks. This self-energy might be a model for simple metals that exhibit similarities to the homogeneous electron gas, like aluminium [3, 60] (see also the discussion in Sec. 3.3). In this work, however, I want to focus on the impact that the dressing of the electron Green's function by the Fan-Migdal self-energy has on the polarizability χ_0. The dressed electron Green's function is obtained from Eq. (45). Then, I can write down the polarizability

$$\begin{aligned}
\chi_0(\mathbf{k},\omega) &= -2i \int \frac{d\mathbf{q}d\omega'}{(2\pi)^4} G(\mathbf{q}+\frac{\mathbf{k}}{2},\omega'+\frac{\omega}{2}) G(\mathbf{q}-\frac{\mathbf{k}}{2},\omega'-\frac{\omega}{2}) \\
&= -2i \int \frac{d\omega'}{(2\pi)} K_\chi(\mathbf{k},\omega,\omega'), \\
\text{with } K_\chi(\mathbf{k},\omega,\omega') &= \int \frac{d\mathbf{q}}{(2\pi)^3} G(\mathbf{q}+\frac{\mathbf{k}}{2},\omega'+\frac{\omega}{2}) G(\mathbf{q}-\frac{\mathbf{k}}{2},\omega'-\frac{\omega}{2})
\end{aligned} \tag{74}$$

where I have defined the kernel for the polarizability K_χ, which is derived in the Appendix B.2. It turns out that the result for K_χ depends on whether none, one or both Green's functions in the integral for K_χ have a finite imaginary self-energy contribution.

To obtain the result for K_χ it is not always possible to use Feynman parametrization. If the self-energy terms in both Green's functions have a finite imaginary part of opposite sign, Feynman parametrization is not applicable. Therefore I followed a different procedure for all three cases. The momentum $\mathbf{q}$ is shifted so that only one Green's function depends on the momentum $\mathbf{k}$ which is, for simplicity, aligned with

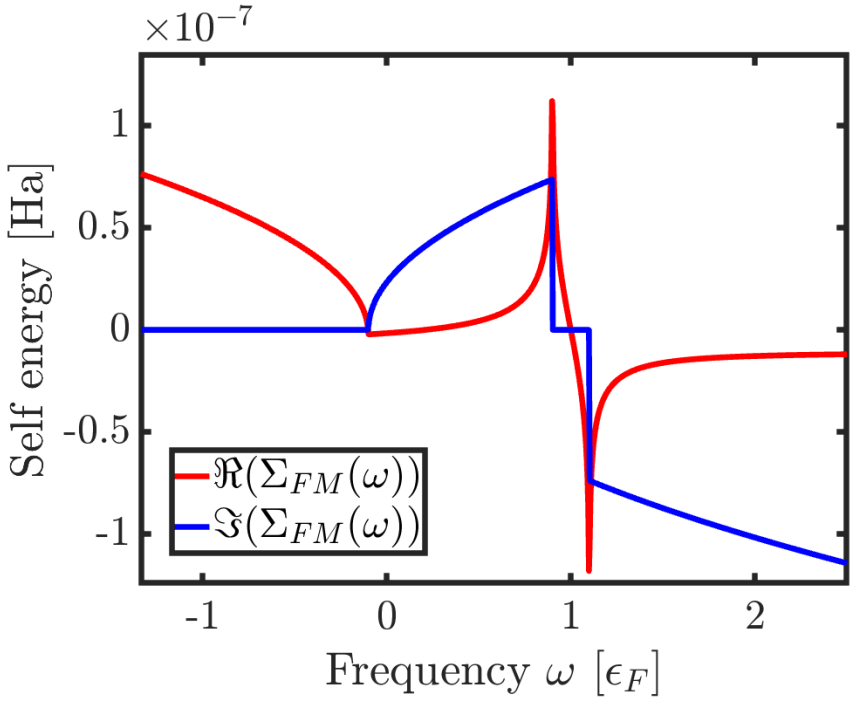

Figure 16: Fan-Migdal self-energy from Eq.(99) for the homogeneous electron gas, with $g = 100\text{meV}$, $\omega_{\text{ph}} = 200\text{meV}$, $m = 0.2$ and $\epsilon_F = 2\text{eV}$.

the z direction

$$K_\chi(\mathbf{k},\omega,\omega') = \int \frac{d\mathbf{q}}{(2\pi)^3} G(\mathbf{q},\omega'+\frac{\omega}{2}) G(\mathbf{q}-\mathbf{k},\omega'-\frac{\omega}{2}) \\ = \int_0^\infty \frac{dq}{(2\pi)^2} q^2 G(\mathbf{q},\omega'+\frac{\omega}{2}) \int_{-1}^1 dx G(\mathbf{q}-\mathbf{k},\omega'-\frac{\omega}{2}) \tag{75}$$

where $x = \cos(\theta)$ and θ is the polar angle, and this works because G only depends on the magnitude $|\mathbf{q}-\mathbf{k}|$. The integration over x is a standard integral and leads to integrals of the type

$$I(a,b,c) = \int_0^\infty \frac{dq\ q}{q^2+a} \left\{\log[(q-b)(q-c)] - \log[(q+b)(q+c)]\right\}. \tag{76}$$

By decomposing the rational function in front in partial fractions, it is possible to transform the integral with partial integration into the form

$$J(a',b',y) = \int_0^y d\xi\ \frac{\log(\xi-a')}{\xi-b'} \tag{77}$$

which can then be rewritten in terms of logarithms and dilogarithms[10]. The final step of

[10]One has to keep track of the contour not to cross any branch cut of the integrand. This is always

carrying out the limit is possible due to the asymptotic expansion of the dilogarithm [72]

$$\mathrm{Li}_2(x) \overset{|x|\gg 1}{\approx} \frac{1}{2}\log(-x)^2 + C \tag{78}$$

with C being a constant. Even though K_χ is known now, this turns out to be not enough to get the dressed polarizability from

$$\chi_0(\mathbf{k},\omega) = -2i\int \frac{d\omega'}{(2\pi)} K_\chi(\mathbf{k},\omega,\omega'). \tag{79}$$

The reason is the behavior of $K_\chi(\mathbf{k},\omega,\omega')$, that for large ω'[11] can be proven, with the aid of Feynman parametrization[12], to be (see Sec. B.2.2)

$$\begin{aligned} K_\chi(\mathbf{k},\omega,\omega') &= \frac{-im^{3/2}}{2^{3/2}\pi\sqrt{|\omega'|}}\int_0^1 \frac{du}{\sqrt{1+\frac{f(u)\epsilon(\mathbf{k})}{|\omega'|}}} \\ &= \frac{-im^{3/2}}{2^{3/2}\pi\sqrt{|\omega'|}} + \mathscr{O}((\omega')^{-1}), \end{aligned} \tag{80}$$

with $f(u) = u^2 + uh_1(\omega,\mathbf{k}) + h_2(\omega,\Sigma_{\mathrm{FM}}(\omega,\omega'))$, where h_1 and h_2 are linear in their arguments. That means the integral in Eq.(79) needs to be renormalized, which is done with the aid of expanding the squareroot in Eq.(80) in $\frac{1}{\omega'} \approx 0$, see Sec. B.2.2. The renormalization procedure has, however, the drawback that two functions of almost identical value (K_χ and it's expansion) are subtracted from each other. This is not numerically stable, especially in the extrapolation procedure where $\chi_0(\mathbf{k},\omega) \overset{\omega\to\infty}{\to} c$. c is the constant to be subtracted from the result for χ_0 to meet the renormalization condition (Eq.(68)). To sufficiently reduce this error, that is estimated in Sec. B.2.2, I expanded K_χ with `Mathematica 11.1` up to order $(\omega')^{-6}$ and then approximated the integral for χ_0

$$\begin{aligned} \chi_0(\mathbf{k},\omega) \approx -2i\int_{-\Lambda}^{\Lambda} \frac{d\omega'}{(2\pi)} K_\chi(\mathbf{k},\omega,\omega') \\ - 2i\left(\int_\Lambda^\infty + \int_{-\infty}^{-\Lambda}\right)\frac{d\omega'}{(2\pi)} K_\chi^{(5)}(\mathbf{k},\omega,\omega') - K_\chi^{(0)}(\omega'), \end{aligned} \tag{81}$$

where $K_\chi^{(n)} = K_\chi + \mathscr{O}((\omega')^{-(n+\frac{3}{2})})$. $K_\chi^{(0)}$ is independent of $(\mathbf{k},\omega)$. This polarizability and the difference to the Lindhard function can be seen in Figs. 17 and 18.

The corrected polarizability is quantitatively only slightly changed due to the electron-phonon interaction. However, the imaginary part of the polarizability, which zero in some regions is without electron-phonon interaction, acquires a finite, though small,

possible, because one can set $\int \frac{dx}{x} = \log(cx)$, with $c \in \mathbb{C}\setminus\{0\}$.

[11] A similar expression, of not-opposite sign, can be proven for large $-\omega'$.

[12] Feynman parametrization is applicable here because the self-energy in both electron Green's functions is $\Sigma_{\mathrm{FM}}(\omega') + \mathscr{O}((\omega')^{-1/2})$.

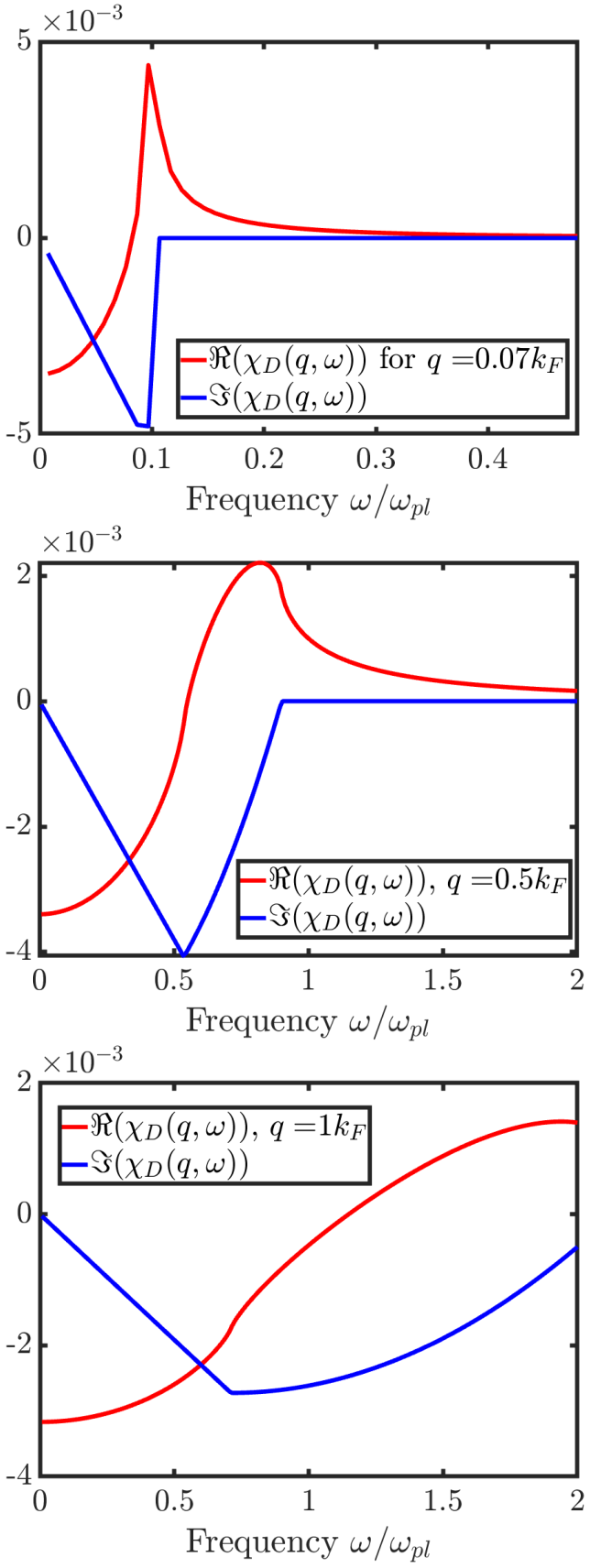

Figure 17: Polarizability with the electron Green's function corrected by the Fan-Migdal self-energy, for three different momenta, $q = 0.07k_F$, (above), $0.5k_F$ (middle) and k_F (below). The left graph has been truncated. These plots look identical to that of the Lindhard function, however, the imaginary part of the polarizability acquires a finite value everywhere. The parameters used for this plot are $g = 100$ meV, $m = 0.2$, $\omega_{\text{ph}} = 60$ meV, and $\epsilon_F = 2$ eV.

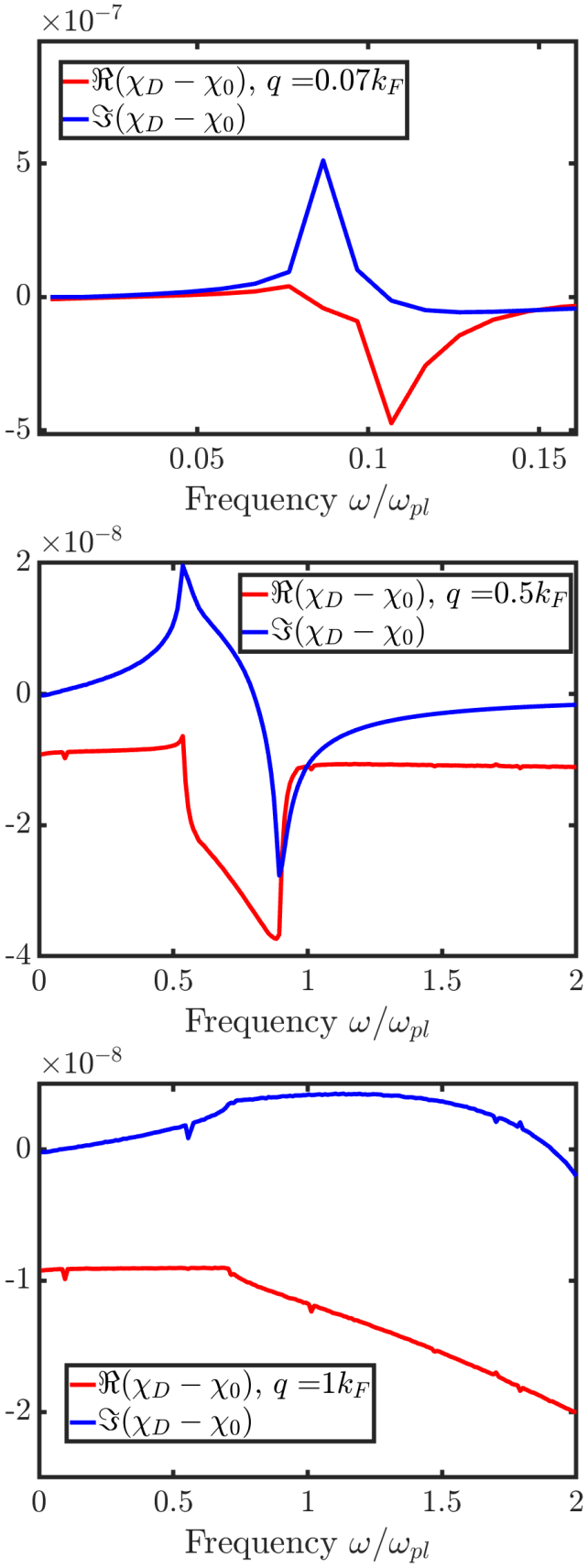

Figure 18: Difference between the Lindhard function and the polarizability with the electron Green's function corrected by the Fan-Migdal self-energy, for three different momenta, $q = 0.07k_F$, (above), $0.5k_F$ (middle) and k_F (below). The left graph has been truncated. The imaginary part of the polarizability acquires, as you can see, finite values everwhere. The change of the polarizability is in all three plots of the order of $g^2\chi_0^L$. The parameters used for this plot are $g = 100$ meV, $m = 0.2$, $\omega_{\text{ph}} = 60$ meV, and $\epsilon_F = 2$ eV.

magnitude. This is both expected, as the electron-phonon interaction should only slightly perturb the system. Though qualitatively, the elementary excitations of the system acquire an additional decay channel through electron-phonon interaction. As the imaginary part is finite everywhere, also the plasmons. This shows up in the loss function

$$\mathscr{L} = \Im(\frac{1}{\varepsilon(\omega, \mathbf{k})}) = \Im(\frac{1}{1 - v(\mathbf{k})\chi_0(\mathbf{k}, \omega)}), \tag{82}$$

by the peaks at $\Re(\varepsilon(\omega, \mathbf{k})) = 0$, where the plasmons acquire a finite lifetime. The discussion about plasmon lifetimes in this interacting theory is found in Sec. 3.3. Reference [18] found with an approximation to the ω integration the same qualitative results, i.e. that the polarizability in the interacting theory is only slightly changed, and that the plasmons of the system acquire a finite lifetime. As the polarizability is only slightly changed, it is plausible that the system can evolve adiabatically into this interacting state, so that this discussion is reasonable.

In real materials, I expect phonons to open new decay channels for elementary excitations of the system, such as plasmons. Additionally, their effect on the properties of the system should be small, except for particular cases, such as superconductors. The results of this section should therefore be a good model for metals that exhibit a homogeneous-electron-gas-like behavior and can be a first guess for the impact of electron-phonon interaction in more complex systems.

3.2. The vertex correction

Having derived an expression for the propagator correction to the polarizability, I proceed to introduce the vertex correction. I calculate the vertex function to order g^2 in the interaction, which represents the phonon-mediated electron-hole interaction to that order. I am then in a position to obtain the correction to the polarizability of this model theory to order g^2 in the interaction.

3.2.1. The vertex function

There is only one corresponding diagram, due to the Lehmann-Symanzik-Zimmermann-reduction formula [61, p.222-230], see Fig. 19. For completeness, I show here the derivation of the integral representation with the aid of the Hedin-Baym equations.

$$\begin{aligned} \Sigma(12) &= ig^2 \int d(34) G(13) \Gamma(324) D(41^+) \\ \Gamma(123) &= \delta(12)\delta(13) + \int d(4567) \frac{\delta\Sigma(12)}{\delta G(45)} G(46) G(75) \Gamma(673) \end{aligned} \tag{83}$$

where the $\frac{\delta\Sigma(12)}{\delta G(45)}$ denotes the functional derivative [71, p.113] of the self-energy with respect to the Green's function. To evaluate this, I simplify the self-energy by setting

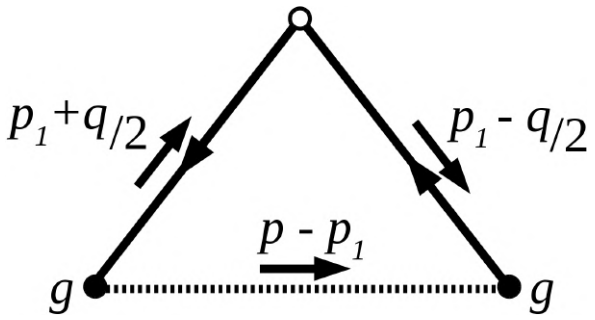

Figure 19: Vertex function to second order in the electron-phonon interaction. The dashed line represents a virtual phonon, the solid lines represent virtual fermions. The external momenta are p and q.

$\Gamma(324) = \delta(23)\delta(34)$. Then, $\Sigma(12) = g^2 G(12) D(21^+)$ and with [49, p.465]

$$\int_{\mathbb{R}} f_1(x) f_2(x) \exp(ikx) dx = \frac{1}{2\pi} \int_{\mathbb{R}} F_1(l) F_2(k-l) dl, \tag{84}$$

where capitalized letters denote the Fourier transforms of the functions. For the Fourier transform of this self-energy, see the last section. With shift invariance I obtain

$$\frac{\delta\Sigma\left[G(1-2)\right]}{\delta G(4-5)} = ig^2 \delta((1-2)-(4-5)) D(12). \tag{85}$$

Plugging this into the vertex, I define the quantity Γ_1 as the first order correction to the vertex function

$$\begin{aligned}
\Gamma_1(123) &= ig^2 \int d(4567)\delta((1-2)-(4-5)) D(12) G(46) G(75) \delta(67)\delta(63) \\
&= ig^2 \int d(456)\delta((1-2)-(4-5)) D(12) G(46) G(65) \delta(63) \\
&= ig^2 \int d(45)\delta((1-2)-(4-5)) D(12) G(43) G(35) \\
&= ig^2 \int d4 D(12) G(43) G((1-2)-(3-4)),
\end{aligned} \tag{86}$$

and with Eq. (84) and some manipulations one obtains the result for the vertex:

$$\frac{1}{g^2}\Gamma_1 = i \int \frac{d\mathbf{k_1} d\omega_1}{(2\pi)^4} D(\omega' - \omega_1) G_0(\mathbf{k_1} + \frac{\mathbf{k}}{2}, \omega_1 + \frac{\omega}{2}) G_0(\mathbf{k_1} - \frac{\mathbf{k}}{2}, \omega_1 - \frac{\omega}{2}). \tag{87}$$

This result could have been obtained as well with the diagram rules of Sec. 2.3. The result of this integral can be found in Sec. B.3. As the phonon Green's function is independent of momentum, the vertex function is independent of the external fermion momentum. I then obtain an analytic expression for the vertex function in terms of logarithms and dilogarithms, but my expression is complicated and bears insight only after close inspection.

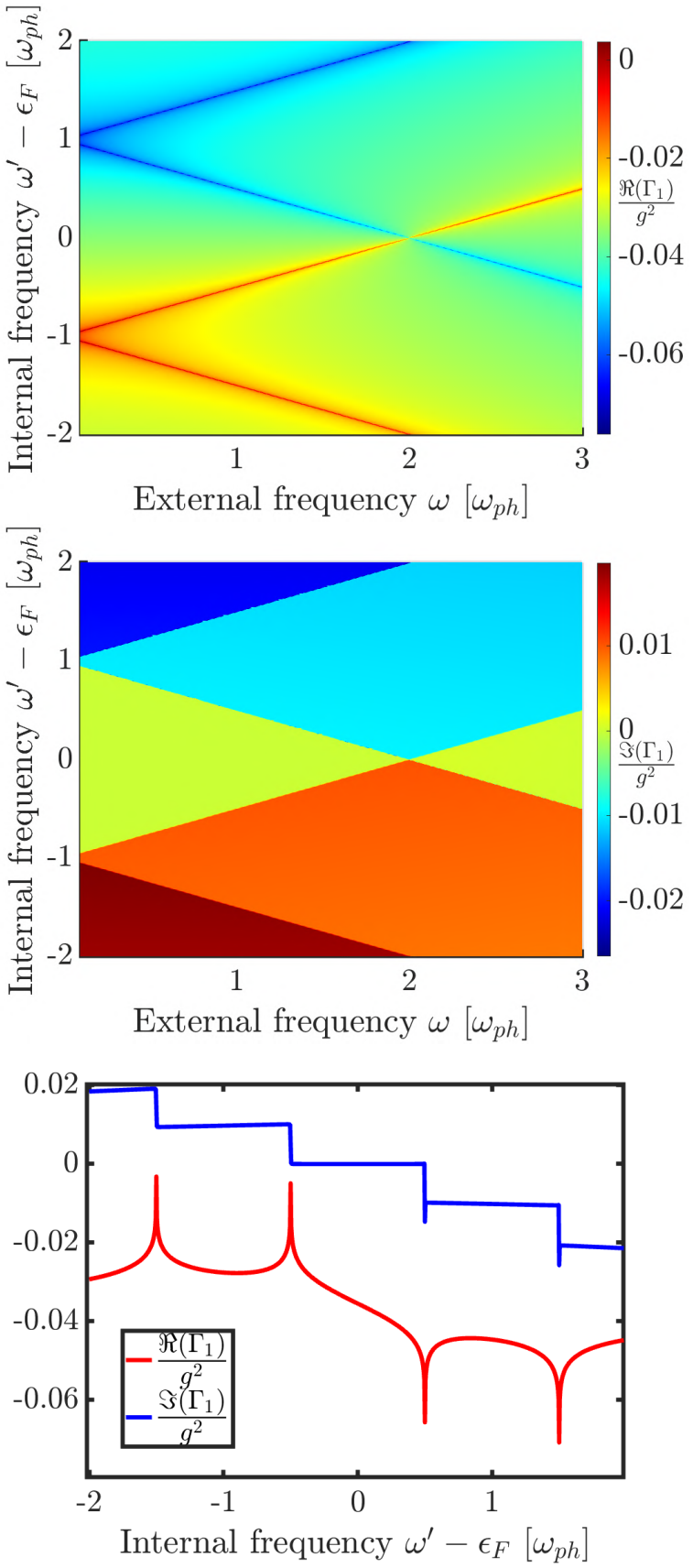

Figure 20: Vertex function to order g^2 is shown in surface plots of the real (above) and imaginary part (middle), and by a cut through this surface at $\omega = \omega_{\text{ph}}$ (below). One can see that the function exhibits branch cut singularities. These singularities correspond to multiparticle excitations [61]. When the external frequency is small, and the internal frequency is close to the Fermi surface, the imaginary part of the vertex function vanishes. The broadening of the logarithmic divergences is artificial, with the infinitesimal set to $\eta = 1\mu$Ha. $k = 0.5k_F$, $m = 0.2$, $\epsilon_F = 2$ eV and $\omega_{\text{ph}} = 100$ meV.

The vertex function is shown in Fig. 20 for small external frequencies and internal frequencies near the Fermi surface. It can be seen that its imaginary part vanishes for small external frequencies ω and internal frequencies ω' near the Fermi energy. This behavior of the function is expected: If a boson in the homogeneous electron gas, with low energy, excites an electron-hole pair, then the energy of this excitation is low as well[13]. This means that both the electron and the hole are in a state close to the Fermi-surface so that the lifetime of this excitation should be large. If the phonon has a larger energy than this excitation, there is no interaction to let this excitation decay, and the lifetime becomes infinite, i.e. the imaginary part of the corresponding correlation function vanishes.

The vertex function exhibits logarithmic divergences whenever $\omega' \pm \frac{\omega}{2} = \epsilon_F \pm \omega_{\text{ph}}$. Also this behavior is expected [61, p.216 par. 2 ff.]: The energies of the particles are such of a multiparticle state, so the correlation function is singular. As this excitation also exists with an infinitesimally changed external energy, the singularity is a branch cut [61, p.225]. As expected, the vertex function is even in ω and is for large $|\omega'|$ proportional to ${\omega'}^{-1/2}$, see Sec. B.3. The presented features of the vertex function represent only a small part of all the properties, and I have yet not interpreted any more of them.

With this insight, I expect the structure of vertex functions in systems with more complex phonon dispersions to be similar with respect to the above mentioned properties: Elementary excitations of the system that have a lower energy than the (lowest) phonon-mode with appropriate momentum, cannot decay via phonon emission, and multiparticle states will also be elementary excitations of more complex systems. Note that this discussion is valid only for excitations with a long lifetime.

3.2.2. Vertex correction to the polarizability

With the vertex function, I can now calculate the vertex correction to the polarizability (multiplied with a minus, by convention for Γ_1)

$$\Delta\chi(\mathbf{k},\omega) = 2i \int \frac{d\omega'}{2\pi} K_\chi(\mathbf{k},\omega,\omega')\Gamma_1(\mathbf{k},\omega,\omega'). \tag{88}$$

Here, I have used that the integration over the loop momentum $\mathbf{q}$ to obtain K_χ is independent of the vertex function. This integral just meets the "convergence expectation" (Eq.(97)), so that $K_\chi\Gamma_1 \propto \frac{1}{\omega'}$, as shown in Sec. B.3.2. This means, that the resulting integral needs to be renormalized, according to the same procedure as in Eq.(79)[14]. The expansion of Γ_1 in terms of ω' can be found in Sec. B.3.3. The error of this integral is shown to be negligible. The resulting corrections to the polarizability are depicted in Fig. 21. The sum of the corrections due to dressing of Green's function and vertex are presented in Fig. 22. Figures 21 and 22 show, that the vertex correction to the polarizability has roughly the same magnitude as the Green's function correction

[13] In the language of [63, p.12].

[14] As for the polarizability I use the condition $\Delta\chi(\mathbf{k},\infty) = 0$.

but, compared to the imaginary part, the opposite sign.

This result shows, that the expectation of Migdal [47], that the vertex correction is negligible, does not hold. For the case of electron-electron interaction, it was shown for silicon and diamond that the vertex correction partially compensates the dressing of the Green's function [9]. One sees a similar effect in the case of electron-phonon interaction. In the case of Ref. [9] this leads to improved agreement with experimental results. I expect that these findings may also apply to metals, that exhibit the most similar behavior to the homogeneous electron gas. However, for more complex materials, further work is needed to estimate the impact of the electron-phonon vertex correction.

3.3. Plasmon lifetimes

Finally, I proceed to investigate the effect of electron-phonon interaction on the lifetimes of plasmons. As explained, the coupling to phonons gives rise to a small but finite imaginary part in the polarizability for most values $\mathbf{k}$ and ω, which causes a finite lifetimes of the plasmons. Physically, the decay of the collective mode happens due to incoherent scattering [63, p.51], when the decay in an electron-hole pair, Landau damping, is forbidden [63, p.50]. Once the decay into a quasiparticle-pair becomes possible, phonon-damping is not the dominant decay channel of the mode anymore. Landau damping is enabled whenever the energy and momentum of a plasmon becomes degenerate with those of electron-hole transitions, provided the necessary phase space for plasmon decay. This happens roughly if [18]

$$k \geq k_F \left[(1 + \omega_{\mathrm{pl}}/\epsilon_F)^{1/2} - 1 \right]. \tag{89}$$

Below this wavevector, phonon-damping is the dominant damping mechanism of the plasmons. The plasmon lifetime can be obtained from their peak width in the loss function [44, p.438 ff.]

$$\begin{aligned} \mathscr{L} &= \Im \left(\frac{1}{\varepsilon(\mathbf{k}, \omega)} \right) \\ &= \frac{-\Im(\varepsilon(\mathbf{k}, \omega))}{\Re(\varepsilon(\mathbf{k}, \omega))^2 + \Im(\varepsilon(\mathbf{k}, \omega))^2} \end{aligned}$$

$$\Rightarrow \tau(\mathbf{k}) = \frac{-\frac{\partial}{\partial \omega} \Re(\varepsilon(\mathbf{k}, \omega))|_{\omega=\omega_{\mathrm{pl}}}}{\Im\varepsilon(\mathbf{k}, \omega_{\mathrm{pl}}(\mathbf{k}))} = \frac{\frac{\partial}{\partial \omega} \Re(\chi_0(\mathbf{k}, \omega))|_{\omega=\omega_{\mathrm{pl}}}}{\Im\chi_0(\mathbf{k}, \omega_{\mathrm{pl}}(\mathbf{k}))}, \tag{90}$$

where the formula in the last line is inspired by the Breit-Wigner formula [61, p.101]. Computing the plasmon lifetime by Eq. (90) suffers a serious problem: The calculated shift of the polarizability χ_0 is accurate only to a certain magnitude. Then, the numerator of Eq. (90), which vanishes for $k \to 0$, is divided by a (shifted) imaginary part that does not vanish for small k, see Fig. 23. I, therefore, acquire the unphysical property, that the lifetime of the plasmons vanish for small momenta k.

In contrast, Ref. [63, p.220] shows, that the imaginary part of the polarizability

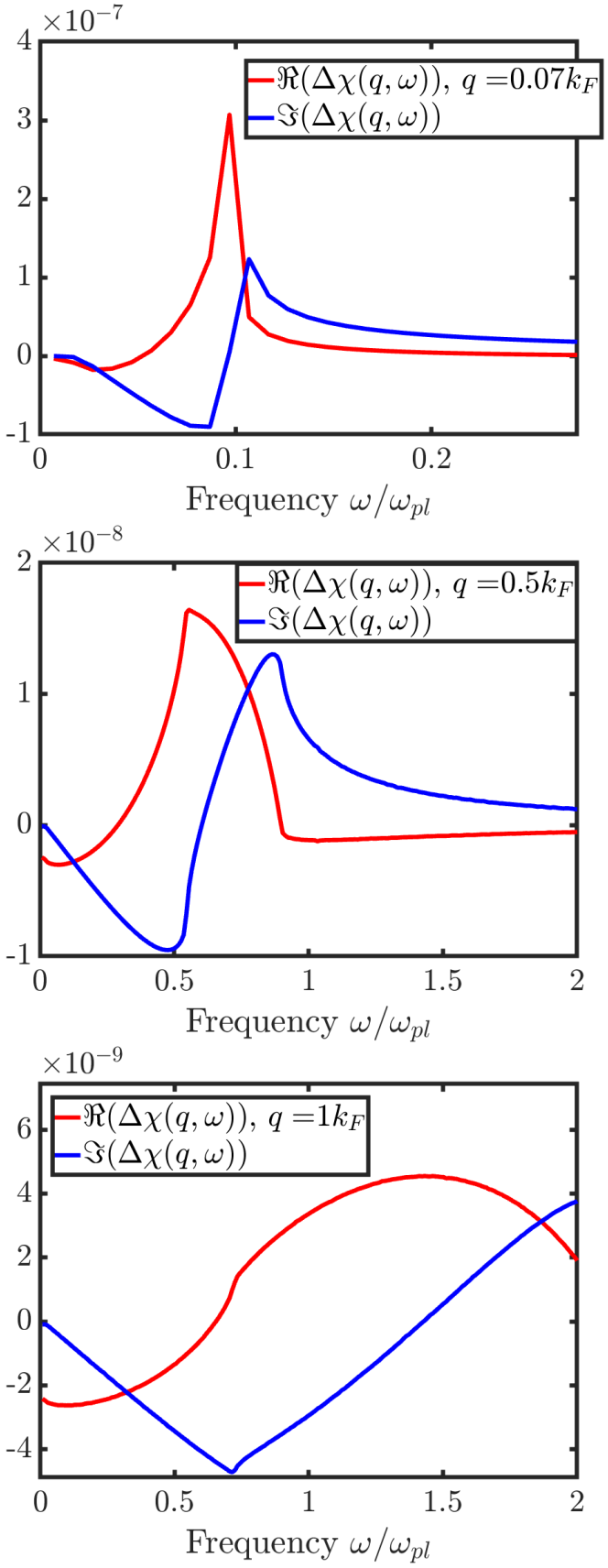

Figure 21: Vertex correction to the polarizability to order g^2, for three different momenta, $q = 0.07k_F$ (above), $0.5k_F$ (middle) and k_F (below). The left graph has been truncated. By comparing to Fig. 17, one can see that the vertex correction and the electron Green's function correction to the polarizability are of the same order of magnitude. The parameters $m = 0.2$, $\epsilon_F = 2$ eV, $g = 100$ meV and $\omega_{\text{ph}} = 60$ meV were used.

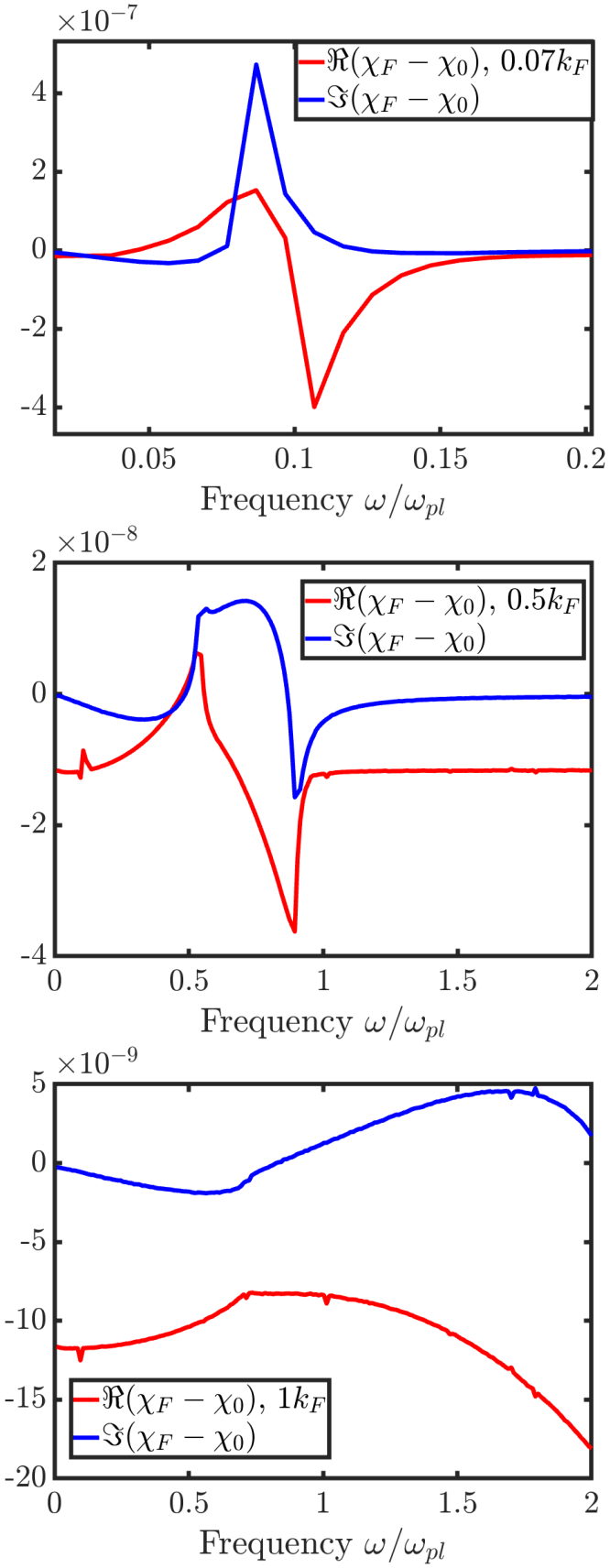

Figure 22: Sum of the corrections to the polarizability due to the dressed Green's function and vertex correction to order g^2, for three different momenta, $q = 0.07k_F$ (above), $0.5k_F$ (middle) and k_F (below). By comparison to Fig. 17, a certain amount of compensation of the Green's function correction due to the vertex takes place, as in the case of Ref. [9]. The parameters $m = 0.2$, $\epsilon_F = 2$ eV, $g = 100$ meV and $\omega_{\rm ph} = 60$ meV have been used.

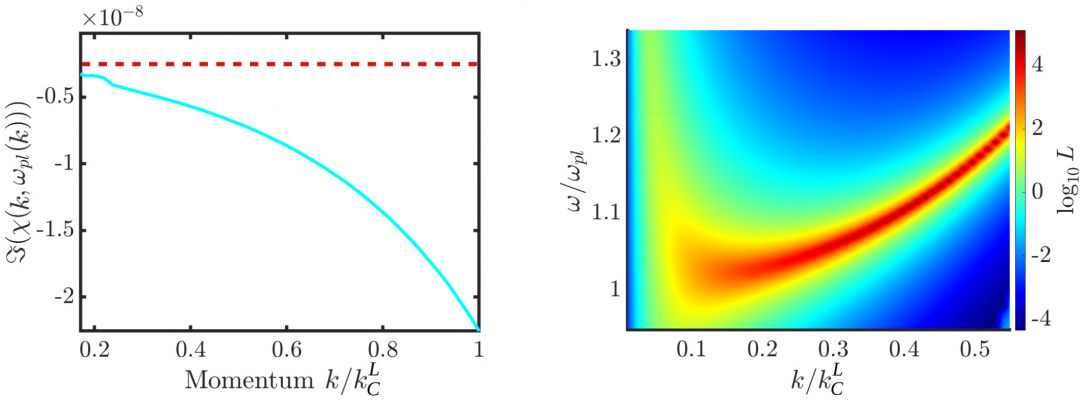

Figure 23: Imaginary part of the polarizability (left) and plasmon peaks in the loss function (right) for the parameters $g = 100$ meV, $\omega_{\text{ph}} = 60$ meV, $\epsilon_F = 2$ eV and $m = 0.2$, zoomed for k small. One can see, that the plasmon peaks broaden for small k. This is caused by the shift of the imaginary part, that is indicated by the red dashed line in the left plot.

should be proportional to k^2 for $k \to 0$. Therefore, I calculate the numerator and denominator of Eq.(90) for values of $k \in [0.2, 1]k_C^L$ and fit the function $f(k) = ak^2 + b$ onto the resulting curves. This fitting procedure leads for the parameters used in Fig. 23 to a relatively small error[15]. Then, the values for the parameters a, of the fitted curves, are divided which leads to a plasmon lifetime of 160fs without the vertex correction, and of 550fs including the vertex correction for these model parameters. The plasmon peaks in the loss function look then like in Fig. 24. Convergence tests of the results can be found in Sec. B.4.

The result for the plasmon lifetime without vertex correction is similar to that of Ref. [18], even though the plasmon lifetimes are slightly larger. Including the vertex correction shows, that the interaction between quasi-electrons and -holes in the system suppresses the incoherent decay of the plasmon modes. Mathematically, this behavior is easily understood and can be traced back to the compensation effects discussed above.

The model Eq. (3) can only be taken into account if the damping through electron-electron interactions in the material is dominated by the phonon-damping, which is for this phonon-model expected if Landau damping is forbidden [2, p.187].

For the discussion how the results apply to real materials, I directly follow Ref. [63, p.228 ff.]. If the plasma frequency of the material is not degenerate with interband transitions in the material (between valence and conduction states), the collective mode is expected to behave analogously to the model system. Simple metals, that have an almost parabolic valence band close to the Fermi surface, may be approximately described with the homogeneous electron gas model. Such simple metals are, for example, gold, silver, aluminium or sodium.

[15]The root mean square error divided by the standard deviation is for both functions smaller than 5%.

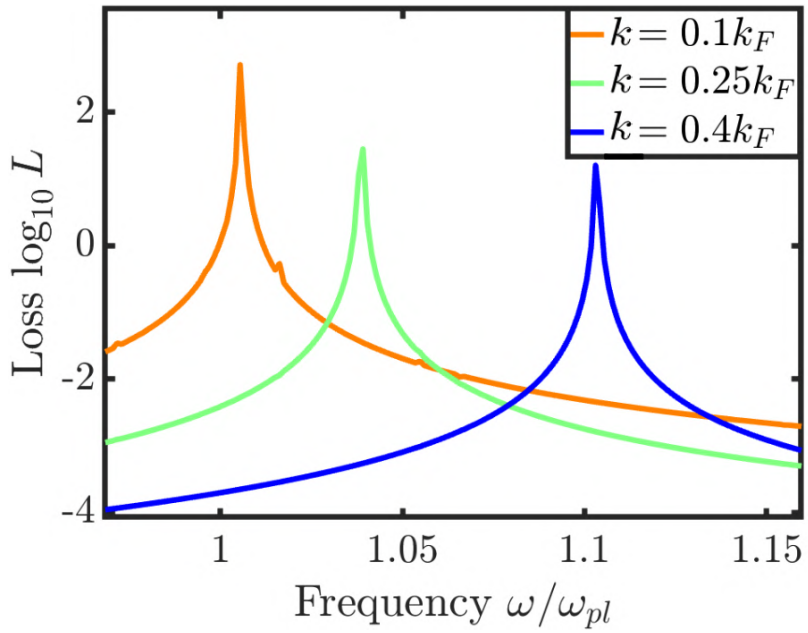

Figure 24: Plasmon peaks in the loss function for three different momenta. A detailed analysis can be found in Sec. B.4. The parameters $g = 100$meV, $\omega_{\text{ph}} = 60$meV, $\epsilon_F = 2$eV and $m = 0.2$ have been used.

4. Conclusions

In this work, I investigated the properties of the homogeneous electron gas including electron-phonon interactions, using the Hedin-Baym equations to second order in the interaction. It was found that the vertex function near the Fermi-surface exhibits a well understandable structure of multiparticle excitations. Even though Migdal's theorem assures that vertex corrections remain small, relevant compensation effects between vertex correction and correction due to the dressing of the Green's function take place, similar to the case of electron-electron interactions, discussed in Ref. [9]. The plasmon lifetimes increase significantly in the model system, when the vertex correction is taken into account.

Vertex functions with logarithmic divergences that correspond to multiparticle excitations should appear also in more complex systems, even though the significance of these excitations may vary. The approximation made in [18] for the correction due to the dressing of the Green's function to the polarizability is very likely to be a good approximation to more complex materials as well, and it seems unnecessary to include the frequency dependence of the self-energy in much detail. Further work is needed to establish whether the compensation effects of the vertex correction on the Green's function correction and their impact on the plasmon lifetimes would apply also to real materials. The best candidates for these findings to apply are the alkali metals, alkaline earths and doped semiconductors [63, p.228] for which the valence band may be approximately described as parabolic.

In the future, one may extend this work to investigate the properties of the two-dimensional homogeneous electron gas, to infer properties of SPP's. Additionally, the calculations of this work can be readily adjusted to any momentum-independent self-energy for the electron Green's function in three dimensions. From the results of this work, it is possible to calculate the electron-electron Green's function of this model system up to order g^4, which might be an interesting model to study superconductivity, according to Ref. [2]. Another another topic that may be addressed with this model system is the impact of polaronic satellites in the spectral function on the polarizability. The calculations of this work may also be extended to higher orders in g using the Hedin-Baym equations. However, the most important task is to develop approximations for the vertex to be used in *ab initio* calculations, to explore how the findings of this work apply to real materials.

References

[1] Abramowitz, M. ; Stegun, I.A.: Handbook of mathematical functions with formulas, graphs, and mathematical table. In: US Department of Commerce. National Bureau of Standards Applied Mathematics series 55, 1965

[2] Abrikosov, Al. A. ; Gor'Kov, LP ; Dzyaloshinskii, I Y.: Quantum Field Theoretical Methods in Statistical Physics. Pergamon Press, 1965

[3] Alfe, D ; De Wijs, GA ; Kresse, G ; Gillan, MJ: Recent developments in ab initio thermodynamics. In: International Journal of Quantum Chemistry 77 (2000), Nr. 5, S. 871–879

[4] Altland, A. ; Simons, B.: Condensed Matter Field Theory. Cambridge University Press, 2010

[5] Antonius, G. ; Louie, S. G.: Theory of the exciton-phonon coupling. In: arXiv preprint arXiv:1705.04245 (2017)

[6] Atwater, H.A. ; Polman, A.: Plasmonics for improved photovoltaic devices. In: Nat. Mater. 9 (2010), Nr. 3, S. 205

[7] Awazu, K. ; Fujimaki, M. ; Rockstuhl, C. ; Tominaga, J. ; Murakami, H. ; Ohki, Y.: Yoshida N and Watanabe T. In: J. Am. Chem. Soc. 2008 (2008), S. 130

[8] Barnes, W.L. ; Dereux, A. ; Ebbesen, T.W.: Surface plasmon subwavelength optics. In: Nat. 424 (2003), Nr. 6950, S. 824

[9] Bechstedt, F ; Tenelsen, K ; Adolph, B ; Del Sole, R: Compensation of dynamical quasiparticle and vertex corrections in optical spectra. In: Phys. Rev. Lett. 78 (1997), Nr. 8, S. 1528

[10] Bernardi, M. ; Mustafa, J. ; Neaton, J.B. ; Louie, S.G.: Theory and computation of hot carriers generated by surface plasmon polaritons in noble metals. In: Nat. Comm. 6 (2015), S. 7044

[11] Bernardi, M. ; Vigil-Fowler, D. ; Lischner, J. ; Neaton, J.B. ; Louie, S.G.: Ab initio study of hot carriers in the first picosecond after sunlight absorption in silicon. In: Phys. Rev. Lett. 112 (2014), Nr. 25, S. 257402

[12] Bernardi, Marco ; Vigil-Fowler, Derek ; Ong, Chin S. ; Neaton, Jeffrey B. ; Louie, Steven G.: Ab initio study of hot electrons in GaAs. In: Proceedings of the National Academy of Sciences 112 (2015), Nr. 17, S. 5291–5296

[13] Brongersma, M. ; Kik, P.G.: Surface plasmon nanophotonics. Bd. 131. Springer, 2007

[14] Brown, AM ; Sundararaman, R ; Narang, P ; Goddard, WA ; Atwater, HA: ACS Nano 10, 957 (2016)

[15] Caruso, F.: Self-consistent GW approach for the unified description of ground and excited states of finite systems, Diss., 2013

[16] Caruso, F. ; Giustino, F.: Theory of electron-plasmon coupling in semiconductors. In: Phys. Rev. B 94 (2016), Nr. 11, S. 115208

[17] Caruso, F. ; Hoesch, M. ; Achatz, P. ; Serrano, J. ; Krisch, M. ; Bustarret, E. ; Giustino, F.: Nonadiabatic Kohn Anomaly in Heavily Boron-Doped Diamond. In: Phys. Rev. Lett. 119 (2017)

[18] Caruso, F. ; Novko, D. ; Draxl, C.: Phonon-assisted damping of plasmons in three-and two-dimensional metals. In: Phys. Rev. B 97 (2018), Nr. 20, S. 205118

[19] Damascelli, A. ; Hussain, Z. ; Shen, Z.-X.: Angle-resolved photoemission studies of the cuprate superconductors. In: Rev. Mod. Phys. 75 (2003), S. 473

[20] Egerton, R.F.: Electron energy-loss spectroscopy in the TEM. In: Rep. Prog. Phys. 72 (2008), Nr. 1, S. 016502

[21] Egerton, R.F.: Electron energy-loss spectroscopy in the electron microscope. Springer Science & Business Media, 2011

[22] Eiguren, A. ; Ambrosch-Draxl, C.: In: Phys. Rev. Lett. 101 (2008), 036402 S.

[23] Eiguren, A. ; Ambrosch-Draxl, C. ; Echenique, P.M.: Self-consistently renormalized quasiparticles under the electron-phonon interaction. In: Phys. Rev. B 79 (2009), Nr. 24, S. 245103

[24] Eustis, S. ; El-Sayed, M. A.: Why gold nanoparticles are more precious than pretty gold: noble metal surface plasmon resonance and its enhancement of the radiative and nonradiative properties of nanocrystals of different shapes. In: Chem. Soc. Rev. 35 (2006), Nr. 3, S. 209–217

[25] García, M. A.: Surface plasmons in metallic nanoparticles: fundamentals and applications. In: Jour. Phys. D 44 (2011), Nr. 28, S. 283001

[26] Giuliani, G. ; Vignale, G.: Quantum theory of the electron liquid. Cambridge university press, 2005

[27] Giustino, F.: Electron-phonon interactions from first principles. In: Rev. Mod. Phys. 89 (2017), Nr. 1, S. 015003

[28] Grimvall, G.: The Electron– Phonon Interaction in Metals. Vol. 16. In: North-Holland Publishing Co., (1981), S. 304

[29] H., Min ; C., Jingyi ; L., Zhi-Yuan ; A., Leslie ; Hartland, G. V. ; L., Xingde ; Marquez, M. ; X., Younan: Gold nanostructures: engineering their plasmonic properties for biomedical applications. In: Chem. Soc. Rev. 35 (2006), Nr. 11, S. 1084–1094

[30] Hedin, L. ; Michiels, J. ; Inglesfield, J.: Transition from the adiabatic to the sudden limit in core-electron photoemission. In: Phys. Rev. B 58 (1998), Nr. 23, S. 15565

[31] Hirsch, L.R. ; Stafford, R. J. ; Bankson, J.A. ; Sershen, S.R. ; Rivera, B. ; Price, R.E. ; Hazle, J.D. ; Halas, N.J. ; West, J.L.: Nanoshell-mediated near-infrared thermal therapy of tumors under magnetic resonance guidance. In: Proc. Natl. Acad. Sci. USA 100 (2003), Nr. 23, S. 13549–13554

[32] Homola, J. ; Yee, S.S. ; Gauglitz, G.: Surface plasmon resonance sensors. In: Sens. Actu. B 54 (1999), Nr. 1-2, S. 3–15

[33] Keating, P.N.: Dielectric screening and the phonon spectra of metallic and nonmetallic crystals. In: Phys. Rev. B 175 (1968), Nr. 3, S. 1171

[34] Khurgin, J.B.: How to deal with the loss in plasmonics and metamaterials. In: Nat. Nanotech. 10 (2015), Nr. 1, S. 2

[35] Kittel, C. ; Stuart Johnson, Patricia M. (Hrsg.): Introduction to Solid State Physics. John Wiley and Sons, Inc, 2005

[36] Kleinert, H.: Particles and quantum fields. World Scientific Singapore, 2016

[37] Knight, M. W. ; Sobhani, H. ; Nordlander, P. ; Halas, N.J.: Photodetection with active optical antennas. In: Sci. 332 (2011), Nr. 6030, S. 702–704

[38] Larsson, E.M. ; Langhammer, C.: Zoric, 1. & Kasemo, B. Nanoplasmonic probes of catalytic reactions. In: Sci. 326 (2009), S. 1091–1094

[39] Lazzeri, M.: M. Lazzeri and F. Mauri, Phys. Rev. Lett. 97, 266407 (2006). In: Phys. Rev. Lett. 97 (2006), S. 266407

[40] Lewin, L.: Dilogarithms and associated functions. (1958)

[41] Link, Stephan ; El-Sayed, Mostafa A.: Spectral properties and relaxation dynamics of surface plasmon electronic oscillations in gold and silver nanodots and nanorods. 1999

[42] Logothetidis, S. ; Petalas, J. ; Polatoglou, H.M. ; Fuchs, D.: Origin and temperature dependence of the first direct gap of diamond. In: Phys. Rev. B 46 (1992), Nr. 8, S. 4483

[43] Luttinger, J.M.: Fermi surface and some simple equilibrium properties of a system of interacting fermions. In: Phys. Rev. 119 (1960), Nr. 4, S. 1153

[44] Mahan, G. D.: Many-Particle Physics. Plenum Press New York, 1990

[45] Maier, S.A.: Effective mode volume of nanoscale plasmon cavities. In: Opt. Quant. Elec. 38 (2006), Nr. 1-3, S. 257–267

[46] Matheu, P. ; Lim, S.H. ; Derkacs, D. ; McPheeters, C. ; Yu, E.T.: Metal and dielectric nanoparticle scattering for improved optical absorption in photovoltaic devices. In: Appl. Phys. Lett. 93 (2008), Nr. 11, S. 113108

[47] Migdal, AB: Interaction between electrons and lattice vibrations in a normal metal. In: Sov. Phys. JETP 7 (1958), Nr. 6, S. 996–1001

[48] Molina-Sánchez, A. ; Palummo, M. ; Marini, A. ; Wirtz, L.: In: Phys. Rev. B 93 (2016), 155435 S.

[49] Morse, P. M. ; Feshbach, H.: Methods of Theoretical Physics, Part 1. Feshbach Publishing, LLC, 1981

[50] Moser, S. ; Moreschini, L. ; Jaćimović, J. ; Barišić, O.S. ; Berger, H. ; Magrez, A. ; Chang, Y.J. ; Kim, K.S. ; Bostwick, A. ; Rotenberg, E. u. a.: Tunable polaronic conduction in anatase TiO 2. In: Phys. Rev. Lett. 110 (2013), Nr. 19, S. 196403

[51] Narayanan, R: Chimica OGGI-Chem. Today 2007, 25, 84–86.(b) Narayanan, R.; El-Sayed. In: J. Phys. Chem 109 (2005), S. 12663–12676

[52] Noffsinger, J. ; Kioupakis, E. ; Walle, C.G. Van d. ; Louie, S.G. ; Cohen, M.L.: Phonon-assisted optical absorption in silicon from first principles. In: Phys. Rev. Lett. 108 (2012), Nr. 16, S. 167402

[53] Nolting, W.: Grundkurs, Theoretische Physik 7, Viel-Teilchen-Theorie. Springer Dordrecht Heidelberg London New York, 2009

[54] Nolting, W.: Magnetostatik. In: Grundkurs Theoretische Physik 3. Springer, 2013, S. 173–220

[55] Novko, D.: D. Novko, Nano Lett. 17, 6991 (2017). In: Nano Lett. 17 (2017), S. 6991

[56] Nozieres, P. ; Pines, D.: Electron interaction in solids. Characteristic energy loss spectrum. In: Physical Review 113 (1959), Nr. 5, S. 1254

[57] O'Neal, D.P. ; Hirsch, L.R. ; Halas, N.J. ; Payne, J.D. ; West, J.L.: Photo-thermal tumor ablation in mice using near infrared-absorbing nanoparticles. In: Canc. Lett. 209 (2004), Nr. 2, S. 171–176

[58] Ozbay, E.: Plasmonics: merging photonics and electronics at nanoscale dimensions. In: Sci. 311 (2006), Nr. 5758, S. 189–193

[59] Patrick, C. E. ; Giustino, F.: Unified theory of electron–phonon renormalization and phonon-assisted optical absorption. In: Jour. Phys. Cond. Mat. 26 (2014), Nr. 36, S. 365503

[60] Pavone, P ; Bauer, R. ; Karch, K. ; Schütt, O. ; Vent, S. ; Windl, W. ; Strauch, D. ; Baroni, S. ; Gironcoli, S. de: In: Physica B 219 (1996), 439 S.

[61] Peskin, M. E. ; Schroeder, D.V.: An Introduction to Quantum Field Theory. Westview Press, 1995

[62] Pillai, S. ; Catchpole, K.R. ; Trupke, T. ; Green, M.A.: Surface plasmon enhanced silicon solar cells. In: Jour. Appl. Phys. 101 (2007), Nr. 9, S. 093105

[63] Pines, D. ; Nozières, P.: The theory of quantum liquids. Bd. 1. WA Benjamin New York, 1966

[64] Piscanec, S.: S. Piscanec, M. Lazzeri, F. Mauri, AC Ferrari, and J. Robertson, Phys. Rev. Lett. 93, 185503 (2004). In: Phys. Rev. Lett. 93 (2004), S. 185503

[65] Pitarke, J.M. ; Silkin, V.M. ; Chulkov, E.V. ; Echenique, P.M.: Theory of surface plasmons and surface-plasmon polaritons. In: Rep. Prog. Phys. 70 (2006), Nr. 1, S. 1

[66] Riley, J.M. ; Caruso, F. ; Verdi, C. ; Duffy, L.B. ; Watson, M.D. ; Bawden, L. ; Volckaert, K. ; Laan, G. van d. ; Hesjedal, T. ; Hoesch, M. u. a.: Crossover from lattice to plasmonic polarons of a spin-polarised electron gas in ferromagnetic EuO. In: Nat. Comm. 9 (2018), Nr. 1, S. 2305

[67] Schwinger, J.: On the Greens functions of quantized fields. I. In: Proc. Natl. Acad. Sci. USA 37 (1951), Nr. 7, S. 452–455

[68] Verdi, C. ; Caruso, F. ; Giustino, F.: Origin of the crossover from polarons to Fermi liquids in transition metal oxides. In: Nat. Comm. 8 (2017), S. 15769

[69] Wang, Z. ; Walker, S. M. ; Tamai, A. ; Wang, Y. ; Ristic, Z. ; Bruno, F. Y. ; De La Torre, A. ; Riccò, S. ; Plumb, N.C. ; Shi, M. u. a.: Tailoring the nature and strength of electron–phonon interactions in the SrTiO 3 (001) 2D electron liquid. In: Nat. Mater. 15 (2016), Nr. 8, S. 835

[70] Weinberg, S.: The quantum theory of fields. Vol. 1: Foundations. Cambridge University Press, 1995

[71] Werner, D.: Funktionalanalysis. Springer, 2006

[72] Wood, D.: The Computation of Polylogarithms / University of Kent, Computing Laboratory. Version: June 1992. http://www.cs.kent.ac.uk/pubs/1992/110. University of Kent, Canterbury, UK, June 1992 (15-92*). – Forschungsbericht. – 182–196 S.

[73] Zacharias, M. ; Giustino, F.: One-shot calculation of temperature-dependent optical spectra and phonon-induced band-gap renormalization. In: Phys. Rev. B 94 (2016), Nr. 7, S. 075125

[74] Zacharias, M. ; Patrick, C.E. ; Giustino, F.: Stochastic approach to phonon-assisted optical absorption. In: Phys. Rev. Lett. 115 (2015), Nr. 17, S. 177401

List of Figures

List of Tables

A. Renormalizability

The method and argumentation in this section stems from Ref. [61, p.321 ff.]. Renormalizability is the property of a field theory, that occurring divergences can be absorbed into a finite number of parameters of the theory, such as the mass of the particles or the coupling strength. If the number of parameters that is needed to absorb the divergences is finite, the number of parameters of the theory, which need to be measured, can be finite. This means, only a renormalizable field theory allows physical predictions. To proof this property, it is enough to show that there is only a finite number of divergent amplitudes in the theory. This is shown, if the convergence of diagrams improves with the number of particles that participate in the process - so that more complex diagrams tend to be more convergent. This considerations can be quantified with the degree of divergence of a quantity $Q(\Lambda) = \int_{-\Lambda}^{\Lambda} dx f(x)$.

Definition 1 (Degree of divergence)**.** *If a quantity $Q(\Lambda)$ diverges as Λ^N with $\Lambda \to \infty$, then, the degree of divergence of Q is defined as*

$$[[Q]] = N. \tag{91}$$

A superficial estimate of the degree of divergence $[Q]$ can be found by counting the dimensions of integration and the asymptotic behaviour of the involved Green's functions. As symmetries might reduce the degree of divergence, the inequality $[[Q]] \leq [Q]$ holds. To reassure, that the considered theory is meaningful, I will show now, that the model theory Eq.(3) is renormalizable. Recall the Feynman rules from Sec. 2.3. The electron Green's function is[16]

$$iG_0(k,\omega) = \frac{i}{\omega - \epsilon(k) + i\eta_k} \propto \frac{1}{\epsilon(k)} \propto \frac{1}{k^2} \tag{92}$$

with $\eta_k = \eta \, \mathrm{sgn}(|k| - k_F)$. η is considered a positive infinitesimal. The phonon Green's function is

$$iD(\omega) = \frac{i}{\omega - \omega_{\mathrm{ph}} + i\eta} - \frac{i}{\omega + \omega_{\mathrm{ph}} - i\eta} \propto \frac{1}{\omega^2} \tag{93}$$

The interaction vertex is non-dispersive. It is thus simply a factor g.

The superficial degrees of divergence of the theory with respect to frequency ω and momentum k are, by the fact that a loop carries an integration over momentum in three dimensions and over frequency in one dimension:

$$\begin{aligned} N_k &= 3N_L - 2F_i \\ N_\omega &= N_L - 2B_i \end{aligned} \tag{94}$$

[16] Throughout the appendix, vectors are implied without bold signs.

where F_i is the number of virtual (internal) electrons (fermions), B_i is the number of internal phonons and N_L is the number of closed loops. The number of loops can now be related to the number of vertices and internal particles. The momenta and energies of all internal fermions and bosons are integrated. So one obtains an integration for each. Every vertex carries a δ function to conserve momentum. Additionally, one delta function enforces overall momentum and energy conservation. So I find, with V the number of vertices

$$N_L = B_i + F_i - V + 1. \tag{95}$$

Then, the number of vertices in a connected diagram can be calculated: From each vertex, three lines come out. An internal particle docks to two vertices; an external particle, denoted by e, docks to one. Then

$$3V = 2(B_i + F_i) + (B_e + F_e). \tag{96}$$

Inserting Eq. (96) in Eq. (95) I have

$$N_L = \frac{B_i + F_i - B_e - F_e}{3} + 1.$$

Inserting this in Eq. (94)

$$\begin{aligned} N_k &= (B_i - F_i) - (B_e + F_e) + 3 \\ N_\omega &= \frac{1}{3}(F_i - 5B_i) - \frac{1}{3}(B_e + F_e) + 1 \end{aligned} \tag{97}$$

The following arguments will proof the renormalizability of the theory: For a given number of external particles, the number of internal bosons in a connected diagram can not grow faster than the number of internal fermions, as for a created boson, also an internal fermion is created, while the boson can be annihilated by exciting more than one fermion - which is impossible vice versa. On the other hand, for a given number of external particles, the number of internal fermions can not grow faster than double the number of internal bosons: an internal boson excites four fermions. But these fermions either contract (connect lines) or emit further bosons, such that they contract. This means, the number of internal fermions cannot grow more than twice as fast as the number of internal bosons. Therefore, the theory is renormalizable, as there is only a finite number of divergent diagrams, so that the theory is expected to give physical predictions.

B. Derivations and validations

This section is organized as follows: in each subchapter first the basic idea of what is calculated is shown, then the result, the expansion for large ω', the calculation and validation. First I will present the calculation for the Fan-Migdal self-energy, then the

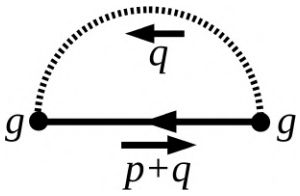

Figure 25: The (only non-constant) self-energy diagram at order g^2.

calculation of the polarizability kernel K_χ, the vertex calculation, and the convergence tests for the integrands and integrals in the polarizability calculation.

B.1. The Fan-Migdal self-energy Σ_{FM}

The only diagram that is non-constant at order g^2 can be seen in Fig. 25.

B.1.1. Result

With the value

$$\Sigma_{\mathrm{FM}}(k,\omega) = ig^2 \int \frac{dq\ d\omega_1}{(2\pi)^4} G(k+q, \omega+\omega_1) D(q,\omega_1). \tag{98}$$

and, as D does not depend on q, I can shift q by $-k$, and see that the self-energy becomes momentum independent.

Theorem 5 (Fan-Migdal self-energy)**.** *The self-energy from electron-phonon interactions in the free electron gas to second order in g is*

$$\Sigma_{FM}(\omega) = \tilde{\Sigma}(\omega) - \tilde{\Sigma}(\epsilon_F) \tag{99}$$

with

$$\tilde{\Sigma}(\omega) = \Sigma_R(\omega - \omega_{ph}, -1) + \sigma(\omega + \omega_{ph}, +1) - \sigma(\omega - \omega_{ph}, -1). \tag{100}$$

Now Σ_R *is*

$$\Sigma_R(\beta,\gamma) = g^2 \frac{m\beta}{2\pi} \sqrt{\frac{2m}{|\beta|}} \begin{cases} isgn(\gamma) & \beta > 0 \\ -1 & \beta < 0 \end{cases} \tag{101}$$

and σ *is*

$$\sigma(\beta,\gamma) = -\frac{mg^2}{\pi^2} \left(k_F + \beta\chi(\beta,\gamma)\right) \tag{102}$$

where

$$\chi(\beta,\gamma)=\begin{cases}-i\sqrt{\frac{m}{2|\beta|}}\left(\log(q-i\sqrt{2m|\beta|})-\log(q+i\sqrt{2m|\beta|})\right)_{q=0}^{k_F} & \beta<0\\ -\chi(-\beta,\gamma)-\frac{m}{k_F}\sqrt{\frac{\beta}{\epsilon_F}}\left(\log(x-\phi_-)-\log(x-\phi_+)\right)_{x=0}^{1} & \beta>0\end{cases} \tag{103}$$

and $\phi_\pm=\frac{1-i}{2}\pm\frac{1+i}{2}\sqrt{\frac{\beta}{\epsilon_F}}$.

B.1.2. Large ω' expansion

For the renormalization of the kernel of the polarizability with dressed propagators, the Fan-Migdal self-energy term needs to be known in orders $\frac{1}{\omega'}$ for large ω'. The procedure to obtain the expansion is, in this case, straight forward: I have implemented the full result in `Mathematica 11.1` and left the expansion to the computer. The validation of this expansion is found below, with the validation of the full result.

B.1.3. Calculation

I use Eq.(73) to bring all poles of Eq.(98) to one side of the contour. Then I contract on the other half plane and by holomorphy, the last integral vanishs:

$$\begin{aligned}\Sigma_{\mathrm{FM}}(\omega)&=ig^2\int\frac{dq\ d\omega_1}{(2\pi)^4}G(q,\omega+\omega_1)D(\omega_1)\\&=ig^2\int\frac{dq\ d\omega_1}{(2\pi)^4}\{2\pi i\delta(\omega+\omega_1-\epsilon(q))\theta(k_F-q)D(\omega_1)+\\&\qquad\frac{1}{\omega+\omega_1-\epsilon(q)+i0}\left(\frac{1}{\omega_1-\omega_{\mathrm{ph}}+i0}-\frac{1}{\omega_1+\omega_{\mathrm{ph}}-i0}\right)\}\\&=ig^2\int\frac{dq\ d\omega_1}{(2\pi)^4}\{2\pi i\delta(\omega+\omega_1-\epsilon(q))\theta(k_F-q)D(\omega_1)+\\&\qquad\frac{1}{\omega+\omega_1-\epsilon(q)+i0}(-2\pi i)\delta(\omega_1+\omega_{\mathrm{ph}})+0\}\end{aligned} \tag{104}$$

The integration over ω_1 then yields

$$\begin{aligned}\Sigma_{\mathrm{FM}}(\omega-\omega_{\mathrm{ph}})=-g^2\int\frac{dq}{(2\pi)^3}\{&\left[\frac{1}{\epsilon(q)-\omega-\omega_{\mathrm{ph}}+i\eta}-\frac{1}{\epsilon(q)-\omega+\omega_{\mathrm{ph}}-i\eta}\right]\times\\&\theta(\epsilon_F-\epsilon(q))+\frac{1}{\epsilon(q)-\omega+\omega_{\mathrm{ph}}-i\eta}\}\end{aligned} \tag{105}$$

It can be seen, that the last fraction's integral is divergent. It is renormalized simply by subtracting a constant from the integrand. The renormalization condition is fixed

later.

$$\Sigma_R(\omega-\omega_{\rm ph},-1) = -g^2\int\frac{dq}{(2\pi)^3}\left(\frac{1}{\epsilon(q)-\omega+\omega_{\rm ph}-i\eta}-\frac{1}{\epsilon(q)}\right)$$
$$= -g^2\int\frac{dq}{(2\pi)^3}\frac{\omega-\omega_{\rm ph}}{\epsilon(q)-\omega+\omega_{\rm ph}-i\eta}\frac{1}{\epsilon(q)}. \tag{106}$$

This can be evaluated:

$$\Sigma_R(\beta,\gamma) = \frac{-mg^2\beta}{\pi^2}\int_0^\infty dq\frac{1}{\epsilon(q)-\beta+i\eta\gamma}. \tag{107}$$

For negative β, the integral is $I(\beta) = \frac{\pi}{2}\sqrt{\frac{2m}{-\beta}}$. For $\beta > 0$ it can be proven that $\Sigma_R(\beta,\gamma) = \Sigma_R(\beta,-\gamma)^*$. For $\gamma > 0$, the pole in the q-plane has negative imaginary location. Thus, I can Wick rotate the contour, noting that the arc of the contour integral does not contribute, and find then, that for $\beta > 0$

$$\Sigma_R(\beta,\gamma) = ig^2{\rm sgn}(\gamma)\frac{m\beta}{2\pi}\sqrt{\frac{2m}{\beta}} \tag{108}$$

and for $\beta < 0$

$$\Sigma_R(\beta,\gamma) = -g^2\frac{m\beta}{2\pi}\sqrt{\frac{2m}{-\beta}} \tag{109}$$

The two other terms are of the type

$$\sigma(\beta,\gamma) = -g^2\int\frac{dq}{(2\pi)^3}\frac{1}{\epsilon(q)-\beta+i\eta\gamma}\theta(\epsilon_F-\epsilon(q))$$
$$= -\frac{mg^2}{\pi^2}\{k_F+\beta\int_0^{k_F}\frac{dq}{\epsilon(q)-\beta+i\eta\gamma}\} \tag{110}$$

I define

$$\chi(\beta,\gamma) = \int_0^{k_F} dq\frac{1}{\epsilon(q)-\beta+i\eta\gamma} \tag{111}$$

I can evaluate this integral in a straight forward fashion, if $\beta < 0$. Then, I decouple the denominator:

$$\frac{1}{\epsilon(q)+|\beta|} = \frac{A}{q-i\sqrt{2m|\beta|}}+\frac{B}{q+i\sqrt{2m|\beta|}} \tag{112}$$

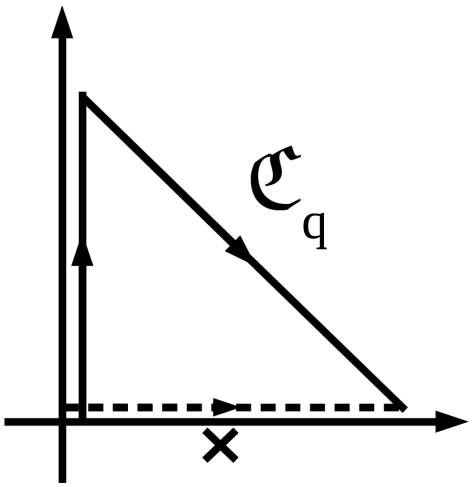

Figure 26: The complex plane for the magnitude of the momentum. The contour for the σ integration is hown by the directed line, and the pole of the integrand by the cross.

Multiplying with the right denominator and comparison yields

$$A = -B = -i\sqrt{\frac{m}{2|\beta|}} \tag{113}$$

so that the integral becomes

$$\begin{aligned}\int_0^{k_F} dq \frac{1}{\epsilon(q)+|\beta|} &= -i\sqrt{\frac{m}{2|\beta|}} \int_0^{k_F} \left(\frac{1}{q - i\sqrt{2m|\beta|}} - \frac{1}{q + i\sqrt{2m|\beta|}} \right) \\ &= -i\sqrt{\frac{m}{2|\beta|}} \left(\log(q - i\sqrt{2m|\beta|}) - \log(q + i\sqrt{2m|\beta|}) \right)_0^{k_F} \end{aligned} \tag{114}$$

When $\beta > 0$, I note that $\sigma(\beta, \gamma) = \sigma(\beta, -\gamma)^*$. For the case $\gamma > 0$ I shift the contour into the upper half plane, as in Fig. 26

$$\chi(\beta, \gamma) = \left(\int_0^{ik_F} + \int_{\gamma_2} \right) \frac{dq}{\epsilon(q) - \beta} \tag{115}$$

Now, the first integral has been computed before, as $\int_0^{ik_F} \frac{dq}{\epsilon(q)-\beta} = -\int_0^{k_F} \frac{dq}{\epsilon(q)+\beta}$. The integral over γ_2 can be computed by parametrizing the contour: I start at $q = ik_F$ and go in a straight line to $q = k_F$. So a simple parametrization is $q(x) = ik_F - x(ik_F - k_F)$.

Then $\frac{dq}{dx} = (1-i)k_F$ and

$$\begin{aligned}\int_{\gamma_2} \frac{dq}{\epsilon(q)-\beta} &= (1-i)k_F \int_0^1 \frac{dx}{\epsilon(q(x))-\beta} \\ &= (1-i)\frac{k_F}{\epsilon_F}\int_0^1 \frac{dx}{-2ix^2+2(1-i)ix-1-\beta/\epsilon_F} \\ &= \frac{m}{k_F}(1+i)\int_0^1 \frac{dx}{x^2-(1-i)x+\frac{-i}{2}(1+\beta/\epsilon_F)} = (*). \end{aligned} \tag{116}$$

Now, I decouple the denominator, just as above by finding the zeros

$$x_0 = \frac{i-1}{2} \pm \frac{1+i}{2}\sqrt{\frac{\beta}{\epsilon_F}} =: \phi_\pm. \tag{117}$$

Now I choose

$$\frac{1}{(x-\phi_-)(x-\phi_+)} = \frac{A}{x-\phi_-} + \frac{B}{x-\phi_+} \tag{118}$$

which, by the sae procedure as above leads to $A = -\frac{1-i}{2}\sqrt{\frac{\beta}{\epsilon_F}} = -B$ and

$$(*) = -\frac{m}{k_F}\sqrt{\frac{\epsilon_F}{\beta}}\left(\log(x-\phi_-) - \log(x-\phi_+)\right)_0^1 \tag{119}$$

This calculation has been done for $\gamma < 0$ as well and is implemented in a `MatLab` implementation. This implementation checks two things about σ, namely,

- Whether the imaginary part vanishs for $\beta \notin [0, \epsilon_F]$
- whether $\sigma(\beta,\gamma) = \sigma(\beta,-\gamma)^*$ holds.

The result for Σ_{FM} obeys importantly $\mathrm{sgn}\Im\Sigma_{\mathrm{FM}}(\omega) = \mathrm{sgn}(\epsilon_F - \omega)$.

B.1.4. Validation of the result

You can see in Fig. 27 that the self-energy is calculated accurately compared to the numerical result for the same integral. In Fig. 28 it can be seen, that the approximation to Σ_{FM} is accurate to machine precision. As both the values for small and large ω' fit the expectation, also comparing to Ref. [27], I expect this result to be correct.

B.2. The kernel of the polarizability K_χ

I aim to compute the integral

$$K_\chi(k,\omega,\omega') = \int \frac{dq}{(2\pi)^3} G(q+\frac{k}{2},\omega'+\frac{\omega}{2})G(q-\frac{k}{2},\omega'-\frac{\omega}{2}), \tag{120}$$

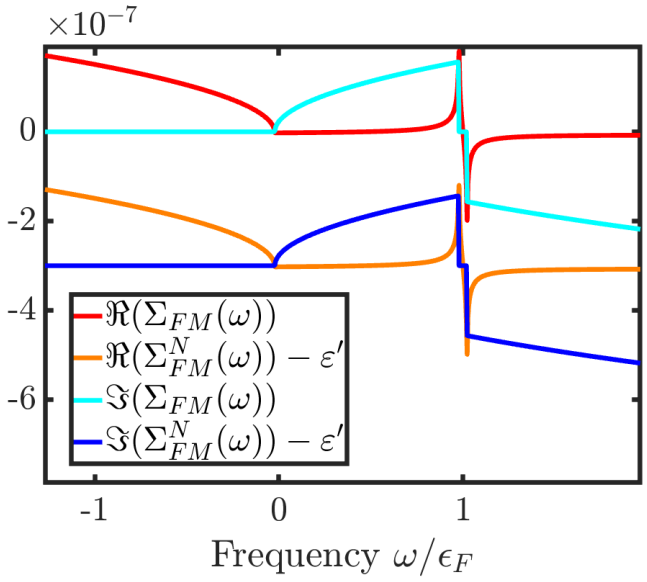

Figure 27: Result for the self-energy (with values in hartree). The numerical calculation gives precisely the same result as the analytically calculated. To see both lines, one has been shifted by ϵ'. The parameters for this calculation are $g = 100\text{meV}$, $\omega_{\text{ph}} = 100\text{meV}$ and $m = 0.2$.

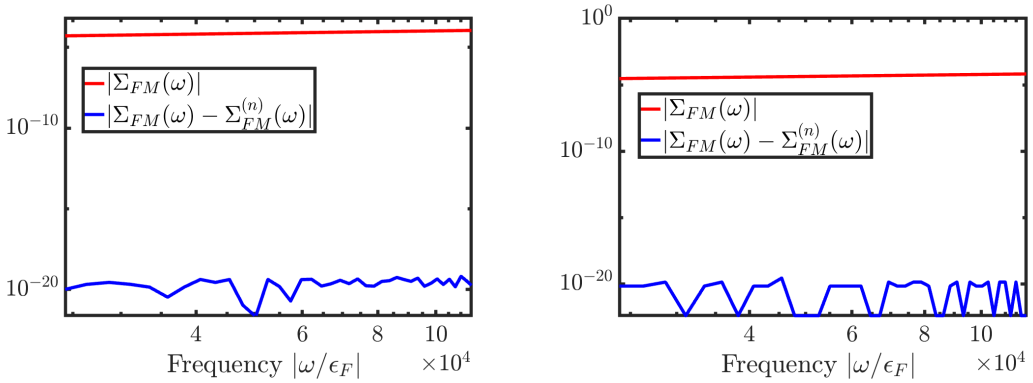

Figure 28: Result for the self-energy (with values in hartree). The approximation to the self-energy $\Sigma^{(n)}_{\text{FM}} = \Sigma_{\text{FM}} + \mathcal{O}(\omega^{-(n+\frac{3}{2})})$, with $n = 5$ is accurate to machine precision in this range for ω', for both positive (left figure) and negative (right figure) frequencies. The parameters for this calculation are $g = 100\text{meV}$, $\omega_{\text{ph}} = 100\text{meV}$ and $m = 0.2$.

which then allows to find the polarizability. The result of this integral has three cases, dependent on whether none, one or two Green's functions have a finite imaginary part. The result is found in the theorem block below, where $I_1(\omega_1, \omega_2) = K_\chi$ and ω_i is the (self-energy shifted) frequency inside the electron Green's function.

B.2.1. The result

Theorem 6 (Kernel of the polarizability)**.** *The kernel of the polarizability is* ***for two real frequencies***

$$I_1 = M + B_1 \tag{121}$$

with

$$M = \frac{m^2}{(2\pi)^2 k} \sum_{a \in \pm\xi_S} \left(S_R(a, \xi_p^+, \xi_p^-) - S_R(a, -\xi_p^+, -\xi_p^-) \right) \tag{122}$$

and $\xi_p^\pm = 1 \pm \frac{\sqrt{-2m\omega_2}}{k}$, $\xi_S = \sqrt{\frac{-\omega_1 + i0 sgn(\omega_1 + \epsilon_F)}{\epsilon(k)}}$ *as well as* $\vartheta = \Re(\sqrt{\frac{-\omega_2}{\epsilon(k)}})$*. If* $\vartheta = 0$

$$S_R(a, b, c) = -\sum_{p \in b,c} I_R(a, p) \tag{123}$$

with $x_0 = \frac{\Im(ab^*)}{\Im(a+b)}$ *it is for* $-\Re(\frac{a+x_0}{b-a}) < 1$

$$I_R(a, b) = \log(a) \log(\frac{b}{b-a}) + \frac{\log(b-a)^2}{2} \tag{124}$$

and otherwise

$$\begin{aligned} I_R(a, b = &- \log(a-b) \left(\log(b-a) - \log(a-b) \right) + \log(a) \log(\frac{b}{b-a}) \\ &+ \log(\frac{a}{a-b}) \left(\log(\frac{b}{b-a}) - \log(\frac{b}{a-b}) \right) \\ &+ \frac{\log(b-a)^2}{2}. \end{aligned} \tag{125}$$

If $\vartheta > 0$

$$\begin{aligned} S_R(a, b, c) = &- \sum_{p \in b,c} \left(\frac{\log(a+p)^2}{2} + \log|p| \log(\frac{a}{a+p}) \right) \\ &+ i\pi \left(\log(\kappa_+ + a) - \log(\kappa_- + a) \right) \end{aligned} \tag{126}$$

with $\kappa_\pm = \max(0, 1 \pm \vartheta)$. *And*

$$B_1 = \frac{im^2}{2\pi k} \sum_{a \in \xi_\pm} [l_1(a) + l_2(a) + l_3(a)] \tag{127}$$

with

$$\begin{aligned} l_1(a) &= \theta(\mu_1) \left(\log(\mu_1 + a) - \log(a)\right) - \log(\mu_2 + a) \\ l_2(a) &= \theta(\epsilon_F + \omega_2) \left(\log(1 + \xi_F + a) - \log(|1 - \xi_F| + a)\right) \\ l_3(a) &= \log(\delta + a). \end{aligned} \tag{128}$$

For one complex frequency, *where* ω_R *is the real frequency*

$$I_1(\omega_R, \omega_C, k) = \frac{-m^2}{(2\pi)^2 k} \sum_{a \in \pm\xi_p} \sum_{b \in \xi_\pm} [P_R(a, b) - P_R(a, -b)] \tag{129}$$

with $\xi_p = \sqrt{-\frac{\omega_R}{\epsilon(k)} - i0 sgn(\omega_R - \epsilon_F)}$ *with now*

$$P_R(a, b) = \begin{cases} P_2(a, b) & a \in \mathbb{R}^+ \\ P_{11}(a, b) & x_0 = -\frac{\Im(ab^*)}{\Im(a+b)} > 0 \text{ and } \Re(\frac{a - x_0}{a+b} - 1) \\ P_{12}(a, b) & else \end{cases} \tag{130}$$

with the three objects

$$\begin{aligned} P_{11}(a, b) = &\log(\frac{a}{a+b} - 1) \log(-a) - \left(\log(\frac{-b}{a+b}) - \log(\frac{b}{a+b})\right) \log(\frac{a}{a+b}) \\ &- \left(-\log(a+b)^2/2 + \log(-(a+b))(\log(a+b) - \log(-(a+b)))\right), \end{aligned} \tag{131}$$

$$P_{12}(a, b) = \log(\frac{b}{a+b}) \log(-a) + \log(a+b)^2, \tag{132}$$

and

$$\begin{aligned} P_2(a, b) = &- i\pi sgn(\Im(a)) \left(\log(\Re(a) + b) - \log(b)\right) - \log(\frac{b}{a+b}) \log(a) \\ &- \log(a+b)^2/2. \end{aligned} \tag{133}$$

For two complex frequencies *I find, with* $\alpha = \omega_1 - \Sigma(\omega_1)$, *and* $\beta = \omega_2 - \Sigma(\omega_2)$

$$I_1(\alpha, \beta, k) = \frac{m^2}{(2\pi)^2 k} \sum_{a \in \pm\xi_S} \sum_{b \in \xi_\pm} \left[J^R(a, b) - J^R(a, -b)\right] \tag{134}$$

with $\xi_S = \sqrt{\frac{\alpha}{\epsilon(k)}}$ *and* $\xi_\pm = 1 \pm \sqrt{\frac{\beta}{\epsilon(k)}}$. *Then, I find*

$$J^R(a,b) = \begin{cases} J_2^R(a,b) & x_0 = -\frac{\Im(ab^*)}{\Im(a+b)} > 0 \text{ and } \Re(\frac{a-x_0}{a+b} - 1) < 0 \\ J_1^R(a,b) & else \end{cases} \tag{135}$$

with

$$J_i^R(a,b) = j_i^R(a,b) - j_i(a,b,0) \tag{136}$$

with

$$\begin{aligned} j_1^R(a,b) &= -\log(a+b)^2/2 + (\log(a+b) - \log(-(a+b)))\log(-(a+b)) \\ j_2^R(a,b) &= -\log(a+b)^2 \\ j_1(a,b,0) &= \log(-a)\log(\frac{-b}{a+b}) + \left(\log(\frac{b}{a+b}) - \log(\frac{-b}{a+b})\right)\log(\frac{a}{a+b}) \\ j_2(a,b,0) &= \log(-a)\log(\frac{b}{a+b}). \end{aligned} \tag{137}$$

B.2.2. Large ω' expansion and error estimation

$$I_1 = -\int \frac{dq}{(2\pi)^3} \frac{1}{\epsilon(q+\frac{k}{2}) - \omega_1 - i\eta_{q+\frac{k}{2}}} \frac{1}{\epsilon(q-\frac{k}{2}) - \omega_2 - i\eta_{q-\frac{k}{2}}} \tag{138}$$

Note here, that the infinitesimals only play a role if the denominator is zero. So I can replace

$$\eta_{q\pm\frac{k}{2}} = \eta \ \mathrm{sgn}(\omega_{1/2} - \epsilon_F) = \eta \ \gamma_{1/2} \tag{139}$$

$$I_1 = -\int \frac{dq}{(2\pi)^3} \frac{1}{\epsilon(q+\frac{k}{2}) - \omega_1 - i\eta\gamma_1} \frac{1}{\epsilon(q-\frac{k}{2}) - \omega_2 - i\eta\gamma_2} \tag{140}$$

Now, it is important to notice, that the frequencies $\omega_i = \omega' \pm \frac{\omega}{2} - \omega_{\mathrm{ph}}$ lead to the same $\gamma_i = \mathrm{sgn}(\omega')$ if $|\omega'| > |\frac{\omega}{2}| + \omega_{\mathrm{ph}} + \epsilon_F$. So, replacing in the integral, $\alpha = \omega_1 + i0\gamma$ and $\beta = \omega_2 + i0\gamma$, I can write

$$I_1 = -\int \frac{dq}{(2\pi)^3} \frac{1}{\epsilon(q+\frac{k}{2}) - \alpha} \frac{1}{\epsilon(q-\frac{k}{2}) - \beta}. \tag{141}$$

That α and β have the same sign in their imaginary part, holds true, also in the dressed

case and is vital, to use Feynman parameters

$$\frac{1}{AB} = \int_0^1 \frac{du}{[uA + (1-u)B]^2}. \tag{142}$$

I can set $A = \epsilon(q + \frac{k}{2}) - \alpha$ and $B = \epsilon(q - \frac{k}{2}) - \beta$. Now, I complete the square

$$\begin{aligned} uA + (1-u)B = u\epsilon(q + \frac{k}{2}) + (1-u)\epsilon(q - \frac{k}{2}) \\ - u\alpha - (1-u)\beta. \end{aligned} \tag{143}$$

The first line of this is

$$\frac{1}{2m}[q^2 + ukq + u\frac{k^2}{4} + (1-u)(-kq) + (1-u)\frac{k^2}{4}] = \frac{1}{2m}[q^2 + (2u-1)kq + \frac{k^2}{4}] = (*) \tag{144}$$

Now I introduce $l = q + \frac{2u-1}{2}k$ so that

$$(*) = \frac{1}{2m}[l^2 + k^2 u(1-u)]. \tag{145}$$

Then I obtain ($|\frac{\partial l}{\partial q}| = 1$)

$$I_1 = -4m \int_0^1 du \int \frac{dl}{(2\pi)^3} \frac{1}{[l^2 + k^2 u(1-u) - 2mu\alpha - 2m(1-u)\beta]^2}. \tag{146}$$

I then define $\phi := k^2 u(1-u) - 2mu\alpha - 2m(1-u)\beta$ and switch to spherical coordinates in l, and note that the integrand is symmetric in l:

$$I_1 = -\frac{m^2}{\pi^2} \int_0^1 du \int_{\mathbb{R}} \frac{l^2 dl}{[l^2 + \phi]^2}. \tag{147}$$

The denominator has zeros at $l_0^{\pm} = \pm\sqrt{-\phi}$. Now, by definition of the squareroot $\mathrm{sgn}(\Im(\sqrt{-\phi})) = -\mathrm{sgn}(\Im(\phi)) =: -\kappa$ and $\mathrm{sgn}(\Im(l_0^{\pm})) = \mp\kappa$. I now choose the contour that circumvents l_0^+. Then I get

$$\int_{\mathbb{R}} \frac{l^2 dl}{[l^2 + \phi]^2} = -\mathrm{sgn}(\kappa) 2\pi i \frac{d}{dl} \frac{l^2}{[l + l_0^+]^2}|_{l=l_0^+} = -\mathrm{sgn}(\kappa) \frac{i\pi}{2l_0^+} \tag{148}$$

and put this back into I_1:

$$I_1 = \frac{im^{3/2}}{2^{3/2}\pi\sqrt{\epsilon(k)}} \mathrm{sgn}(\kappa) \int_0^1 \frac{du}{\sqrt{u^2 + u\left(\frac{\alpha-\beta}{\epsilon(k)} - 1\right) + \frac{\beta}{\epsilon(k)}}}. \tag{149}$$

Now, as I aim to expand the object in ω', I identify $\alpha - \beta = \mathscr{O}(\omega'^0)$ and $\beta = \mathscr{O}(\omega')$.

This means, if

$$|\omega'| > |\beta - \omega'| + |\alpha - \beta - \epsilon(k)| + \epsilon(k), \tag{150}$$

I can expand in ${\omega'}^{-1}$. I define $f(u) = u^2 + u\left(\frac{\alpha-\beta}{\epsilon(k)} - 1\right) + \frac{\beta-\omega'}{\epsilon(k)}$. Now, for $\omega' > 0$,

$$I_1 = \frac{-im^{3/2}}{2^{3/2}\pi\sqrt{|\omega'|}} \int_0^1 \frac{du}{\sqrt{1 + \frac{f(u)\epsilon(k)}{|\omega'|}}}. \tag{151}$$

and for $\omega' < 0$

$$I_1 = \frac{-m^{3/2}}{2^{3/2}\pi\sqrt{|\omega'|}} \int_0^1 \frac{du}{\sqrt{1 - \frac{f(u)\epsilon(k)}{|\omega'|}}}. \tag{152}$$

The integrand can now be expanded in terms of $\frac{f(u)\epsilon(k)}{|\omega'|}$, and integrated term by term, leading to an asymptotic expansion of I_1. This is implemented in a `Mathematica 11.1` script and linked to `MatLab` to compute corrections to the integrals over I_1, see Sec.C. The generalization to the dressed case, lies in including the expansion for Σ_{FM} in $f(u)$. This converges because $|\Sigma_{\text{FM}}(\omega)| < |\omega|$ for $|\omega|$ large.

The error estimation for the polarizability in Eq.(81) can now be calculated.

I aim to calculate the polarizability. To do this I start with the following integral

$$\tilde{\chi}(k,\omega) = \int_{-\Lambda}^{\Lambda} \frac{d\omega'}{2\pi} \left(K_\chi(k,\omega,\omega') - f(\omega')\right) + \mathscr{O}(\omega^{-1/2}) + c. \tag{153}$$

Now, introducing correction terms, I can reduce the error with respect to the threshold:

$$\tilde{\chi}(k,\omega) = \int_{-\Lambda}^{\Lambda} \frac{d\omega'}{2\pi} \left(K_\chi(k,\omega,\omega') - f(\omega')\right) + \mathscr{O}(\omega^{-n}) + c. \tag{154}$$

To now find the polarizability, I have to extract the constant c with the `fixPolarizabilityAsymptot` procedure. Then I obtain the polarizability as

$$\chi(k,\omega) = \int_{-\Lambda}^{\Lambda} \frac{d\omega'}{2\pi} \left(K_\chi(k,\omega,\omega') - f(\omega')\right) + \mathscr{O}(\omega^{-n}) + (c - \tilde{c}). \tag{155}$$

The task of this section is to estimate the calculation errors that are introduced. The three errors are caused by, first, the accuracy of the integration routine, that can be defined by an input parameter, secondly the error made, when the integral is truncated, which can be reduced by introducing higher order corrections and, lastly, the error due to the back-shift procedure determining c. The error by the correction terms can be

calculated as follows. I take the identity $K_\chi = I_1$ and Eq. (151) for large $|\omega'|$

$$I_1 = \frac{im^{3/2}}{2^{3/2}\pi\sqrt{|\omega'|}} \int_0^1 \frac{du}{\sqrt{1 + \frac{f(u)\epsilon(k)}{|\omega'|}}}. \tag{156}$$

I define now

$$F(x) = \frac{1}{\sqrt{1+x}} \tag{157}$$

and it's approximating functions to be polynomials with $F^{(n)}(x) = \sum_i^n a_n x^n$ so that $F(x) - F^{(n)}(x) = \mathscr{O}(x^{n+1})$. Then I find from Ref. [49, p.376]

$$|F(x) - F^{(n)}(x)| = |R_{n+1}(x)| \leq \frac{M_{|x|}|x|^{n+1}}{1-|x|} = \frac{|x|^{n+1}}{(1-|x|)^{3/2}} \tag{158}$$

I define the helping function

$$I_1^{(n)} = \frac{im^{3/2}}{2^{3/2}\pi\sqrt{|\omega'|}} \int_0^1 du F^{(n)}(x(u)). \tag{159}$$

The difference $I_1 - I_1^{(n)}$ can now be calculated as

$$\begin{aligned} |I_1 - I_1^{(n)}| &= \frac{m^{3/2}}{2^{3/2}\pi\sqrt{|\omega'|}} | \int_0^1 du F(x(u)) - F^{(n)}(x(u))| \\ &\leq \frac{m^{3/2}}{2^{3/2}\pi\sqrt{|\omega'|}} \max_{x(u)|u\in[0,1]} |F(x(u)) - F^{(n)}(x(u))|. \end{aligned} \tag{160}$$

Now I want to estimate $|F(x(u)) - F^{(n)}(x(u))|$.

$$|F(x(u)) - F^{(n)}(x(u))| \leq \frac{|x|^{n+1}}{(1-|x|)^{3/2}} \tag{161}$$

and

$$
\begin{aligned}
x(u) &= \frac{f(u)\epsilon(k)}{|\omega'|} \\
|f(u)| &= |u^2 + u\left(\frac{\alpha-\beta}{\epsilon(k)} - 1\right) + \frac{\beta-\omega'}{\epsilon(k)}| \\
&\leq 1 + |\frac{\alpha-\beta}{\epsilon(k)} - 1| + |\frac{\beta-\omega'}{\epsilon(k)}| = \widehat{f} \\
\rightarrow |x(u)| &\leq \frac{\widehat{f}\epsilon(k)}{|\omega'|} = \widehat{x}(\omega') \\
\rightarrow |F(x(u)) - F^{(n)}(x(u))| &\leq \frac{\widehat{x}(\omega')^{n+1}}{(1-\widehat{x}(\Lambda))^{3/2}}
\end{aligned} \tag{162}
$$

Looking back to Eq.(155), I find the error $\mathscr{O}(\Lambda^{-n})$ as

$$
\begin{aligned}
\Delta_2 &= 4\int_\Lambda^\infty \frac{d\omega'}{2\pi}|I_1 - I_1^{(n)}| \\
&\leq \frac{m^{3/2}}{\sqrt{2}\pi^2}\frac{(\widehat{f}\epsilon(k))^{n+1}}{(1-\widehat{x}(\Lambda))^{3/2}}\frac{1}{(n+\frac{1}{2})\Lambda^{n+\frac{1}{2}}}
\end{aligned} \tag{163}
$$

Note that, with the dressed propagator, I additionally need to expand the self-energy. When this is done, an additional correction of the order $g^2\Delta_2$ appears, that is neglected here. The last equation can be evaluated and yields for the extrapolation frequencies around $\omega = 10^3\epsilon_F$ for $n = 1$ an estimate of 4.2×10^{-4}, for $n = 4$ an estimate of 4.1×10^{-7} and for $n = 5$ an estimate of 1.3×10^{-8}. The parameters for this calculation are $g = 100$meV, $\omega_{\text{ph}} = 100$meV and $m = 0.2$, $k = k_F$. This error is in for small frequencies negligible, if $n > 2$. Note that, for large external frequencies, $\widehat{x}(\omega') = \frac{3\omega}{2\omega'}$. So, for large frequencies, this procedures delivers the largest error - therefore the order of the expansion needs to be pushed ahead, if c should be calculated accurately. The error of the shift procedure is determined within the routine see Sec.C. The absolute error of the integration routine is set to be 10^{-11}, which is tested internally in `MatLab`'s `integral` routine, see `https://www.mathworks.com/help/matlab/ref/integral.html` (looked up on the 10^{th} of march 2019 at 10:44:24).

B.2.3. The calculation of K_χ

To avoid confusion: I_1 and K_χ are the same integrals.

The computation of I_1 for two real frequencies.

$$
\begin{aligned}
I_1 &= -\int \frac{dq}{(2\pi)^3} \frac{1}{\epsilon(q+\frac{k}{2}) + \omega_{\rm ph} - \omega' - \frac{\omega}{2} - i\eta_{q+\frac{k}{2}}} \frac{1}{\epsilon(q-\frac{k}{2}) + \omega_{\rm ph} - \omega' + \frac{\omega}{2} - i\eta_{q-\frac{k}{2}}} \\
&= -\int_0^\infty dq \frac{q^2}{(2\pi)^2} \frac{1}{\epsilon(q) + \omega_{\rm ph} - \omega' - \frac{\omega}{2} - i\eta_q} \times \\
&\quad \int_{-1}^1 dx \frac{1}{-\frac{qk}{m}x + \frac{q^2+k^2}{2m} + \omega_{\rm ph} - \omega' + \frac{\omega}{2} - i\eta_{q-k}} \\
&= \frac{m}{k}\int_0^\infty dq \frac{q}{(2\pi)^2} \frac{1}{\epsilon(q) + \gamma - i\eta_q} A(\phi) \\
&= \frac{m}{k}\int_0^\infty dq \frac{q}{(2\pi)^2} \frac{1}{\epsilon(q) + \gamma - i\eta_q} \{\log(1+\phi - i\eta) - \log(-1+\phi - i\eta) \\
&+ 2\pi i\{(\theta(k - k_F - q) + \theta(q - k_F - k))\theta(-(1+\phi)) \\
&+ \theta(q + k_F - k)\theta(q + k - k_F)\theta(k_F + k - q)\theta(-(\phi + x_0)) \\
&- \theta(q + k - k_F)\theta(1-\phi)\}\}
\end{aligned} \tag{164}
$$

with $\gamma = \omega_{\rm ph} - \omega' - \frac{\omega}{2}$, $\phi = \frac{m}{qk}\left(-\frac{q^2+k^2}{2m} - \omega_{\rm ph} + \omega' - \frac{\omega}{2}\right)$ and A from Eq. (192) below. I will first take care about the first line, which I call M. Without any change, I multiply both logarithm arguments by $\frac{qk}{m}$ and can then write them as

$$
\log(-(q-q_p^+)(q-q_p^-) - i\eta) - \log(-(q+q_p^+)(q+q_p^-) - i\eta) \tag{165}
$$

with $\tilde{\eta} = \omega_{\rm ph} - \omega' + \frac{\omega}{2}$ and $q_p^\pm = k \pm \sqrt{-2m\tilde{\eta}}$. Then I decouple $\frac{q}{\epsilon(q)+\gamma-i\eta_q}$ with $q_S = \sqrt{-2m(\gamma + i\eta{\rm sgn}(\epsilon_F + \gamma))}$ and change variables $\xi = q/k$

$$
\begin{aligned}
M = \frac{m^2}{(2\pi)^2 k} \sum_{a\in\pm\xi_S} \int_0^\infty \frac{d\xi}{\xi + a} (&\log(-(\xi - \xi_p^+)(\xi - \xi_p^-) - i\eta) \\
&- \log(-(\xi + \xi_p^+)(\xi + \xi_p^-) - i\eta)).
\end{aligned} \tag{166}
$$

In order to solve this integral, I define the helping quantity

$$
S_s(a,b,c;y) = \int_0^y \frac{d\xi}{\xi + a} \log(-(\xi - b)(\xi - c) - i\eta) \tag{167}
$$

with $y \gg 1$. Note that b, c are real, or their complex conjugates:

$$
\begin{aligned}
b &= s + 1/k\sqrt{-2m\tilde{\eta}} \\
c &= s - 1/k\sqrt{-2m\tilde{\eta}} \\
s &= \pm 1
\end{aligned} \tag{168}
$$

I split the logarithms real and imaginary part to obtain

$$S(a,b,c;y) = \int_0^y \frac{d\xi}{\xi+a} \log|-(\xi-b)(\xi-c)| \\ - i\pi\theta((\xi-b)(\xi-c)) \tag{169}$$

In order to have an analytic function again, I split the region of integration into three. I call $\vartheta = \Re(\sqrt{-2m\tilde{\eta}}/k)$ and $\kappa_\pm = \max(0, s \pm \vartheta)$. Then

$$S(a,b,c;y) = \left(\int_0^{\kappa_-} + \theta(\vartheta) \int_{\kappa_-}^{\kappa_+} + \int_{\kappa_+}^{y} \right) \frac{d\xi}{\xi+a} \log|-(\xi-b)(\xi-c)| - i\pi\theta((\xi-b)(\xi-c)). \tag{170}$$

Case 1: ϑ is zero. Then I find the indefinite integrals of the functions above with

$$T(\xi) = \int d\xi \frac{\log((\xi-b)(\xi-c))}{\xi+a} \\ = \log(\xi+a)\log((\xi-b)(\xi-c)) - \sum_{g\in b,c} \int \frac{\log(\xi+a)}{\xi-g} \tag{171}$$

$$S(a,b,c;y) = T(y) - T(0) - i\pi\left[\log(y+a) - \log(a)\right]. \tag{172}$$

Now I define

$$I(a,b;y) = \int_0^y \frac{\log(\xi+a)}{\xi-b}. \tag{173}$$

I have to be sure, the new contour crosses no branch cut. I find with

$$x_0 = \frac{1}{y}\frac{\Im(ab^*)}{\Im(b-a)}, \tag{174}$$

that if $-\Re(\frac{a+x_0 y}{b-a}) < 1$ and $x_0 \in [0,1]$, the integral is

$$I(a,b;y) = \{\log((a+b)\psi)\log(1-\psi) + \mathrm{Li}_2(\psi)\}_{\frac{a}{a+b}}^{\frac{a+y}{a+b}} \tag{175}$$

and otherwise

$$I(a,b;y) = \{\log((a+b)\psi)\log(\psi-1) + \mathrm{Li}_2(\psi) + \\ \log(\psi)(\log(1-\psi) - \log(\psi-1))\}_{\frac{a}{a+b}}^{\frac{a+y}{a+b}}. \tag{176}$$

To find the implemented functions, I will now separate the terms that cancel each other in the limit $y \to \infty$. The rest, or regularized term, I call S_R. I use the asymptotic expansion of the dilogarithm ($|y| \gg 1$) [72]

$$\mathrm{Li}_2(y) = -\frac{1}{2}\log(-y)^2 + C \tag{177}$$

with C some constant. Then, for the first case

$$\begin{aligned} I(a,b;y \gg 1) = \log(y+a)\log(\frac{b-y}{a+b}) + \mathrm{Li}_2(\frac{a+y}{a+b}) \\ - \log(a)\log(\frac{a}{a+b}) - \mathrm{Li}_2(\frac{a}{a+b}). \end{aligned} \tag{178}$$

I call the second line $-I_l(a,b)$ and use that for $y \gg 1$: $\Im(\log(y+a)) \approx 0$ for every $a \in \mathbb{C}$, so that $\log((y+a)/b) = \log(y+a) - \log(b)$ without an extra phase

$$\begin{aligned} I(a,b;y \gg 1) &= \log(y+a)\left(\log(y-b) - \log(-(a+b))\right) \\ &\quad - \frac{\left(\log(y+a) - \log(-(a+b))\right)^2}{2} + C - I_l(a,b) \\ &= \frac{1}{2}\log(y+a)\log(y-b) - \frac{1}{2}\log(-(a+b))^2 + C - I_l(a,b) \end{aligned} \tag{179}$$

and for the second case

$$\begin{aligned} I(a,b;y \gg 1) &= \frac{1}{2}\log(y+a)\log(y-b) - \frac{1}{2}\log(-(a+b))^2 \\ &\quad + \log(a+b)\left[\log(-(a+b)) - \log(a+b)\right] + C - \log(a)\log(\frac{-b}{a+b}) \\ &\quad + \mathrm{Li}_2(\frac{a}{a+b}) + \log(\frac{a}{a+b})\left[\log(\frac{b}{a+b}) - \log(\frac{-b}{a+b})\right] \end{aligned} \tag{180}$$

where I call $I_l^{(2)}(a,b) = \log(a)\log(\frac{-b}{a+b}) + \mathrm{Li}_2(\frac{a}{a+b}) + \log(\frac{a}{a+b})\left[\log(\frac{b}{a+b}) - \log(\frac{-b}{a+b})\right]$. Then I can define their regularized contribution to the integral: I can extinct all y dependent functions by subtraction of $I(a,b;y) - I(a,-b;y)$ and just keep the rest term:

$$I_R(a,b) = \log(a)\log(\frac{b}{b-a}) + \frac{\log(b-a)^2}{2} \tag{181}$$

and

$$\begin{aligned} I_R(a,b) &= -\log(a-b)\left(\log(b-a) - \log(a-b)\right) + \log(a)\log(\frac{b}{a-b}) \\ &\quad + \log(\frac{a}{a-b})\left(\log(\frac{b}{b-a}) - \log(\frac{b}{a-b})\right) + \frac{\log(b-a)^2}{2}. \end{aligned} \tag{182}$$

And the regularized S then is

$$S_R(a,b,c) = -\sum_{p\in b,c} I_R(a,p). \tag{183}$$

Case 2: for non-zero ϑ I find

$$\begin{aligned}
S(a,b,c;y) &= \int_0^y d\xi \frac{\log(|(\xi-b)(\xi-c)|)}{\xi+a} \\
&\quad - i\pi\left[\log(y+a) - \log(\kappa_+ + a) + \log(\kappa_1 + a) - \log(a)\right] \\
&= \sum_{g\in b,c} \theta(g) \int_0^g d\xi \frac{\log(g-\xi)}{\xi+a} + \int_{\max(0,g)}^y d\xi \frac{\log(\xi-g)}{\xi+a} \\
&\quad - i\pi\left[\log(y+a) - \log(\kappa_+ + a) + \log(\kappa_- + a) - \log(a)\right] \\
&= \sum_{g\in b,c} \left[\log|\xi-g| \log(\frac{\xi+a}{a+g}) + \mathrm{Li}_2(\frac{g-\xi}{a+g})\right]_0^y \\
&\quad - i\pi\left[\log(y+a) - \log(\kappa_+ + a) + \log(\kappa_1 + a) - \log(a)\right]
\end{aligned} \tag{184}$$

this becomes for large y

$$\begin{aligned}
S(a,b,c;y) &= \sum_{g\in b,c} \left[\frac{1}{2}\log(y-g)^2 - \frac{1}{2}\log(a+g)^2 - \log|g| \log(\frac{a}{a+g}) - \mathrm{Li}_2(\frac{g}{a+g})\right] \\
&\quad - i\pi\left[\log(y+a) - \log(\kappa_+ + a) + \log(\kappa_1 + a) - \log(a)\right]
\end{aligned} \tag{185}$$

and the regularized part of this is

$$\begin{aligned}
S_R(a,b,c) &= -\sum_{p\in b,c} \left(\frac{\log(a+p)^2}{2} + \log|p| \log(\frac{a}{a+p})\right) \\
&\quad + i\pi\left(\log(\kappa_+ + a) - \log(\kappa_- + a)\right)
\end{aligned} \tag{186}$$

with $\vartheta = \Re(\sqrt{-2m\tilde{\eta}}/k)$ and $\kappa_\pm = \max(0, s \pm \vartheta)$. With these equations, I have found the solution of M

$$M = \frac{m^2}{(2\pi)^2 k} \sum_{a\in\pm\xi_S} \left(S_R(a,\xi_p^+,\xi_p^-) - S_R(a,-\xi_p^+,-\xi_p^-)\right) \tag{187}$$

The θ functions yield now an extra term of

$$B_1 = \frac{im^2}{2\pi k} \sum_{a\in\pm\xi_S} \left[l_1(a) + l_2(a) + l_3(a)\right] \tag{188}$$

l_i corresponds to the i^{th} line of the θ functions in the integral. With $\tilde{\eta} = \omega_{\mathrm{ph}} - \omega' + \frac{\omega}{2}$, $\vartheta = \Re(\sqrt{-2m\tilde{\eta}})/k$, $\mu_1 = \min(1-\xi_F, 1-\vartheta)$, $\mu_2 = \max(1+\xi_F, 1+\vartheta)$ and $\delta =$

$\max(0, \xi_F - 1, \vartheta - 1)$, I have

$$\begin{aligned} l_1(a) &= \theta(\mu_1)\left(\log(\mu_1 + a) - \log(a)\right) - \log(\mu_2 + a) \\ l_2(a) &= \theta(\epsilon_F + \tilde{\eta})\left(\log(1 + \xi_F + a) - \log(|1 - \xi_F| + a)\right) \\ l_3(a) &= \log(\delta + a) \end{aligned} \tag{189}$$

Then $I_1 = M + B_1$.

And here I used especially the auxiliary integral $A(\phi)$

$$A(\phi) = \int_{-1}^{1} \frac{dx}{x + \phi + i\eta_{q-k}}. \tag{190}$$

The indefinite integral is $\log(x + \phi + i\eta_{q-k})$. So that I have to find out, where the infinitesimal switches sign, and when this happens in $x \in [-1, 1]$. The function switches for $x < -1$ if $k + q < k_F$; for $x > 1$ if $k - q > k_F$; and at $x_0 = \frac{q^2 + k^2 - k_F^2}{2k_1 k}$ in the third case.

The x integral depends on the infinitesimal involved. So the integral splits. The latter integral becomes

$$\begin{aligned} A(\phi) =& \theta(k_F - k - q)\{\log(1 + \phi - i\eta) - \log(-1 + \phi - i\eta)\} \\ &+(\theta(k - k_F - q) + \theta(q - k_F - k))\{\log(1 + \phi + i\eta) - \log(-1 + \phi + i\eta)\} \\ &+\theta(q + k_F - k)\theta(q + k - k_F)\theta(k_F + k - q) \\ &\quad \{\log(1 + \phi - i\eta) - \log(-1 + \phi + i\eta) + 2\pi i\theta(-(\phi + x_0))\}. \end{aligned} \tag{191}$$

I note, that for $q < k_F$ the last θ in the second row is wrong; while the third in the third row is true. Now I can proceed by using the the integrated version of Eq. (73), which I already used once for $\log(x_0 + \phi + i\eta) - \log(x_0 + \phi - i\eta) = 2\pi i\theta(-(\phi + x_0))$ for $\phi \in \mathbb{R}$. I shift all infinitesimals to negative sign, with

$\log(a + \phi + i\eta) = \log(a + \phi - i\eta) + 2\pi i\theta(-(a + \phi))$.

Then, I obtain

$$\begin{aligned} A(\phi) = \log(1 + \phi - i\eta) - \log(-1 + \phi - i\eta) \\ +2\pi i\{(\theta(k - k_F - q) + \theta(q - k_F - k))\theta(-(1 + \phi)) \\ + \theta(q + k_F - k)\theta(q + k - k_F)\theta(k_F + k - q)\theta(-(\phi + x_0)) \\ - \theta(q + k - k_F)\theta(1 - \phi)\} \end{aligned} \tag{192}$$

The integral I_1 for two complex frequencies.

$$I_1(\alpha, \beta, k) = -\int_{\mathbb{R}^3} \frac{dq}{(2\pi)^3} \frac{1}{\epsilon(q + \frac{k}{2}) - \alpha} \frac{1}{\epsilon(q - \frac{k}{2}) - \beta}. \tag{193}$$

Now, I shift $q \to q - \frac{k}{2}$ and can write, in spherical coordinates with $x = \cos(\theta)$

$$\begin{aligned}\epsilon(q-k) - \beta &= \frac{1}{2m}[q^2 - 2kqx + k^2 - 2m\beta] \\ &= \frac{-kq}{m}[x - \frac{q^2 + k^2 - 2m\beta}{2kq}]\end{aligned} \tag{194}$$

so that

$$\int_{-1}^{1} \frac{dx}{\epsilon(q-k) - \beta} = -\frac{m}{kq} \log(x - \frac{q^2 + k^2 - 2m\beta}{2kq})|_{x=-1}^{1}. \tag{195}$$

Then

$$I_1 = \frac{m}{(2\pi)^2 q} \int_0^\infty dq \frac{q}{\epsilon(q) - \alpha} \left(\log(-(q-k)^2 - 2m\beta) - \log(-(q+k)^2 - 2m\beta)\right) \tag{196}$$

Now I split the first fraction apart:

$$\frac{q}{\epsilon(q) - \alpha} = \frac{m}{q - \sqrt{2m\alpha}} + \frac{m}{q + \sqrt{2m\alpha}}. \tag{197}$$

with $q_S := \sqrt{2m\alpha}$ I obtain

$$I_1 = \frac{m^2}{(2\pi)^2 q} \sum_{a \in \pm q_S} \int_0^\infty \frac{dq}{q - a} \left(\log(-(q-k)^2 - 2m\beta) - \log(-(q+k)^2 - 2m\beta)\right). \tag{198}$$

I substitute $\xi = q/k$ ($\xi_S = q_S/k$) and get

$$I_1 = \frac{m^2}{(2\pi)^2 q} \sum_{a \in \pm \xi_S} \int_0^\infty \frac{d\xi}{\xi - a} \left(\log(-(\xi-1)^2 - \frac{\beta}{\epsilon(k)}) - \log(-(\xi+1)^2 - \frac{\beta}{\epsilon(k)})\right). \tag{199}$$

Decoupling the log's argument gives with $\xi_\pm = 1 \pm \sqrt{\frac{\beta}{\epsilon(k)}}$ yields

$$I_1 = \frac{m^2}{(2\pi)^2 q} \sum_{a \in \pm \xi_S} \int_0^\infty \frac{d\xi}{\xi - a} \left(\log(-(\xi - \xi_+)(\xi - \xi_-)) - \log(-(\xi + \xi_+)(\xi + \xi_-))\right). \tag{200}$$

Using partial integration I get

$$I_1 = -\frac{m^2}{(2\pi)^2 q} \sum_{a \in \pm \xi_S} \sum_{b \in \xi_\pm} \int_0^\infty d\xi \left(\frac{1}{\xi + b} - \frac{1}{\xi - b}\right) \log(\xi - a). \tag{201}$$

To evaluate this, I define

$$J(a,b,y) = \int_0^y d\xi \frac{\log(\xi - a)}{\xi + b}. \tag{202}$$

I aim to reduce this to a dilogarithm. For this purpose, I substitute $\phi = \xi - a$

$$J(a,b,y) = \int_{-a}^{y-a} d\xi \frac{\log(\phi)}{\phi + a + b}. \tag{203}$$

and $\chi = -\phi/(a+b)$

$$J(a,b,y) = \int_{\frac{a}{a+b}}^{-\frac{y-a}{a+b}} d\xi \frac{\log(-\chi(a+b))}{\chi - 1}. \tag{204}$$

I aim to use partial integration once more. But I have to exercise caution, as the integral contour is not allowed to hit a branch cut of the integrand. For that reason, I note

$$\int d\chi \frac{1}{1-\chi} = -\log(1-\chi) + C_1 = -\log(\chi - 1) + C_2. \tag{205}$$

Which integration I choose, depends on the parameters: Look at the function $\log(\chi - 1)$ along our contour from $\frac{a}{a+b}$ to $-\frac{y-a}{a+b}$. If, for an $x \in [0,y]$ I have $\Im(-\frac{x-a}{a+b} - 1) = 0$ and $\Re(-\frac{x-a}{a+b} - 1) < 0$, I cross a branch cut. The condition for the imaginary part yields $x = -\frac{\Im(ab*)}{\Im(a+b)}$. If now $\Re(-\frac{x-a}{a+b} - 1) < 0$, I have to integrate in the other illustrated fashion (case 2). In case 1, I get

$$\begin{aligned}
J_1(a,b,y) &= \int_{\frac{a}{a+b}}^{-\frac{y-a}{a+b}} d\xi \frac{\log(-\chi(a+b))}{\chi - 1} \\
&= \left[\log(-(a+b)\chi)\log(\chi-1)\right]_{\chi=\frac{a}{a+b}}^{-\frac{y-a}{a+b}} \\
&- \int_{\frac{a}{a+b}}^{-\frac{y-a}{a+b}} \frac{\log(\chi-1)}{\chi} d\chi \\
&= (\log(-(a+b)\chi)\log(\chi-1) + \mathrm{Li}_2(\chi) \\
&+ (\log(1-\chi) - \log(\chi-1))\log(\chi))_{\chi=\frac{a}{a+b}}^{-\frac{y-a}{a+b}}
\end{aligned} \tag{206}$$

In case two I get

$$\begin{aligned} J_2(a,b,y) &= \int_{\frac{a}{a+b}}^{-\frac{y-a}{a+b}} d\xi \frac{\log(-\chi(a+b))}{\chi-1} \\ &= [\log(-(a+b)\chi)\log(1-\chi)]_{\chi=\frac{a}{a+b}}^{-\frac{y-a}{a+b}} \\ &- \int_{\frac{a}{a+b}}^{-\frac{y-a}{a+b}} \frac{\log(1-\chi)}{\chi} d\chi \\ &= [\log(-(a+b)\chi)\log(1-\chi) + \mathrm{Li}_2(\chi)]_{\chi=\frac{a}{a+b}}^{-\frac{y-a}{a+b}} . \end{aligned} \tag{207}$$

Now, I can again use the asymptotic expansion of the dilogarithm [72] for large input values. I define j_1 and use this expansion for large y

$$\begin{aligned} j_1(a,b,y) &= \log(y-a)\log(-\frac{y+b}{a+b}) + \mathrm{Li}_2(-\frac{y-a}{a+b}) + \\ &+ (\log(\frac{y+b}{a+b}) - \log(-\frac{y+b}{a+b}))\log(-\frac{y-a}{a+b}) \\ &\approx \frac{1}{2}\log(y-a)^2 - \frac{1}{2}\log(a+b)^2 + (\log(a+b) - \log(-(a+b)))\times \\ &\times \log(-(a+b)) \\ &= \frac{1}{2}\log(y-a)^2 + j_1^R(a,b) \end{aligned} \tag{208}$$

then, I define j_2 similarly

$$\begin{aligned} j_2(a,b,y) &= \log(y-a)\log(\frac{y+b}{a+b}) + \mathrm{Li}_2(-\frac{y-a}{a+b}) \\ &= \frac{1}{2}\log(y-a)^2 - \frac{1}{2}\log(a+b)^2 \\ &= \frac{1}{2}\log(y-a)^2 + j_2^R(a,b). \end{aligned} \tag{209}$$

Then, I obtain in general

$$J_i(a,b,y) = j_i(a,b,y) - j_i(a,b,0) = j_i^R(a,b) - j_i(a,b,0) + f(y) \tag{210}$$

and by subtraction, I can define

$$J_i^R(a,b) = j_i^R(a,b) - j_i(a,b,0) \tag{211}$$

and then have found

$$I_1 = \frac{m^2}{(2\pi)^2 q} \sum_{a\in\pm\xi_S} \sum_{b\in\xi_\pm} \left[J^R(a,b) - J^R(a,-b)\right] \tag{212}$$

I_1 **for one complex and one real frequency** is obtained in a similar fashion.

$$I_1^s(\omega_R,\omega_C,k)=\frac{2m^2}{(2\pi)^2k}\int_0^\infty d\xi\frac{\xi}{\xi^2+\frac{\omega_R}{\epsilon(k)}-i0\mathrm{sgn}(\omega_R-\epsilon_F)}\times \\ \times\left[\log(-(\xi-\xi_0^+)(\xi-\xi_0^-))-\log(-(\xi+\xi_0^+)(\xi+\xi_0^-))\right] \tag{213}$$

where $\omega_R\in\mathbb{R}$. I split the leading fraction

$$\xi^2+\frac{\omega_R}{\epsilon(k)}-i0\mathrm{sgn}(\omega_R-\epsilon_F)=(\xi-\xi_P)(\xi+\xi_P) \\ \frac{\xi}{\xi^2+\frac{\omega_R}{\epsilon(k)}-i0\mathrm{sgn}(\omega_R-\epsilon_F)}=\frac{1}{2}\left(\frac{1}{\xi-\xi_P}+\frac{1}{\xi+\xi_P}\right) \tag{214}$$

so that then

$$I_1^s(\omega_R,\omega_C,k)=\frac{-m^2}{(2\pi)^2k}\sum_{a\in\pm\xi_P}\int_0^\infty\frac{1}{\xi-a}(\log(-(\xi-\xi_0^+)(\xi-\xi_0^-)) \\ -\log(-(\xi+\xi_0^+)(\xi+\xi_0^-))). \tag{215}$$

with $\xi_P=\sqrt{\frac{-\omega_R}{\epsilon(k)}+i0\mathrm{sgn}(\omega_R-\epsilon_F}$ and $\xi_0^\pm=-1\pm\sqrt{-\frac{-\omega_C}{\epsilon_F}}$. Then, I again use partial integration, with

$$\frac{d}{d\xi}\log(-(\xi-\xi_0^+)(\xi-\xi_0^-))=\frac{1}{\xi-\xi_0^+}+\frac{1}{\xi-\xi_0^-} \tag{216}$$

and find

$$I_1^s(\omega_R,\omega_C,k)=\frac{m^2}{(2\pi)^2k}\sum_{a\in\pm\xi_P}\sum_{b\in\xi_0^\pm}\int_0^\infty\left(\frac{1}{\xi-b}-\frac{1}{\xi+b}\right)\log(\xi-a). \tag{217}$$

To evaluate this integral, I define

$$P(a,b,y)=\int_0^y\frac{d\xi}{\xi+b}\log(\xi-a). \tag{218}$$

Note, that a can be positive real (+ an infinitesimal). So, the integral has to be calculated in two cases. In the case where a is not positive real, the integral can be computed just as in the complex case. If a is real, it is easiest to split the integral in two: $\xi\in[0,a]$ and $\xi\in[a,y]$. For the first integral I find

$$\int_0^a\frac{d\xi}{\xi+b}\log(\xi-a)=-i\pi\ \mathrm{sgn}\ (\Im(a))\,(\log(a+b)-\log(b)) \\ -\log(\frac{a}{a+b})\log(a)-\mathrm{Li}_2(\frac{a}{a+b}). \tag{219}$$

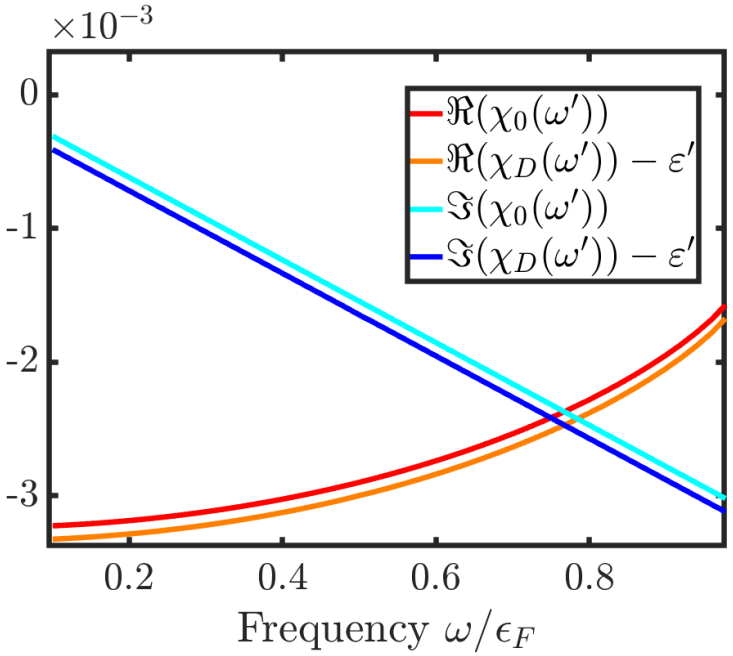

Figure 29: Convergence of the integral over I_1 against the Lindhard function. Note that one function was shifted to make both lines visible to the reader. The momentum is randomly chosen. The parameters for this calculation are $g = 100\text{meV}$, $\omega_{\text{ph}} = 100\text{meV}$ and $m = 0.2$.

The second integral can now be calculated as follows

$$\begin{aligned}\int_a^y \frac{d\xi}{\xi+b}\log(\xi-a) &= \int_0^{y-a}\frac{d\phi\log(\phi)}{\phi+a+b}\\ &= -\int_0^{-\frac{y-a}{a+b}}\frac{d\chi\log(-(a+b)\chi)}{1-\chi}\\ &= \log(1-\chi)\log(-(a+b)\chi)+\text{Li}_2(\chi)|_{\chi=\frac{a-y}{a+b}}\end{aligned} \tag{220}$$

I now execute the old program to find the limit of this object for $y \to \infty$ in the correct subtraction order. It turns out that the upper bound yields $-\frac{1}{2}\log(a+b)^2$, and the lower stays as it is. Implementing all three integrals for I_1 then enables us to compute the corrected polarizability.

B.2.4. Validation of the result

The first test is, whether the integral over I_1 (or K_χ) without coupling, leads after renormalizing to the Lindhard function, as one would expect, see Fig. 29.

Then, I tested whether the integrals with and without dressed propagator I_1 (or K_χ) do converge against each other if the coupling vanishes $g \to 0$, and how the scaling of this difference is, with g, see Figs. 30 and 31.

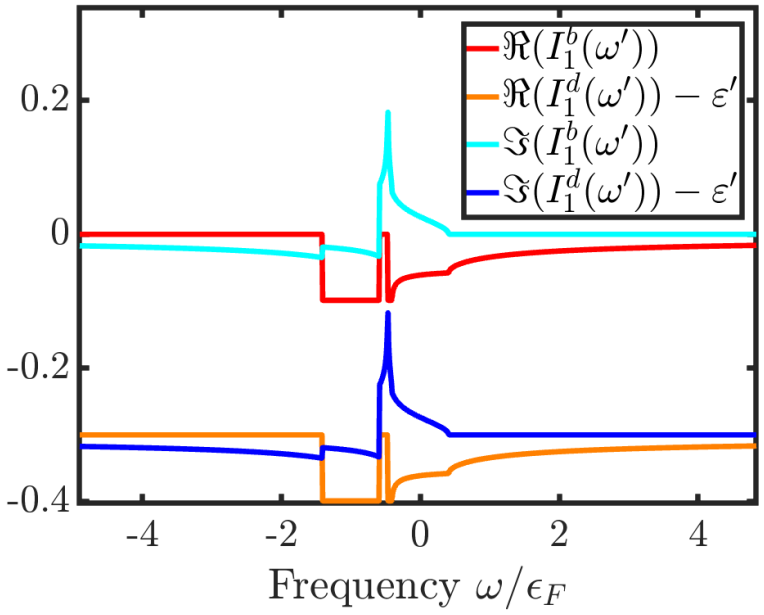

Figure 30: Convergence of the integrals I_1 for vanishing g. One function is shofted, to make both visible, one can see how the functions exhibit same behavior. The parameters for this calculation are $g = 100\text{meV}$, $\omega_{\text{ph}} = 100\text{meV}$ and $m = 0.2$, $k = k_F$.

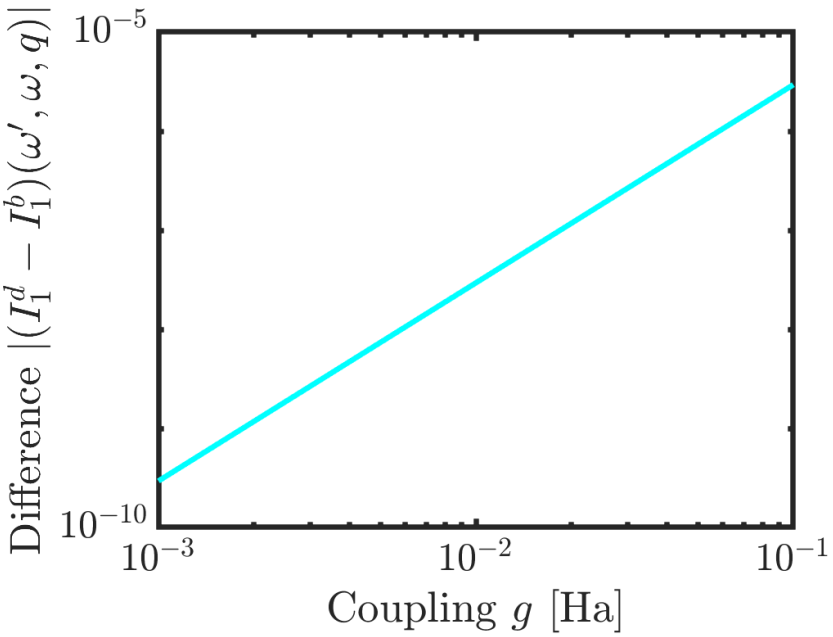

Figure 31: Convergence of the integrals I_1 for vanishing g. The convergence resembles a g^2 dependence as expected. The parameters for this calculation are $g = 100\text{meV}$, $\omega_{\text{ph}} = 100\text{meV}$ and $m = 0.2$, $k = k_F$.

Then, I tested whether the integrals with and without dressed propagator I_1 (or K_χ) do converge against their asymptotic expectations, see Fig. 32.

Table 1: The leading exponents for the integral I_1 subtracted by it's approximation for large $|\omega'|$, positive or negative ω'. The measurements have been made in regions, where the approximation is not everywhere accurate to double precision. The values for the approximation to order 5 do not fit the expectation, because at double precision the scaling cannot be shown with the computer anymore. "o.a." stands for "order of approximation", which means for o.a. n that the exponent should be equal to $-n - \frac{1}{2}$.

Description	Exponent
Positive ω', without self-energy, o.a. 1	-1.5051.
Negative ω', without self-energy, o.a. 1	-1.495.
Positive ω', with self-energy, o.a. 1	-1.5052.
Negative ω', with self-energy, o.a. 1	-1.4724.
Positive ω', without self-energy, o.a. 5	-2.8851.
Negative ω', without self-energy, o.a. 5	-2.9755.
Positive ω', with self-energy, o.a. 5	-3.1666.
Negative ω', with self-energy, o.a. 5	-3.0117.

Then, I tested whether the integral over I_1 with the dressed propagators converges against the Lindhard function, see Fig. 33. Note that the scaling is not perfect, because of the shift error, see above.

Additionally to these tests, I have compared the calculated integrals for K_χ with their numerical implementations. The results can be seen in Tab. 4.

B.3. The vertex correction

The vertex correction to order g^2 corresponds to the diagram in Fig. 34

B.3.1. The result

Theorem 7 (The vertex correction to the theory)**.** *The vertex correction to order g^2 can be written as*

$$\Gamma_1(\omega, \omega', k) = g^2(I_1(\omega' + \omega/2 - \omega_{ph}, \omega' - \omega/2 - \omega_{ph}, k) + I_2 + I_3) \tag{221}$$

where I_1 has real frequency entries and is shown in Sec.B.2. Now, I find I_2 as

$$I_2 = K(-\omega/2, -{\omega_{ph}}^+, -\omega) - K(-\omega/2, {\omega_{ph}}^-, -\omega) \tag{222}$$

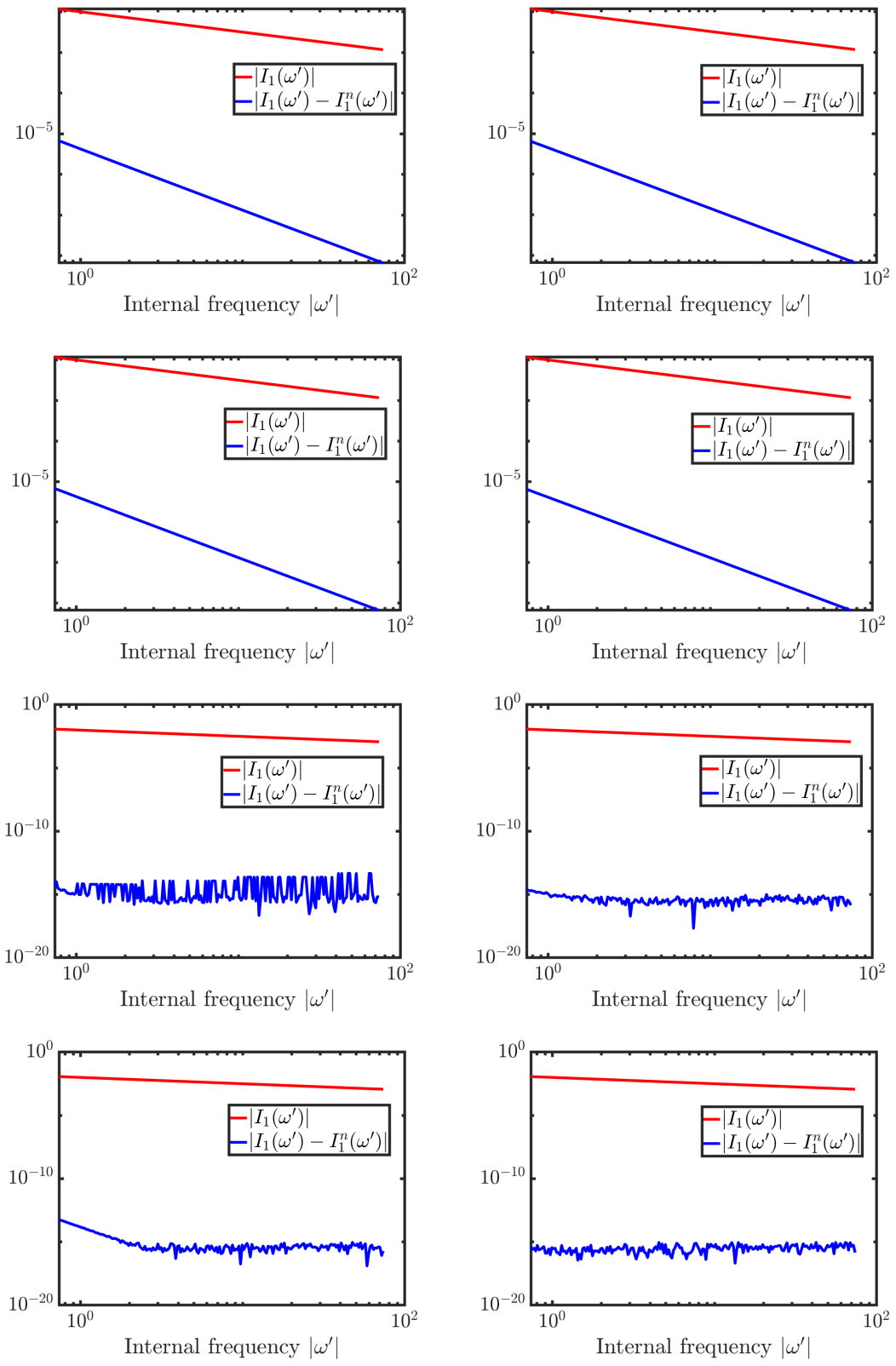

Figure 32: Convergence of the integrals I_1 against their asymptotic expectation. To the left the convergence for positive frequencies is shown, to the right, the convergence with respect to negative frequencies. The second and fourth row represent the self-energy corrected calculations, the upper four calculations have only the terms for renormalization subtracted, the lower plots show subtraction up to order $\omega^{-6.5}$. With the `getScaling` procedure see Sec.C. I have then calculated the exponents of the differences, see Tab. 1. The parameters for this calculation (when used) are $g = 100\text{meV}$, $\omega_{\text{ph}} = 100\text{meV}$ and $m = 0.2$, $k = k_F$.

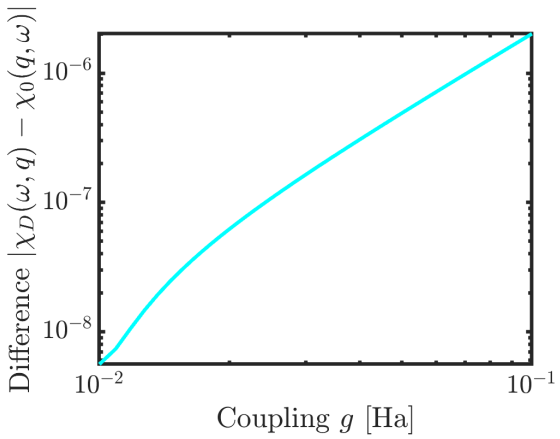

Figure 33: Absolute difference between the integral over the dressed I_1 and the Lindhard function. The convergence resembles a g^2 dependence only for large enough g because of the shift error. Note that above, I tested whether the integrands converge against each other, which they do, much better. The parameters for this calculation are $g = 100\text{meV}$, $\omega_{\text{ph}} = 100\text{meV}$ and $m = 0.2$, $k = k_F$.

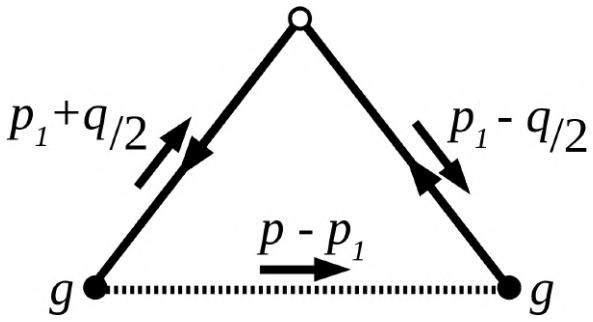

Figure 34: The vertex function to order g^2 in the electron-phonon interacting electron gas. The dashed line represents a virtual phonon, the solid lines represent virtual fermions.

with $L(\alpha,\psi) = K(\tau,\sigma,\rho)$, $\alpha = \tau + \sigma - \omega'$, $\psi = \frac{m}{k}(\rho - \epsilon(k))$ *and* $L = L_1 + B_2$ *with*

$$\begin{aligned} L_1(\xi_S,\xi_F,\psi) = \frac{m^2}{(2\pi)^2 k} \sum_{a\in\pm\xi_S} (&-\log|1-\xi_F|\log(\frac{a+\xi_F}{a+1}) + \\ &\log(\xi_F+1)\log(\frac{\xi_F+a}{a-1}) + Li_2(\frac{\xi_F+1}{1-a}) - Li_2(\frac{1-\xi_F}{1+a}) + \\ &i\pi\theta(\xi_F-1)\left(\log(\xi_F-a)-\log(-a)\right)) \end{aligned} \tag{223}$$

and $\xi_F = k_F/|\psi|$, $\xi_S = \frac{\sqrt{-2m\alpha}}{|\psi|}$. *I find*

$$B_2 = \frac{im^2}{2\pi k} \sum_{a\pm\xi_S} \left(\theta(-\psi)\left(\log(\gamma_1+a)-\log(a)\right) + \log(\gamma_3+a) - \log(\gamma_2+a)\right) \tag{224}$$

with $\gamma_1 = \max(\min(\xi_S - \xi_F, \xi_F, 1), 0)$, $\gamma_2 = \min(\xi_F, \max(\Re(\sqrt{\phi}), |\xi_S - \xi_F|, 0)))$, $\phi = \xi_F^2 - 2sgn(\psi)\xi_S - {\xi_S}^2$ *and* $\gamma_3 = \min(\xi_F, \max(sgn(\psi), \xi_F - \xi_S, 0))$. *The solution of integral* I_3 *turns out to be a spin-off of the last integrals's calculation:*

$$I_3 = L_1(\beta_1,\psi,k) - L_1(\beta_2,\psi,k) + C \tag{225}$$

with $\beta_1 = \frac{\omega}{2} - \omega' - \omega_{ph} + i0$, $\beta_2 = \frac{\omega}{2} - \omega' + \omega_{ph} + i0$ *and* $C = D(\gamma_1) - D(\gamma_2)$ *with* $\gamma_i = \sqrt{-2m\beta_i}/|\psi|$ *and* $\Delta = \max(1, \xi_F)$

$$\begin{aligned} D(\beta) = \frac{im^2}{2\pi k} \sum_{\alpha\in\pm\xi_S} &\theta(-\psi)(\log(\Delta-\alpha) - \log(\xi_F-\alpha)) \\ &- \theta(\psi)\theta(\xi_F-1)(\log(\xi_F-\alpha) - \log(1-\alpha)). \end{aligned} \tag{226}$$

B.3.2. Properties of the vertex function

The leading term for large ω' comes from the I_1 contribution. This means that for large $|\omega'|$: $|\Gamma_1| \propto |\omega'|^{-1/2}$.

Symmetry of the vertex function From the equation

$$\frac{i}{g^2}\Gamma_1 = \int \frac{dqd\omega_1}{(2\pi)^4} D(\omega'-\omega_1) G(q+\frac{k}{2}, \omega_1+\frac{\omega}{2}) G(q-\frac{k}{2}, \omega_1-\frac{\omega}{2}) \tag{227}$$

I reflect the integral variable $q \to -q$ and use $G(q,\omega) = G(-q,\omega)$ to find

$$\Gamma_1(\omega,k,\omega') = \Gamma_1(-\omega,k,\omega') \tag{228}$$

The meromorphism of the vertex function. I found logarithmic divergences at $\omega' = \epsilon_F \pm \omega_{\rm ph}, \omega = 0$. They occur, when the $L(\alpha,\psi)$ integral is evaluated at $-\alpha = \epsilon_F$ which is $\omega' = \epsilon_F + q_1\omega_{\rm ph} + q_2\frac{\omega}{2}$ and $q_i = \pm 1$.

Other candidates are the lines where $\xi_S = \xi_p^{\pm}$ which are $\omega = \omega_{\text{ph}} + \frac{(\omega-\epsilon(k))(\omega+\epsilon(k))}{4\epsilon(k)}$

B.3.3. Large ω' expansion

The expansion for I_1 is found in Sec. B.2.2. I now need to do the same expansion for the integral L, which will enable us to compute corrections accurately in practice.

$$L(\alpha,\psi) = \frac{m}{k}\int_0^{k_F}\frac{dq}{(2\pi)^2}\frac{q}{\epsilon(q)+\alpha}\int_{-1}^{+1}\frac{dx}{x+\psi/q+i\eta_{q-k}} =:\therefore \tag{229}$$

I transform the infinitesimal

$$\frac{1}{x+\frac{\psi}{q}+i\eta_{q-k}} = \frac{1}{x+\frac{\psi}{q}+i\eta} + 2\pi i\delta(x+\frac{\psi}{q})\theta(\epsilon_F-\epsilon(q-k)) \tag{230}$$

$$:\!= \Phi(\alpha,\psi) + C(\alpha,\psi), \tag{231}$$

with

$$\Phi(\alpha,\psi) = \frac{m}{k}\int_0^{k_F}\frac{dq}{(2\pi)^2}\frac{q}{\epsilon(q)+\alpha}\int_{-1}^{+1}\frac{dx}{x+\psi/q+i\eta} \tag{232}$$

The x integration can now be performed right away

$$\Phi(\alpha,\psi) = \frac{m}{k}\int_0^{k_F}\frac{dq}{(2\pi)^2}\frac{q}{\epsilon(q)+\alpha}\log(x+\psi/q+i\eta)|_{x=-1}^{1} = \Phi_+(\alpha,\psi)-\Phi_-(\alpha,\psi) \tag{233}$$

with

$$\Phi_\pm(\alpha,\psi) = \frac{m}{k}\int_0^{k_F}\frac{dq}{(2\pi)^2}\frac{q}{\epsilon(q)+\alpha}\log(\pm 1+\psi/q+i\eta) =:\therefore \tag{234}$$

Now, I aim to expand this function in $\frac{1}{\omega'}$, as $\alpha = \alpha' - \omega'$ with $\alpha' = \mathscr{O}((\omega')^0)$. Then I will exploit this by [1]

$$F(q,n) = \int dq q^n\log(q) = q^{n+1}\left(\frac{\log(q)}{n+1} - \frac{1}{(n+1)^2}\right) + C. \tag{235}$$

Someone might conceivably object here, that this way of inserting the integrated function is unfeasible because of the logarithm's branch-cut. However, such an objection is overly doubtful as a geometric argument explains: The logarithm has a branch cut along the negative real axis. The integral contour goes from the origin to $k_F \in \mathbb{R}$, which is perfectly parallel. As the logarithm has a positive infinitesimal it is at the

correct branch for this integral formula to hold.

$$\begin{aligned}
\therefore &= \frac{m}{\omega' k}\int_0^{k_F}\frac{dq}{(2\pi)^2}\frac{q}{1+\frac{\epsilon(q)+\alpha'}{\omega'}}\log(\pm 1+\psi/q+i\eta)\\
&= \frac{m}{\omega' k}\int_0^{k_F}\frac{dq}{(2\pi)^2}q\sum_{n=0}^{\infty}\left(-\frac{\epsilon(q)+\alpha'}{\omega'}\right)^n\log(\pm 1+\psi/q+i\eta)\\
&= \frac{m}{\omega' k}\sum_{n=0}^{\infty}\frac{(-1)^n}{(\omega')^n}\int_0^{k_F}\frac{dq}{(2\pi)^2}q\left(\epsilon(q)+\alpha'\right)^n\log(\pm 1+\psi/q+i\eta)\\
&= \frac{m}{(2\pi)^2\omega' k}\sum_{n=0}^{\infty}\frac{(-1)^n}{(2m\omega')^n}\int_0^{k_F}dqq\left(q^2+2m\alpha'\right)^n\log(\pm 1+\psi/q+i\eta)\\
&= \frac{m}{(2\pi)^2\omega' k}\sum_{n=0}^{\infty}\frac{(-1)^n}{(2m\omega')^n}\sum_{p=0}^{n}(2m\alpha')^{n-p}\binom{n}{p}\int_0^{k_F}dqq^{2p+1}\log(\pm 1+\psi/q+i\eta)
\end{aligned}\tag{236}$$

I use, that I can multiply the log by any positive constant, such as q and now the ways of $\Phi_\pm$ split. For Φ_+ I substitute $\rho=\psi+q$

$$\begin{aligned}
\Phi_+(\alpha,\psi) &= \frac{m}{(2\pi)^2\omega' k}\sum_{n=0}^{\infty}\frac{(-1)^n}{(2m\omega')^n}\sum_{p=0}^{n}(2m\alpha')^{n-p}\binom{n}{p}\times\\
&\quad\times\int_{\psi}^{k_F+\psi}d\rho(\rho-\psi)^{2p+1}\log(\rho+i\eta)\\
&= \frac{m}{(2\pi)^2\omega' k}\sum_{n=0}^{\infty}\frac{(-1)^n}{(2m\omega')^n}\sum_{p=0}^{n}(2m\alpha')^{n-p}\binom{n}{p}\sum_{q=0}^{2p+1}\binom{2p+1}{q}(-\psi)^q\times\\
&\quad\times\int_{\psi}^{k_F+\psi}d\rho\rho^{2p+1-q}\log(\rho)\\
&= \frac{m}{(2\pi)^2\omega' k}\sum_{n=0}^{\infty}\frac{(-1)^n}{(2m\omega')^n}\sum_{p=0}^{n}(2m\alpha')^{n-p}\binom{n}{p}\sum_{q=0}^{2p+1}\binom{2p+1}{q}(-\psi)^q\times\\
&\quad\times\left(F(k_F+\psi,2p+1-q)-F(\psi,2p+1-q)\right).
\end{aligned}\tag{237}$$

For Φ_- I substitute $\rho = -q + \psi$, use $2p+1$ is odd,

$$\begin{aligned}
\Phi_+(\alpha,\psi) &= \frac{m}{(2\pi)^2\omega' k}\sum_{n=0}^{\infty}\frac{(-1)^n}{(2m\omega')^n}\sum_{p=0}^{n}(2m\alpha')^{n-p}\binom{n}{p}\times \\
&\quad\times\int_{\psi}^{-k_F+\psi} d\rho(\rho-\psi)^{2p+1}\log(\rho+i\eta) \\
&= \frac{m}{(2\pi)^2\omega' k}\sum_{n=0}^{\infty}\frac{(-1)^n}{(2m\omega')^n}\sum_{p=0}^{n}(2m\alpha')^{n-p}\binom{n}{p}\sum_{q=0}^{2p+1}\binom{2p+1}{q}(-\psi)^q\times \\
&\quad\times\int_{\psi}^{-k_F+\psi} d\rho\rho^{2p+1-q}\log(\rho) \\
&= \frac{m}{(2\pi)^2\omega' k}\sum_{n=0}^{\infty}\frac{(-1)^n}{(2m\omega')^n}\sum_{p=0}^{n}(2m\alpha')^{n-p}\binom{n}{p}\sum_{q=0}^{2p+1}\binom{2p+1}{q}(-\psi)^q\times \\
&\quad\times\left(F(-k_F+\psi,2p+1-q)-F(\psi,2p+1-q)\right). \qquad (238)
\end{aligned}$$

which boils down to

$$\begin{aligned}
\Phi(\alpha,\psi) &= \frac{m}{(2\pi)^2\omega' k}\sum_{n=0}^{\infty}\frac{(-1)^n}{(2m\omega')^n}\sum_{p=0}^{n}(2m\alpha')^{n-p}\binom{n}{p}\sum_{q=0}^{2p+1}\binom{2p+1}{q}(-\psi)^q\times \\
&\quad\times\left(F(k_F+\psi,2p+1-q)-F(\psi-k_F,2p+1-q)\right). \qquad (239)
\end{aligned}$$

this is already all I need for I_3, where I truncate n at a certain value (here $n=8$) for reasonable accuracy and limited execution time. For I_2 the only missing thing now is $C(\alpha,\psi)$.

$$C(\alpha,\psi) = \frac{im}{2\pi q}\int_0^{k_F}\frac{dq}{(2\pi)^2}\frac{q}{\epsilon(q)+\alpha}\int_{-1}^{1}dx\delta(x+\psi/q)\theta(\epsilon_F-\epsilon(q)+\rho) \qquad (240)$$

where I have used the δ function.

$$\begin{aligned}
C(\alpha,\psi) &= \frac{im}{2\pi q}\int_0^{k_F} dq \frac{q}{\epsilon(q)+\alpha}\theta(q-|\psi|)\theta(\epsilon_F-\epsilon(q)+\rho) \\
&= \frac{im}{2\pi q}\int_\lambda^{\Lambda} dq \frac{q}{\epsilon(q)+\alpha} \\
&= \frac{im}{2\pi\omega' q}\int_\lambda^{\Lambda} dq \frac{q}{1+\frac{\epsilon(q)+\alpha'}{\omega'}} \\
&= \frac{im}{2\pi\omega' q}\sum_{n=0}^{\infty}\frac{1}{(-\omega')^n}\int_\lambda^{\Lambda} dq q\left(\epsilon(q)+\alpha'\right)^n \\
&= \frac{im}{4\pi\omega' q}\sum_{n=0}^{\infty}\frac{1}{(-2m\omega')^n}\int_{\sqrt{\lambda}}^{\sqrt{\Lambda}} dl\left(l+2m\alpha'\right)^n \\
&= \frac{im}{4\pi\omega' q}\sum_{n=0}^{\infty}\frac{1}{(-2m\omega')^n}\sum_{p=0}^{n}\binom{n}{p}(2m\alpha')^{n-p}\int_{\sqrt{\lambda}}^{\sqrt{\Lambda}} dl l^p \\
&= \frac{im}{4\pi\omega' q}\sum_{n=0}^{\infty}\frac{1}{(-2m\omega')^n}\sum_{p=0}^{n}\binom{n}{p}\frac{(2m\alpha')^{n-p}}{p+1}\left(\sqrt{\Lambda}^{p+1}-\sqrt{\lambda}^{p+1}\right). \qquad (241)
\end{aligned}$$

B.3.4. Error estimation for Φ and L

In the following, I will argue why the error of the vertex correction to the polarizability is negligible. Therefore I will show that the error of Φ and L, that compose I_2 and I_3 are negligible compared to I_1.

The integrals are then $L(\alpha,\psi)=\Phi(\alpha,\psi)+C(\alpha,\psi)$. Now for Φ I have

$$\begin{aligned}
\Phi(\alpha,\psi) &= \Phi_+(\alpha,\psi)-\Phi_-(\alpha,\psi) \\
\Phi_\pm(\alpha,\psi) &= \frac{m}{\omega' k}\int_0^{k_F}\frac{dq}{(2\pi)^2}\frac{q}{1+\frac{\epsilon(q)-\alpha'}{\omega'}}\log(\pm q+\psi+i0) \qquad (242)
\end{aligned}$$

Then, the approximated function is $F(x)=\frac{1}{1+x}$, so that $|R_{n+1}(x)|\leq\frac{|x|^{n+1}}{(1-|x|)^2}$ and our x is $|x|=|\frac{\epsilon(q)+\alpha'}{\omega'}|\leq\frac{\epsilon_F+|\alpha'|}{|\omega'|}=\widehat{x}(\omega')$. The estimate becomes

$$\begin{aligned}
|\Phi_\pm(\alpha,\psi)-\Phi_\pm^{(n)}(\alpha,\psi)| &\leq \left|\frac{m}{\omega' k}\frac{\widehat{x}^{n+1}}{(1-\widehat{x})^2}\int_0^{k_F}\frac{dq}{(2\pi)^2}q\log(\pm q+\psi+i0)\right| \\
&\leq \left|\frac{mk_F^2}{(2\pi)^2\omega' k}\frac{\widehat{x}^{n+1}}{(1-\widehat{x})^2}(\pi+\log(|k_F|+|\psi|))\right|. \qquad (243)
\end{aligned}$$

The only integral that I have to calculate now is $C(\alpha,\psi)$.

$$C(\alpha,\psi)=\frac{im}{2\pi k}\int_\lambda^{\Lambda} dq\frac{q}{\epsilon(q)+\alpha} \qquad (244)$$

and $0 \leq \lambda \leq \Lambda \leq k_F$. Then

$$|C(\alpha,\psi) - C^{(n)}(\alpha,\psi)| \leq \frac{mk_F^2}{4\pi k\omega'} \frac{\widehat{x}^{n+1}}{(1-\widehat{x})^2} \tag{245}$$

and the same $\widehat{x}$ as for $\Phi_\pm$. Comparing I_1's error and I_2's or I_3's error[17] yields now, that the error for the vertex correction has the leading term of $g^2\Delta(I_1^2)$ where $\Delta(f)$ means the error of f. Then $g^2\Delta(I_1^2) = 2g^2 I_1 \Delta I_1$, which is negligibly small compared to the error of I_1 and is therefore neglected.

B.3.5. Calculation

$$\frac{1}{g^2}\Gamma_1 = i\int \frac{dk_1 d\omega_1}{(2\pi)^4} D(\omega-\omega_1) G_0(k_1+\frac{k}{2}, \omega_1+\frac{\omega}{2}) G_0(k_1-\frac{k}{2}, \omega_1-\frac{\omega}{2}) \tag{246}$$

To perform the ω_1 integration, I can read of the poles from the definition of the propagators. I aim to push all poles to one side of the contour by Eq.(73). By the residue theorem, a contour that does not contain any poles in a complex plane is zero. As the integrand of our integral vanishes, I can, without mistake, add the arcbow to the contour (which is zero) and use holomorphy. With these definitions in advance, the ω_1 integration can be performed. I define

$$\omega_{s,1} = \omega' - \omega_{\mathrm{ph}} \tag{247}$$
$$\omega_{s,2} = \omega' + \omega_{\mathrm{ph}} \tag{248}$$
$$\omega_{s,3} = \epsilon(k_1+\frac{k}{2}) - \frac{\omega}{2} \tag{249}$$
$$\omega_{s,4} = \epsilon(k_1-\frac{k}{2}) + \frac{\omega}{2}. \tag{250}$$

and write the vertex as

$$\frac{i}{g^2}\Gamma_1 = \int \frac{dk_1 d\omega_1}{(2\pi)^4} \{\frac{1}{\omega_1 - (\omega_{s,2} - i\eta)} - \frac{1}{\omega_1 - (\omega_{s,1} + i\eta)}\} \\ \frac{1}{\omega_1 - (\omega_{s,3} - i0_{k_1+\frac{k}{2}})} \frac{1}{\omega_1 - (\omega_{s,4} - i0_{k_1-\frac{k}{2}})} = (*). \tag{251}$$

[17] The errors of these terms are smaller, because they are expanded three orders more.

Now, as explained, I use Eq.(73).

$$
\begin{aligned}
(*) &= \int \frac{dk_1 d\omega_1}{(2\pi)^4} - 2\pi i\delta(\omega_1-\omega_{s,1})\frac{1}{\omega_1-(\omega_{s,3}-i0_{k_1+\frac{k}{2}})}\frac{1}{\omega_1-(\omega_{s,4}-i0_{k_1-\frac{k}{2}})} \\
&+ \int \frac{dk_1 d\omega_1}{(2\pi)^4}\{\frac{1}{\omega_1-(\omega_{s,2}-i\eta)}-\frac{1}{\omega_1-(\omega_{s,1}-i\eta)}\}\frac{1}{\omega_1-(\omega_{s,3}-i0_{k_1+\frac{k}{2}})}\times \\
&\quad\times\frac{1}{\omega_1-(\omega_{s,4}-i0_{k_1-\frac{k}{2}})} \\
&= \int \frac{dk_1 d\omega_1}{(2\pi)^4} - 2\pi i\delta(\omega_1-\omega_{s,1})\frac{1}{\omega_1-(\omega_{s,3}-i0_{k_1+\frac{k}{2}})}\frac{1}{\omega_1-(\omega_{s,4}-i0_{k_1-\frac{k}{2}})} \\
&+ \int \frac{dk_1 d\omega_1}{(2\pi)^4}\{\frac{1}{\omega_1-(\omega_{s,2}-i\eta)}-\frac{1}{\omega_1-(\omega_{s,1}-i\eta)}\}\frac{1}{\omega_1-(\omega_{s,4}-i0_{k_1-\frac{k}{2}})} \\
&2\pi i\theta(\epsilon_F-\epsilon(k_1+\frac{q}{2}))\delta(\omega_1-\omega_{s,3}) \\
&+ \int \frac{dk_1 d\omega_1}{(2\pi)^4}\{\frac{1}{\omega_1-(\omega_{s,2}-i\eta)}-\frac{1}{\omega_1-(\omega_{s,1}-i\eta)}\}\frac{1}{\omega_1-(\omega_{s,3}-i\eta)}\times \\
&\quad\times\frac{1}{\omega_1-(\omega_{s,4}-i0_{k_1-\frac{k}{2}})} \\
&= \int \frac{dk_1 d\omega_1}{(2\pi)^4} - 2\pi i\delta(\omega_1-\omega_{s,1})\frac{1}{\omega_1-(\omega_{s,3}-i0_{k_1+\frac{k}{2}})}\frac{1}{\omega_1-(\omega_{s,4}-i0_{k_1-\frac{k}{2}})} \\
&+ \int \frac{dk_1 d\omega_1}{(2\pi)^4}\{\frac{1}{\omega_1-(\omega_{s,2}-i\eta)}-\frac{1}{\omega_1-(\omega_{s,1}-i\eta)}\}\frac{2\pi i}{\omega_1-(\omega_{s,4}-i0_{k_1-\frac{k}{2}})}\times \\
&\quad\times\theta(\epsilon_F-\epsilon(k_1+\frac{q}{2}))\delta(\omega_1-\omega_{s,3}) \\
&+ \int \frac{dk_1 d\omega_1}{(2\pi)^4}\{\frac{1}{\omega_1-(\omega_{s,2}-i\eta)}-\frac{1}{\omega_1-(\omega_{s,1}-i\eta)}\}\frac{2\pi i}{\omega_1-(\omega_{s,3}-i\eta)}\times \\
&\quad\times\delta(\omega_1-(\omega_{s,4})\theta(\epsilon_F-\epsilon(k_1-\frac{k}{2})) \qquad (252)
\end{aligned}
$$

Now, I carry out the ω_1 integrations.

$$
\begin{aligned}
\frac{\Gamma_1}{g^2} = \int \frac{dk_1}{(2\pi)^3}\{ &-\frac{1}{\omega_{s,1}-\omega_{s,3}+i0_{k_1+\frac{k}{2}}}\frac{1}{\omega_{s,1}-\omega_{s,4}+i0_{k_1-\frac{k}{2}}} \\
&+\left(\frac{1}{\omega_{s,3}-\omega_{s,2}+i\eta}-\frac{1}{\omega_{s,3}-\omega_{s,1}+i\eta}\right)\frac{\theta(k_F-|k_1+\frac{k}{2}|)}{\omega_{s,3}-\omega_{s,4}+i0_{k_1-\frac{k}{2}}} \\
&+\left(\frac{1}{\omega_{s,4}-\omega_{s,2}+i\eta}-\frac{1}{\omega_{s,4}-\omega_{s,1}+i\eta}\right)\frac{\theta(k_F-|k_1-\frac{k}{2}|)}{\omega_{s,4}-\omega_{s,3}+i\eta}\}. \qquad (253)
\end{aligned}
$$

Now, I define each line of Eq. (253) to be an integral I_1, I_2, I_3. Note, that the ω

integration for $GG\Gamma$ in terms of two k-integrations is simple.

The integral I_2 Recall the integrals from above. I define

$$K(\tau,\sigma,\rho) = \int \frac{dq}{(2\pi)^3} \frac{1}{\epsilon(q+\frac{k}{2})+\tau+\sigma-\omega'} \frac{\theta(k_F-|q+\frac{k}{2}|)}{\frac{q\cdot k}{m}+\rho+i\eta_{q-k/2}} \tag{254}$$

with $\omega_{\rm ph}^- = \omega_{\rm ph} - i\eta$ and note that then

$$I_2 = K(-\frac{\omega}{2}, -\omega_{\rm ph}^+, -\omega) - K(-\frac{\omega}{2}, \omega_{\rm ph}^-, -\omega) \tag{255}$$

A shift $q \to q - \frac{k}{2}$ and two definitions $\alpha := \tau+\sigma-\omega'$, $\psi := \frac{m}{k}\left(\rho - \frac{k^2}{2m}\right)$ lead to

$$K(\tau,\sigma,\rho) = L(\alpha,\psi) = \int \frac{dq}{(2\pi)^3} \frac{1}{\epsilon(q)+\alpha} \frac{\theta(k_F-|q|)}{\frac{q\cdot k}{m}+\frac{k}{m}\psi+i\eta_{q-k}}. \tag{256}$$

I switch to spherical coordinates and rotate the sphere, such that $k \propto e_z$. Then

$$L(\alpha,\psi) = \frac{m}{k}\int_0^{k_F} \frac{dq}{(2\pi)^2} \frac{q}{\epsilon(q)+\alpha} \int_{-1}^{+1} \frac{dx}{x+\psi/q+i\eta_{q-k}}. \tag{257}$$

and with Eq. (192)

$$\begin{aligned} L(\alpha,\psi) = \frac{m}{k}\int_0^{k_F} \frac{dq}{(2\pi)^2} \frac{q}{\epsilon(q)+\alpha} \{ &\log(1+\psi/q-i\eta) - \log(-1+\psi/q-i\eta) \\ &+ 2\pi i\{\theta(k-k_F-q)+\theta(q-k_F-k))\theta(-(1+\psi/q)) \\ &+ \theta(q+k_F-k)\theta(q+k-k_F)\theta(k_F+k-q)\theta(-(\psi/q+x_0)) \\ &- \theta(q+k-k_F)\theta(1-\psi/q)\}\} \end{aligned} \tag{258}$$

Note that there might be a pole close to the real axis in $[0,k_F]$ at $q_S = \sqrt{-2m\alpha}$. The first line of L I call L_1. I perform the transform $\xi = \frac{q}{|\psi|}$, and denote $\xi_{S/F} = \frac{q_{S/F}}{|\psi|}$.

$$\begin{aligned} L_1(\xi_S,\xi_F,\psi) = \frac{m^2}{k}\int_0^{\xi_F} \frac{d\xi}{(2\pi)^2} \left(\frac{1}{\xi-\xi_S}+\frac{1}{\xi+\xi_S}\right) \times \\ \times \{\log(\xi+\mathrm{sgn}(\psi)-i\eta) - \log(-\xi+\mathrm{sgn}(\psi)-i\eta)\} \end{aligned} \tag{259}$$

To simplify the calculation I note that the cases $\psi > 0$ and $\psi < 0$ give the exact opposite results, with one single difference:

$$\begin{aligned} \log(\xi+1-i\eta) - \log(-\xi+1-i\eta) + \log(\xi-1-i\eta) - \log(-\xi-1-i\eta) \\ = 2\pi i\theta(\xi-1). \end{aligned} \tag{260}$$

The whole result takes the form $\mathrm{sgn}(\psi)F + \theta(-\psi)C$, with $F = L_1(\xi_S, \xi_F, |\psi|)$ and $C = \frac{im^2}{2\pi k}\theta(\xi_F - 1)\left(\log(\xi_F - \xi_S) - \log(-\xi_S) + \log(\xi_F + \xi_S) - \log(\xi_S)\right)$.

Case 1 : Assume ξ_S is not near the real axis, then

$$L_1(\xi_S, \xi_F, |\psi|) = \frac{m^2}{k}\int_0^{\xi_F} \frac{d\xi}{(2\pi)^2}\left(\frac{1}{\xi - \xi_S} + \frac{1}{\xi + \xi_S}\right)\left\{\log(\xi + 1) - \log(-\xi + 1 - i\eta)\right\} \tag{261}$$

In the implementation, I use for each logarithm a function $F_\pm(a) = \int_0^{\xi_F} \frac{d\xi}{(2\pi)^2}\frac{1}{\xi + a}\log(\xi \pm 1 - i0)$ Where the first logarithm yields, with suppressed prefactor $\frac{m^2}{(2\pi)^2 k}$

$$\begin{aligned}
&\mathrm{Li}_2\left(\frac{\xi_F + 1}{\xi_S + 1}\right) + \log(\xi_F + 1)\log\left(1 - \frac{\xi_F + 1}{\xi_S + 1}\right) + \mathrm{Li}_2\left(\frac{\xi_F + 1}{1 - \xi_S}\right) \\
&+ \log(\xi_F + 1)\log\left(1 - \frac{\xi_F + 1}{1 - \xi_S}\right) - \mathrm{Li}_2\left(\frac{1}{\xi_S + 1}\right) - \mathrm{Li}_2\left(\frac{1}{1 - \xi_S}\right).
\end{aligned} \tag{262}$$

Case 2 is more delicate in one special case: If $\xi_F < 1$, the phase only of the ξ_S survives. For this case, the result is

$$\begin{aligned}
&\mathrm{Li}_2\left(\frac{1 - \xi_F}{1 - \xi_S}\right) + \log(1 - \xi_F)\log\left(1 - \frac{1 - \xi_F}{1 - \xi_S}\right) + \mathrm{Li}_2\left(\frac{1 - \xi_F}{\xi_S + 1}\right) \\
&+ \log(1 - \xi_F)\log\left(1 - \frac{1 - \xi_F}{\xi_S + 1}\right) - \mathrm{Li}_2\left(\frac{1}{1 - \xi_S}\right) - \mathrm{Li}_2\left(\frac{1}{\xi_S + 1}\right)
\end{aligned} \tag{263}$$

For $\xi_F > 1$ I get rid off the logarithmic infinitesimal by noting that

$$\log(-\xi + 1 - i\eta) = \log|1 - \xi| - i\pi\theta(\xi - 1) \tag{264}$$

and obtain

$$\begin{aligned}
&- i\pi\left[\log(\xi_F - \xi_S) - \log(1 - \xi_S) + \log(\xi_F + \xi_S) - \log(1 + \xi_S)\right]\theta(\xi_F - 1) \\
&- \mathrm{Li}_2\left(\frac{1}{1 - \xi_S}\right) - \mathrm{Li}_2\left(\frac{1}{\xi_S + 1}\right) + \mathrm{Li}_2\left(\frac{\xi_F - 1}{\xi_S - 1}\right) + \log(\xi_F - 1)\log\left(1 - \frac{\xi_F - 1}{\xi_S - 1}\right) \\
&+ \mathrm{Li}_2\left(\frac{\xi_F - 1}{-\xi_S - 1}\right) + \log(\xi_F - 1)\log\left(1 - \frac{\xi_F - 1}{-\xi_S - 1}\right)
\end{aligned} \tag{265}$$

which means, the polylogarithm stay as they have been before. The final result for the second integral becomes

$$
\begin{aligned}
&- i\pi \left[\log(\xi_F - \xi_S) - \log(1-\xi_S) + \log(\xi_F + \xi_S) - \log(1+\xi_S)\right] \theta(\xi_F - 1) \\
&- \mathrm{Li}_2\left(\frac{1}{1-\xi_S}\right) - \mathrm{Li}_2\left(\frac{1}{\xi_S+1}\right) + \mathrm{Li}_2\left(\frac{\xi_F-1}{\xi_S-1}\right) + \log|\xi_F - 1| \log\left(1 - \frac{\xi_F-1}{\xi_S-1}\right) \\
&+ \mathrm{Li}_2\left(\frac{\xi_F-1}{-\xi_S-1}\right) + \log|\xi_F - 1| \log\left(1 - \frac{\xi_F-1}{-\xi_S-1}\right)
\end{aligned} \tag{266}
$$

with $\xi_F \in \mathbb{R}$. Then the full integral L_1 is

$$
\begin{aligned}
L_1(\xi_S, \xi_F, \psi) = \frac{m^2}{(2\pi)^2 k} \sum_{a \in \pm\xi_S} \mathrm{sgn}(\psi) \{ &\log|1-\xi_F| \left(-\log\left(\frac{a+\xi_F}{a+1}\right)\right) \\
&+ \log(\xi_F + 1) \log\left(\frac{a+\xi_F}{a-1}\right) \\
&+ \mathrm{Li}_2\left(\frac{\xi_F+1}{1-a}\right) - \mathrm{Li}_2\left(\frac{1-\xi_F}{a+1}\right) \\
&+ i\pi\theta(\xi_F - 1)\left(\log(\xi_F - a) - \log(-a)\right)\}.
\end{aligned} \tag{267}
$$

The θ functions now yield the following extra term

$$
B_2 = \frac{im^2}{2\pi k} \sum_{a \in \pm\xi_S} \{\theta(-\psi)(\log(\gamma_1 + a) - \log(a)) + (\log(\gamma_3 + a) - \log(\gamma_2 + a))\} \tag{268}
$$

with $\gamma_1 = \max(\min(\tilde{\xi} - \xi_F, \xi_F, 1), 0)$, $\gamma_2 = \min(\xi_F, \max(\Re(\sqrt{\phi}), |\tilde{\xi} - \xi_F|, 0)))$, $\phi = \xi_F^2 - 2\mathrm{sgn}(\psi)\tilde{\xi} - \tilde{\xi}^2$ and $\gamma_3 = \min(\xi_F, \max(\mathrm{sgn}(\psi), \xi_F - \tilde{\xi}, 0))$.

I_3 is now simple, and left to the interested reader.

B.3.6. Validation

At first, I have tested the calculated integrals against their numerical counterparts and the results can be found in Tab. 4.

Then, I tested the asymptotic expansions of all the participarting integrals, see Figs. 35 and 36.

Then, I tested whether the integrands and integrals for the vertex converge against each other, if $g \to 0$. These tests are illustrated in Figs.37, 38 and 39.

B.4. Plasmon peaks

The plasmon peaks have been converged for $\epsilon_F = 2\mathrm{eV}$, $g = 100\mathrm{meV}$, $\omega_{\mathrm{ph}} = 60\mathrm{meV}$, $m = 0.2$. Then, I have plotted below the peaks first for multiple values of η and then

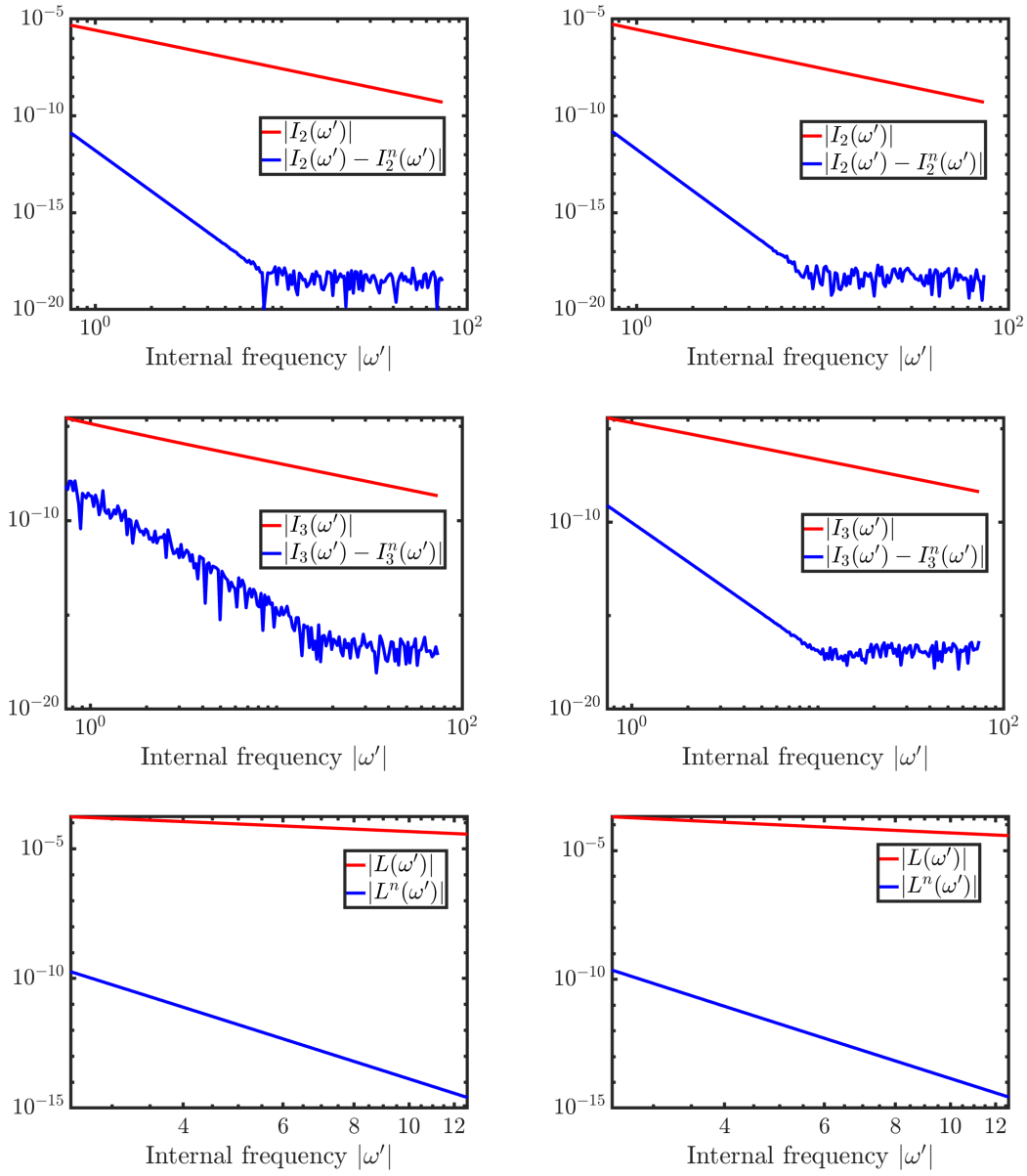

Figure 35: Convergence of the integrals I_2 (first row), I_3 (second row) and L (third row) against their asymptotic expectation. To the left the convergence for positive frequencies is shown, to the right, the convergence with respect to negative frequencies. The plots show subtraction up to order $\omega^{-6.5}$. With the `getScaling` procedure see Sec. C I have then calculated the exponents of the differences, see Tab. 2. The parameters for this calculation are $g = 100\text{meV}$, $\omega_{\text{ph}} = 100\text{meV}$ and $m = 0.2$, $k = k_F$.

Table 2: The leading exponents for the integrals I_2 and I_3 subtracted by the approximation for large $|\omega'|$, positive or negative ω'. The measurements have been made in regions, where the approximation is not everywhere accurate to double precision. The values for the approximation to order 8 do not fit the expectation, because at double precision the scaling cannot be shown with the computer anymore. "o.a." stands for "order of approximation", which means for o.a. n that the exponent should be equal to $-n - \frac{1}{2}$.

Description	Exponent
For positive ω', I_2 with o.a. 8	-3.9542.
For negative ω', I_2 with o.a. 8	-3.7477.
For positive ω', I_3 with o.a. 8	-3.9823.
For negative ω', I_3 with o.a. 8	-4.476.
For positive ω', L with o.a. 8	-3.4898.
For negative ω', L with o.a. 8	-3.4898.

Table 3: The leading exponents for the integrals Γ_1 and $I_1\Gamma_1$ subtracted by the approximation for large $|\omega'|$, positive or negative ω'. The measurements have been made in regions, where the approximation is not everywhere accurate to double precision. The values for the approximation to order 8 do not fit the expectation, because at double precision the scaling cannot be shown with the computer anymore. "o.a." stands for "order of approximation", which means for o.a. n that the exponent should be equal to $-n - \frac{1}{2}$.

Description	Exponent
For positive ω', Γ_1 with o.a. 5	-4.5059.
For negative ω', Γ_1 with o.a. 5	-4.3828.
For positive ω', $I_1\Gamma_1$ with o.a. 5	-3.4742.
For negative ω', $I_1\Gamma_1$ with o.a. 5	-3.4875.
For positive ω' with self-energy, $I_1\Gamma_1$ with o.a. 5	-3.5265.
For negative ω', with self-energy, $I_1\Gamma_1$ with o.a. 5	-3.4898.

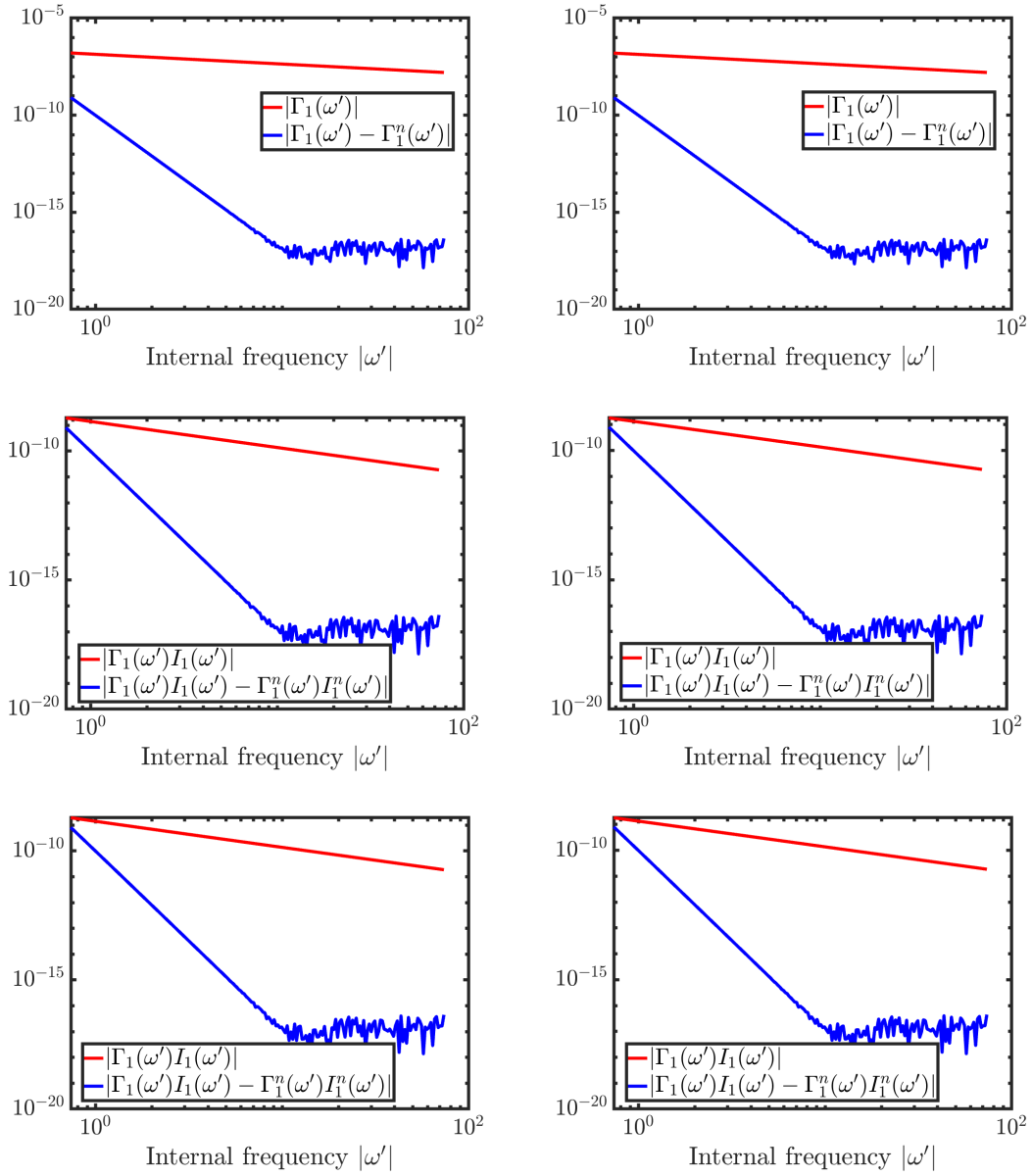

Figure 36: Convergence of the integrals Γ_1 (first row), $I_1^b\Gamma_1$ (second row) and $I_1^d\Gamma_1$ (second row) against their asymptotic expectation, b stands for bare, without self-energy correction, d for dressed. To the left the convergence for positive frequencies is shown, to the right, the convergence with respect to negative frequencies. The plots show subtraction up to order $\omega^{-6.5}$. With the `getScaling` procedure see Sec. C I have then calculated the exponents of the differences, see Tab. 3. The parameters for this calculation are $g = 100\text{meV}$, $\omega_{\text{ph}} = 100\text{meV}$ and $m = 0.2$, $k = k_F$.

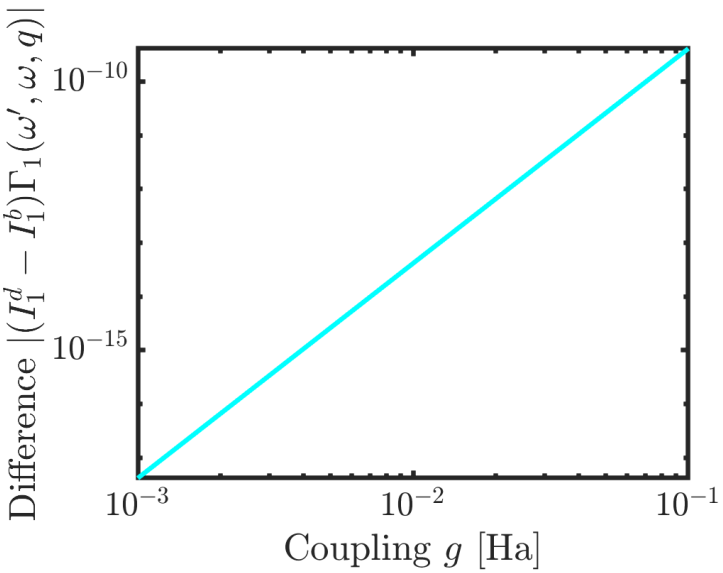

Figure 37: Difference between the kernels of the integral for the vertex correction (dressed and undressed) for a random value (k, ω, ω'), with $g \to 0$. The scaling is g^4, as was expected. The measurement with `getScaling` gives the exponent -4.02. The parameters for this calculation are $\omega_{\text{ph}} = 100\text{meV}$ and $m = 0.2$, $k = k_F$.

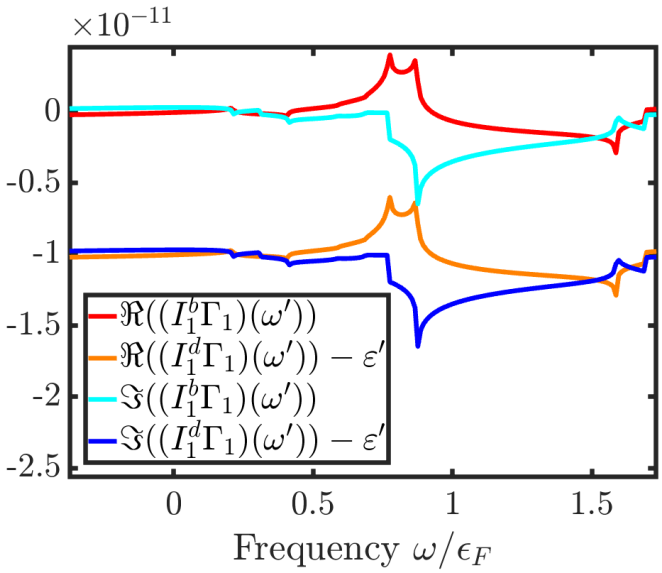

Figure 38: Difference between the kernel of the integral for the vertex correction for a random value (k, ω, ω'), with $g \to 0$. To make both curves visible, one has been shifted by a constant value. The parameters for this calculation are $\omega_{\text{ph}} = 100\text{meV}$ and $m = 0.2$, $k = k_F$.

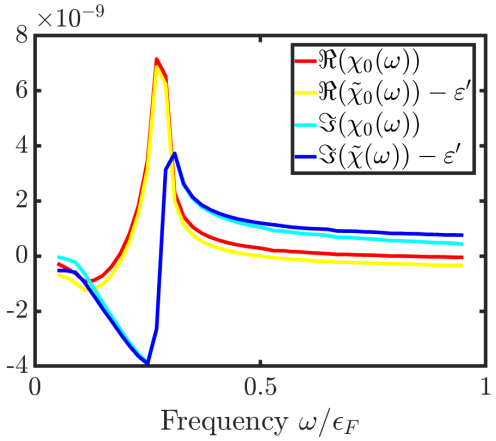

Figure 39: Difference between the vertex correction, with and without self-energy in K_χ for a random value (k, ω), with $g \to 0$. To make both curves visible, one has been shifted by a constant value. The parameters for this calculation are $g = 10\text{meV}$, $\omega_{\text{ph}} = 100\text{meV}$ and $m = 0.2$, $k = k_F$.

of the grid density. The results for the lifetime are also given below and seem well converged, see Figs. 40 and 41.

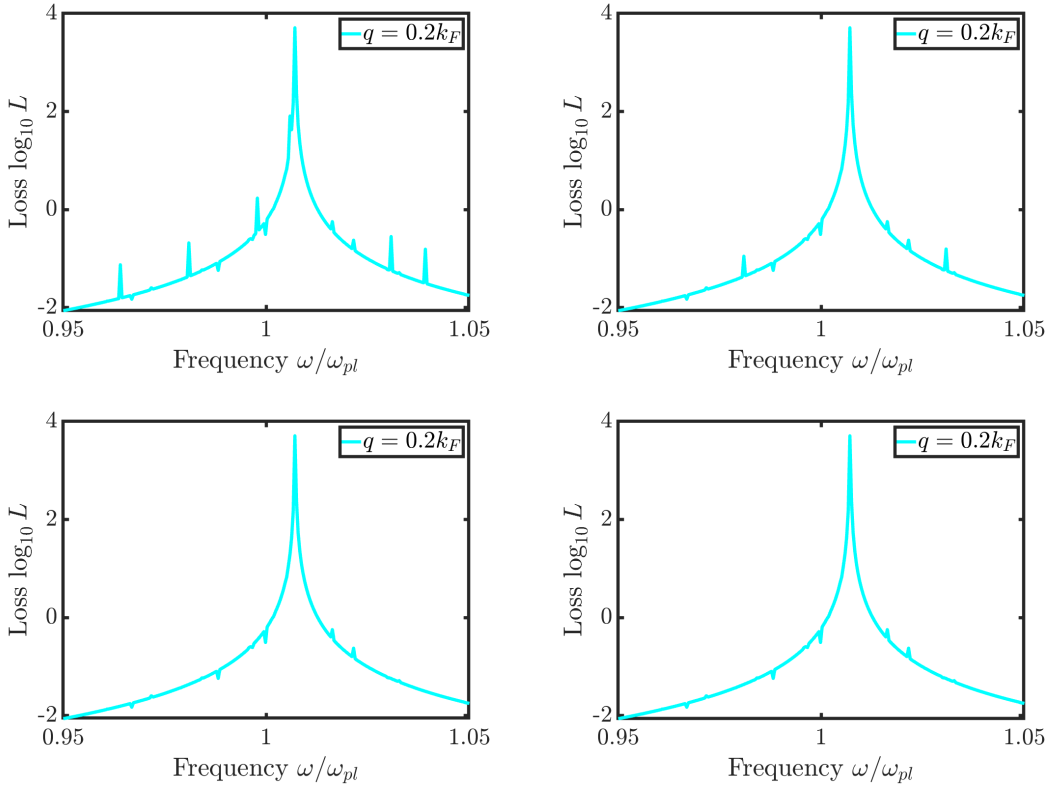

Figure 40: Plasmon peaks in loss function for different values of the broadening η, with values clockwise from the upper right 6×10^{-10}, 4×10^{-10}, 4×10^{-14} and 10^{-12} with a resolution of $4 \times 10^{-4}\omega_{\mathrm{pl}}$. The parameters for this calculation are $g = 10\mathrm{meV}$, $\omega_{\mathrm{ph}} = 100\mathrm{meV}$ and $m = 0.2$, $k = 0.2k_F$.

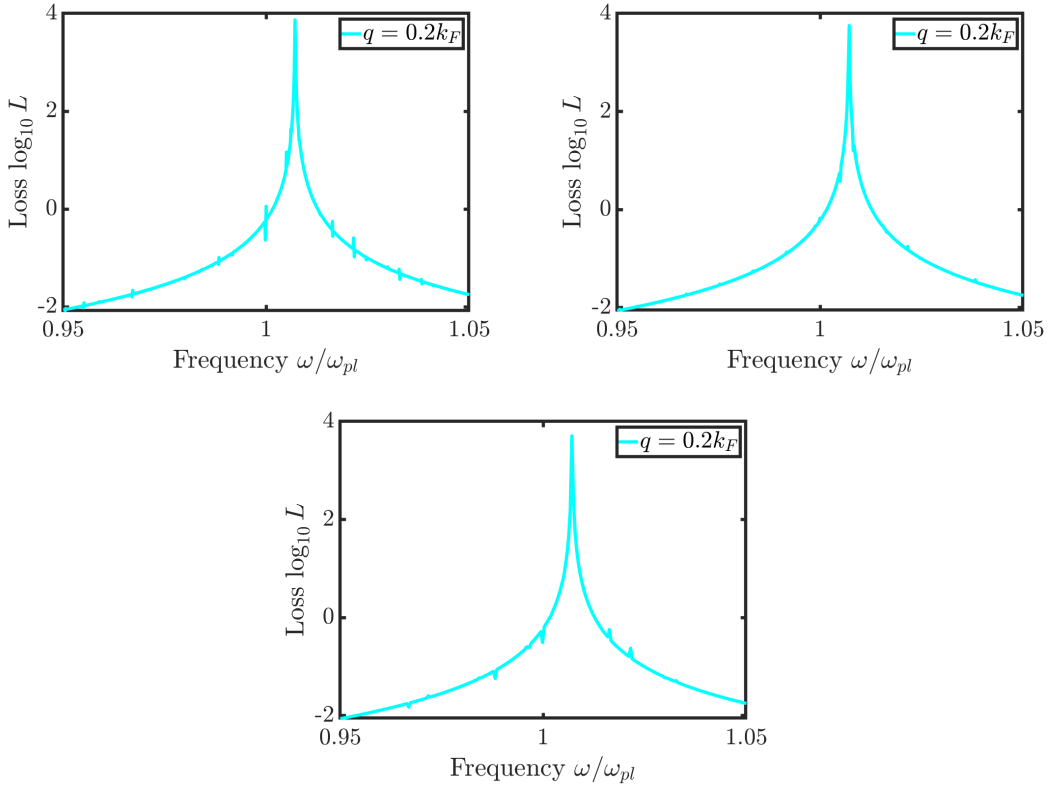

Figure 41: Plasmon peaks in loss function with $\eta = 10^{-12}$ for different grid densities of resolution of $1 \times 10^{-4}\omega_{\mathrm{pl}}$, $2 \times 10^{-4}\omega_{\mathrm{pl}}$ and $4 \times 10^{-4}\omega_{\mathrm{pl}}$. The results for the plasmon lifetimes are all about 170fs. The parameters for this calculation are $g = 10\mathrm{meV}$, $\omega_{\mathrm{ph}} = 100\mathrm{meV}$ and $m = 0.2$, $k = 0.2k_F$.

C. Implementation details

In the following I will sketch the software implementation for my master thesis. The system consists of more than 200 scripts with over 11000 lines of code (6th of march 2019), for the calculations, validations and plots (pls notify me if you want the implementation: "huebner@physik.hu-berlin.de"). To calculate the impact of electron-phonon coupling on the spectral function and polarizability of the free electron gas, I have calculated the Fan-Migdal self energy, the kernel of the polarizability and the vertex function of the interacting electron-phonon system to second order in the interaction and implemented these functions, their expansions for large ω' and the other methods, explained in this text, in `Matlab R2018b`.

The implementation falls into three parts: the library functions, the self-energy and the vertex function. The validation procedures are also implemented and their results are found in Sec.B above.

C.1. Library

The library has the following purposes,

- Read the parameters of the electron gas,
- support the methods explained in this text, such as fixing the renormalization condition,
- compute necessary functions, such as the dilogarithm,
- convert units,
- provide interfaces to run all necessary calculations,
- compute the observables from the polarizability and the spectral density, such as the spectral density and plasmon lifetimes
- and call all tests of the system.

With this, it simplifies the programming task and supports the implementation of the other elements.

There are the following functions in the package. The Lindhard function for the free electron gas is computed according to Ref. [26]. The functions that can be measured by spectroscopy are computed, namely the loss function from EEL spectroscopy

$$\mathscr{L} = \Im(\varepsilon^{-1}) \tag{269}$$

the spectral density

$$S = \frac{1}{\pi}\Im(G^{\mathrm{ret}}) \tag{270}$$

the absorption function

$$A = \Im(\varepsilon) \tag{271}$$

and the dielectric function

$$\varepsilon = 1 - \frac{4\pi}{q^2}\chi_0. \tag{272}$$

Another important function is the dilogarithm Li_2. As `MatLab`'s routine `dilog`, is slower, I used a routine, made by Didier Clamond, that is in my code called `canonicalDilogarithm`. It transforms the dilogarithm into the Debye function and applies the rational approximation (that is exact within machine precision) [40, 72].

Next to this, I implemented the routine `fixPolarizabilityAsymptotics` to capture the constant that is introduced during the renormalization procedure, c. I extract the constant by evaluating the function of interest, the polarizability χ, for large frequencies. The values of the function are then used in a fitting procedure: I assume a form of the polarizability, motivated by the f-sum rule

$$\chi(q,\omega) + c = c + \alpha_{-2}(q)\omega^{-2} + \mathscr{O}(\omega^{-3}). \tag{273}$$

Then, I define my test functions to be $f_1(\omega) = 1$ and $f_2(\omega) = \omega^{-2}$. I compute the functions at the frequencies at which χ was evaluated to determine c. These "correlations" are put into the correlation matrix X. Then, I perform a singular value decomposition of the correlation matrix. The left-singular matrix U then enables us, to compute the standard deviation of the shift at each momentum: The error is proportional to the root mean square error of the fit. This is, when χ is approximated as $\tilde{\chi}(\omega, q_i) = c + \alpha_{-2}(q)\omega^{-2}$

$$\mathrm{RMSE}(q) = \left(\frac{1}{n}\sum_{i=1}^{n} |\chi(\omega_i, q) - \tilde{\chi}(\omega_i, q)|^2\right)^{\frac{1}{2}}. \tag{274}$$

Now, we have

$$\chi(\omega, q) - \tilde{\chi}(\omega, q) = (1 - UU')\chi(\omega, q) \tag{275}$$

with χ interpreted as a vector with an entry per frequency. Then, the error of c can be calculated for this momentum:

$$\Delta c(q) = ||U_1||_2 \mathrm{RMSE}(q) \tag{276}$$

where U_1 is the first column of U and $||\bullet||_2$ is the euclidean norm. c, which is q independent, can be calculated for each momentum

$$c(q) = V_1 \Sigma^{-1} U' \chi(q, \omega) \tag{277}$$

with V the right-singular matrix of X and Σ the diagonal matrix that contains the singular values of X. The averaged shift is computed via Gauss propagation of uncertainty

$$\begin{aligned} \overline{c} &= \frac{1}{\sum_q \Delta c(q)^{-2}} \sum_q \frac{c(q)}{\Delta c(q)^2} \\ \overline{\Delta c} &= \left(\sum_q \Delta c(q)^{-2} \right)^{-1/2} . \end{aligned} \tag{278}$$

Then, the polarizability is corrected by $\overline{c}$, and the routine warns, if the uncertainty $\overline{\Delta c}$ is larger than the predefined relative tolerance of the system. Additionally the routine tests, if the coefficient $\alpha_{-2}(q)$ meets the expectation from the f-sum rule.

To test whether the expansions of $g(x, y)$ in x^{-1}, that are calculated by `Mathematica`, are accurate, I assume that the subtracted function scales like

$$g(x, y) - g_n(x, y) \propto x^{-\beta(n)} \tag{279}$$

with $\beta \in \mathbb{Q}$. To obtain β, that should be linear in n, I use that for $k(x) = a_{-\gamma} x^{-\gamma} + \mathscr{O}(x^{-\gamma-d})$, ($a_{-\gamma}$ and $d > 0$)

$$\gamma \approx -\frac{d \log |k(x)|}{d \log(x)}. \tag{280}$$

This formula is implemented in the routine `getScaling`, which also includes an error estimation: The routine uses N calculations of $k(x)$ on a manifold of points for $x \gg 0$ or $x \ll 0$. The differential quotient, that approximates the derivative in Eq.(280), obtains then $N - 1$ values for γ. I assume then a Gaussian distribution of the values of γ and by this obtain a standard deviation of the distribution.

If this standard deviation is larger than 1, it usually hints at that the subtraction leads to double precision errors in the result. In this case, I will test, whether the relative error of our approximation of g is of the order of the machine precision. If the error is not of this order, the routine returns a warning.

C.2. Self-energy

The tasks of this part are

- Compute the Fan-Migdal approximation to the electron-phonon self energy in jellium,
- the self-energy corrected polarizability and
- the effects of satellites in the spectral function on the polarizability.

The corrected polarizability needs a correction term to be extrapolated accurately. The reasoning and error calculation have been presented in Sec. B.2.4. The correction

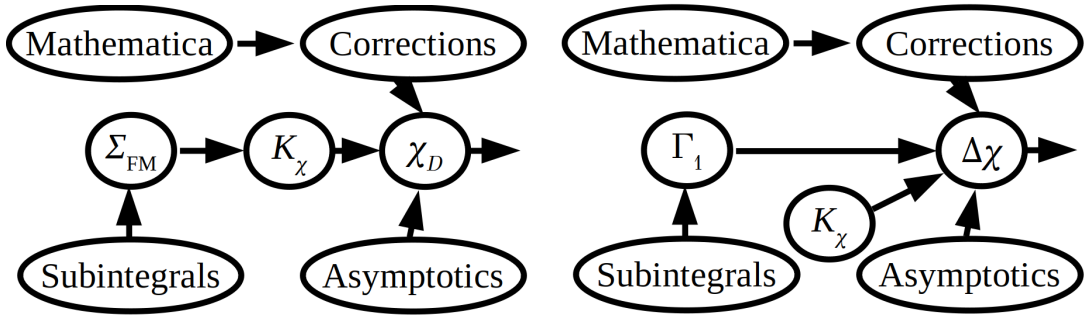

Figure 42: Workflows to calculate the polarizability χ_D and it's vertex correction $\Delta\chi$.

terms stem now from the expansion of the integral I_1, that is the kernel of the corrected polarizability χ_D:

$$I_1 = \frac{-m^{3/2}}{2^{3/2}\pi\sqrt{|\omega'|}} \int_0^1 \frac{du}{\sqrt{1 - \frac{f(u)\epsilon(q)}{|\omega'|}}}. \tag{281}$$

I aim to compute correction terms, that are

$$c_n(\Lambda) = \int_\Lambda^\infty \frac{d\omega'}{2\pi} I_1^{(n)}(\omega')|_C, \tag{282}$$

where $I_1^{(n)}$ is the function that $I_1 - I_1^{(n)} = \mathscr{O}(\omega^{-(n+\frac{3}{2})})$. To find $I_1^{(n)}$ I expand the squareroot in the representation of I_1 to order n. For the convergence discussions see Sec. B.2.4. Then, the expanded integrand is a polynomial in $f(u)$. The integral in u can be solved exactly. To solve it, I have implemented the procedure in `Mathematica 11.1` and use the `ToMatlab` package, by Harri Ojanen[18], to convert the resulting expressions to `MatLab` executables. The resulting functions $I^{(n)}$ and their integrals $c_n(\Lambda)$ are then tested by the `getScaling` routine to meet the defining condition $I_1 - I_1^{(n)} = \mathscr{O}(\omega^{-(n+\frac{3}{2})})$. Then the correction terms, that are calculated analytically, are compared to the numerical integrals over $I_1^{(n)} - I_1^{(0)}$. Note that, in the case of the corrected polarizability, the function $f(u)$ depends on the Fan-Migdal self energy, and so Σ_{FM} has to be expanded in $\frac{1}{\omega'}$ as well. The integral for the polarizability is then

$$\chi_D(q,\omega) = \int_{-\Lambda}^{\Lambda} \frac{d\omega'}{2\pi} I_1(q,\omega,\omega') + c_n(\Lambda) + \tilde{c}_n(-\Lambda) + \mathscr{O}(\Lambda^{-n+1}). \tag{283}$$

Finally the corrected polarizability is adjusted by `fixPolarizabilityAsymptotics`, so that $\chi(q,\infty) = 0$.

The procedure to calculate the polarizability is depicted in Fig. 42 and applies also to the vertex correction.

[18]See `http://library.wolfram.com/infocenter/MathSource/577/`, called 10^{th} of march, 2019, 12:15:37.

C.3. The vertex correction

The main purposes of the vertex part are

- the computation of the vertex function
- and of the vertex correction to the polarizability.

Additionally I have tested the vertex function for its monodromy and calculated the average of the vertex correction around the Fermi surface. This might, in a later work, help to find approximations for *ab initio* calculations.

To compute the integrals correctly, I needed to expand the integrals I_2 and I_3 for large ω'. The expansions of these function have then again been tested with `getScaling`. The correction terms for the vertex function are calculated numerically only, as their components have been tested in-depth before. The function finally needs to be corrected by a constant, using `fixPolarizabilityAsymptotics`.

To test the monodromy, I have calculated $|\Gamma_1(q, \omega, \omega')|$ for $\approx 10^9$ points in the box $q \in [0, 3k_F]$, $\omega \in [0, 2\epsilon_F]$ and $\omega' \in [-5\epsilon_F, 5\epsilon_F]$ and have looked for sharp local peaks of the function, that may indicate branch cut divergences. The divergences may correspond to elementary excitations of the system, as explained in Sec.3.2.

C.4. Additional tests for the integrals

Additionally, I tested the calculated integrals against their integral representation numerically. This has been done for thousand random sets of input parameters for each integral. The maximum relative error can be seen in Tab. 4. These tests have been carried out for all my integrals: $I_1, I_2, I_3, L, L_1, K, \Gamma_1, \sigma, \Sigma_R, \Sigma_{\mathrm{FM}}$.

To make sure that the integrals (that have been calculated pointwise above) are also calculated correctly if parallelized, I have checked their serialized versions against their parallelized results. These results you can see in the Tab. 5.

The correction terms to my integrals $\int_\Lambda^\infty g_n(x)dx = c_n$ can be obtained analytically (and have been, with `Mathematica`), and are tested against their integral representations. The results you can see in Tab. 6.

The reader is welcomed to ask for a copy of the package. Write to the e-mail: "huebner@physik.hu-berlin.de".

Table 4: Maximum relative error of the calculated integrals in this work with respect to their integral representations. Both values have been evaluated numerically for thousand random sets of input parameters for each integral. This table also includes subintegrals of the integrals shown in the text: F_1, F_2, B_1^{FM} and B_2^{FM}.

Output	Relative Error
Integral I_1 for two real input frequencies	3.89×10^{-8}
Integral I_1 for one real input frequency	1.43×10^{-8}
Integral I_1 for two complex input frequencies	9.46×10^{-11}
Integral I_1 interface for two complex input frequencies	2.56×10^{-13}
Integral I_2	6.71×10^{-9}
Integral I_3	2.93×10^{-8}
Integral F_1	3.97×10^{-11}
Integral F_2	6.05×10^{-9}
Integral L_1	7.66×10^{-9}
Integral L	5.09×10^{-7}
Integral M	8.15×10^{-9}
Σ_{FM}	1.18×10^{-5}
Σ_R	4.31×10^{-16}
σ function	1.17×10^{-15}
Integral B_1^{FM}	1.17×10^{-15}
Integral B_2^{FM}	2.91×10^{-15}
Li_2	$2.22\times10^{-}16$

Table 5: The integrals implementations are tested in serialized and parallelized fashion, for vector and matrix inputs in all input parameters, are compared here (1000 calculations per test, or table row). I_1^c means the implementation of I_1 for complex input frequencies. Therefore, I expect the implementation to work well, as the integrals have been tested in the pointwise form in Sec. B. "p.w." stands for "parallelized with respect to".

Description	**Error**
Integral I_1 p.w. k	0
Integral I_1 p.w. ω'	0
Integral I_1 p.w. ω	0
Integral I_1 p.w. all inputs	0
Integral I_1^c p.w. k	0
Integral I_1^c p.w. ω'	0
Integral I_1^c p.w. ω	0
Integral I_1^c p.w. all inputs	0
Integral M p.w. k	0
Integral M p.w. ω'	0
Integral M p.w. ω	0
Integral M p.w. all inputs	0
Integral S_R p.w. first input	0
Integral S_R p.w. second input	0
Integral S_R p.w. third input	0
Integral S_R p.w. all inputs	0
Integral I_R p.w. first input	0
Integral I_R p.w. second input	0
Integral I_R p.w. all inputs	0
Integral L p.w. k	0
Integral L p.w. α	0
Integral L p.w. ψ	0
Integral L p.w. all inputs	0
Li_2 with vector input	0
Li_2 with matrix input	0
Γ_1 p.w. k and ω'	0
Γ_1 p.w. all inputs	0

Table 6: Test of the analytically calculated corrections to the polarizability, compared to their numerical integrals over $(I_1^{(n)} - I_1^{(0)})(x)$. The values to the left represent relative errors, for different integration domains ($[\Lambda, \infty]$ and $[-\infty, -\Lambda]$) with and without self-energy corrected Green's function.

Case	Relative Error
For positive frequencies without self-energy	2.3362×10^{-8}.
For negative frequencies without self-energy	3.6119×10^{-9}.
For positive frequencies with self-energy	1.5082×10^{-9}.
For negative frequencies with self-energy	1.4197×10^{-8}.

Acknowledgements

I want to address special thanks to my academic advisor and first evaluator, Prof. Dr. Dr. h.c. Claudia Draxl, for all her help, suggestions and tips and all the time she invested, starting from finding the right topic for me up to revising this text.

Furthermore, I would particularly thank my tutor, Dr. Fabio Caruso, for supervising my work and redacting this thesis. I want to give thanks to Dr. habil. Pasquale Pavone for his advises and to Rouven Koch and Dr. Santiago Rigamonti, for counterreading my thesis.

Additionally I want to thank the institute for informatics for the title page design.

Humboldt-Universität zu Berlin
Philosophische Fakultät II

Name: Huebner Vorname: Axel Felix

Matrikelnummer: 556649

Eidesstattliche Erklärung zur

☐	**Hausarbeit**	☐	**Take Home-Klausur**
☐	**Bachelorarbeit**	☐	**Diplomarbeit**
☒	**Masterarbeit**	☐	**Magisterarbeit**

Ich erkläre ausdrücklich, dass es sich bei der von mir eingereichten schriftlichen Arbeit mit dem Titel

Vertex correction due to electron-phonon interactions in the homogeneous electron gas

um eine von mir erstmalig, selbstständig und ohne fremde Hilfe verfasste Arbeit handelt.

Ich erkläre ausdrücklich, dass ich *sämtliche* in der oben genannten Arbeit verwendeten fremden Quellen, auch aus dem Internet (einschließlich Tabellen, Grafiken u. Ä.) als solche kenntlich gemacht habe. Insbesondere bestätige ich, dass ich ausnahmslos sowohl bei wörtlich übernommenen Aussagen bzw. unverändert übernommenen Tabellen, Grafiken u. Ä. (Zitaten) als auch bei in eigenen Worten wiedergegebenen Aussagen bzw. von mir abgewandelten Tabellen, Grafiken u. Ä. anderer Autorinnen und Autoren (Paraphrasen) die Quelle angegeben habe.

Mir ist bewusst, dass Verstöße gegen die Grundsätze der Selbstständigkeit als Täuschung betrachtet und entsprechend der fachspezifischen Prüfungsordnung und/oder der Allgemeinen Satzung für Studien- und Prüfungsangelegenheiten der HU (ASSP) bzw. der Fächerübergreifenden Satzung zur Regelung von Zulassung, Studium und Prüfung der Humboldt-Universität (ZSP-HU) geahndet werden.

Datum 17.03.2019 Unterschrift

,